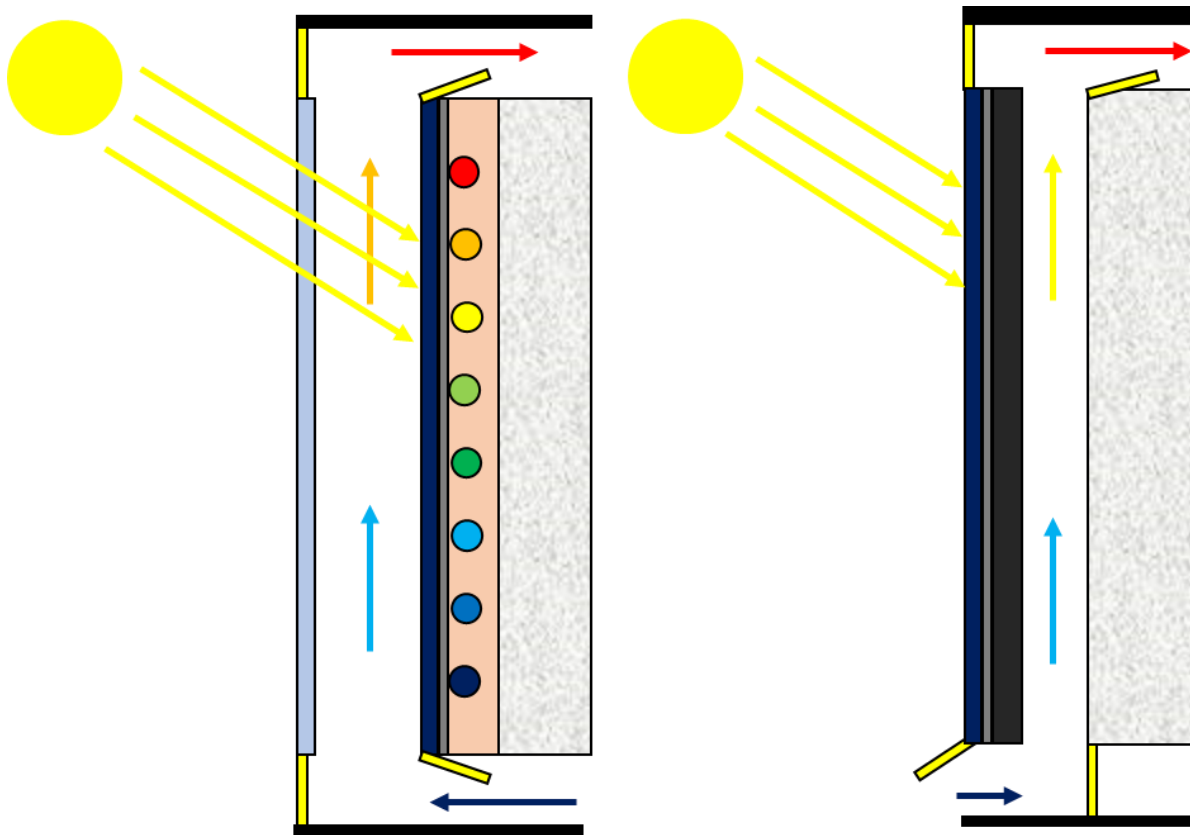


Thermal and Electric Performance of PV/T Solar Chimney System



KYRIAKOS VATTIS
Delft University of Technology

Thermal and Electric Performance of PV/T Solar Chimney System

By

Kyriakos Vattis (4899180)

in partial fulfilment of the requirements for the degree of

Master of Science in Sustainable Energy Technology

at the Delft University of Technology,

to be defended publicly on Friday July 17, 2020 at 2:00 PM.

Project duration:	05 November 2019 – 17 July 2020		
Thesis Committee:	Dr. Ir. O.Isabella	Associate Professor-Tu Delft	Supervisor
	Prof. Ir. P.Luscuere	Professor- Tu Delft	External committee member
	Dr. P. Manganiello	Assistant Professor-Tu Delft	
	Ir. J.C.Ortiz	Phd Candidate-Tu Delft	Daily supervisor
	Ir. Z.Haghighi	Phd Candidate- Tu Delft	

This thesis is confidential and cannot be made public until August 31, 2021

Abstract

The residential and service sectors are responsible for the 39% of the total energy consumption. 80% of this energy is used for heating purposes. Achieving nearly zero energy buildings is a major goal for the near future. The design of an integrated electrical and thermal system can substantially help to reach such objective. The façade is the biggest area of a building and could be utilised to convert incident solar energy to electrical and thermal energy. In previous work (2019), the combination of building integrated PV modules with solar chimney on a façade was investigated to study its energetic performance. One of the main findings was that using the thermal energy from the photovoltaic modules on the air inside the cavity of the chimney is not possible due to its low quality of heat. It was concluded that the utilization of heat could be better by using auxiliary systems, like photovoltaic thermal systems for water heating. The aim of this work is to create a computational model to calculate the thermal and electrical performance of PV thermal (PV/T) modules combined with a solar chimney.

Two new designs for better heat utilization were considered and compared. The first design is for the PV modules to be installed at the front of the solar chimney with fins (Fins design) and the second design is to couple the PV modules installed on the wall inside the solar chimney with water pipe system (Water pipe design). These designs are also compared with the same configurations but without the thermal systems (No fins & No water pipes designs). In addition, two new strategies are introduced to improve the performance of the model. The first strategy is the optimization of the solar chimney openings with respect of time for the highest power generation. The second strategy is the variation of the water mass flow with respect to time for highest water-thermal energy and optimum cooling of the PV cells.

The model was developed in MATLAB and it is based on 2D finite difference transient implicit method. To reduce the computational time, the density of the nodes varies in respect of temperature gradient. In addition, secondary models were created to increase the accuracy and sensibility of the model such as water tank and water pump models.

The models were studied for a building in Delft, Netherlands, and the scale of the chosen system is 10m². It is concluded that Water pipes design provides the overall best energetic performance mainly because of the high water-thermal energy with yearly energy efficiency of 64.3%. However, the best electrical performance is observed from the Fins design and the best air-thermal performance from the No water pipes design.

Acknowledgment

First, I would like to thank my family for all the support during my MSc degree. Without them this journey would not be possible. In addition, I want to express my deepest gratitude to my long-time partner Georgia who was always next to me with love and support.

I also wish to express my sincere appreciation to my supervisor, Dr. Olindo Isabella who provided an excellent supervision and guidance. Furthermore, I would like to pay my special regards to my daily supervisor, Juan Camilo Ortiz who was always there to help and support me for several challenges that I faced during this period.

Lastly, I wish to thank all the people who supported me with their friendship. Abdallah, Sushen and Samrid thank you.

Contents

1	Introduction	1
2	State of the art	3
2.1	Solar chimney/ Trombe wall	3
2.2	Building integrated photovoltaic	3
2.3	Photovoltaic thermal	4
2.3.1	PV/T water	5
2.3.2	PV/T air.....	6
2.3.3	PV/T air and water	6
2.4	Combinations.....	7
3	System designs and strategies	9
3.1	Designs	9
3.1.1	Water pipes design	10
3.1.2	Fin design	10
3.2	System.....	10
3.3	Strategies	12
3.3.1	Door openings.....	12
3.3.2	Water mass-flow variable speed	13
4	Methodology.....	16
4.1	Introduction	16
4.2	Irradiance model.....	16
4.3	Thermal model.....	18
4.3.1	Introduction to heat transfer	18
4.3.2	Finite difference method	19
4.3.3	Thermal model approach.....	22
4.3.4	Convection coefficients.....	24
4.3.5	View factor of radiation	26
4.4	Air mass-flow model choice	29
4.5	Electrical model.....	31
4.6	Water tank model	32
4.7	Energy yield model.....	34
4.7.1	Electrical energies	34
4.7.2	Thermal energies	35
5	Results and discussion	36

5.1	Introduction	36
5.1.1	General description of results.....	36
5.1.2	Main Inputs and parameters	36
5.2	Yearly results.....	38
5.2.1	Energies.....	38
5.2.2	Ventilation.....	41
5.2.3	Efficiencies	43
5.2.4	Temperatures.....	45
5.3	Scenario results.....	47
5.3.1	Highest Irradiance	47
5.3.2	Lowest Irradiance.....	54
5.3.3	Highest ambient temperature	58
5.3.4	Lowest ambient temperature	65
6	Conclusion.....	70
7	Recommendations	72
	Appendix A: Designs without thermal systems	73
	Appendix B: Weather data of scenarios	74
	Bibliography	77

1 Introduction

It is well known that greenhouse gases cause serious problems worldwide with carbon dioxide being of the biggest contributor. The most important effect is the rise of average global temperature, which is estimated to rise on a worst case scenario about 3°C in the current century [1]. This will lead to droughts, rise of sea level and many other effects on nature and humanity [2]. Therefore, renewable energy is the solution for the reduction of CO₂ emissions and fossil fuel consumption.

Figure 1-1-a displays the energy consumption per sector in Europe. The highest energy consumption sector is buildings (residential and services). In addition, Figure 1-1-b illustrates the different usages of energy in the residential sector [3]. Heating takes up to 80% of the overall energy usage and therefore is the most important energy to tackle.

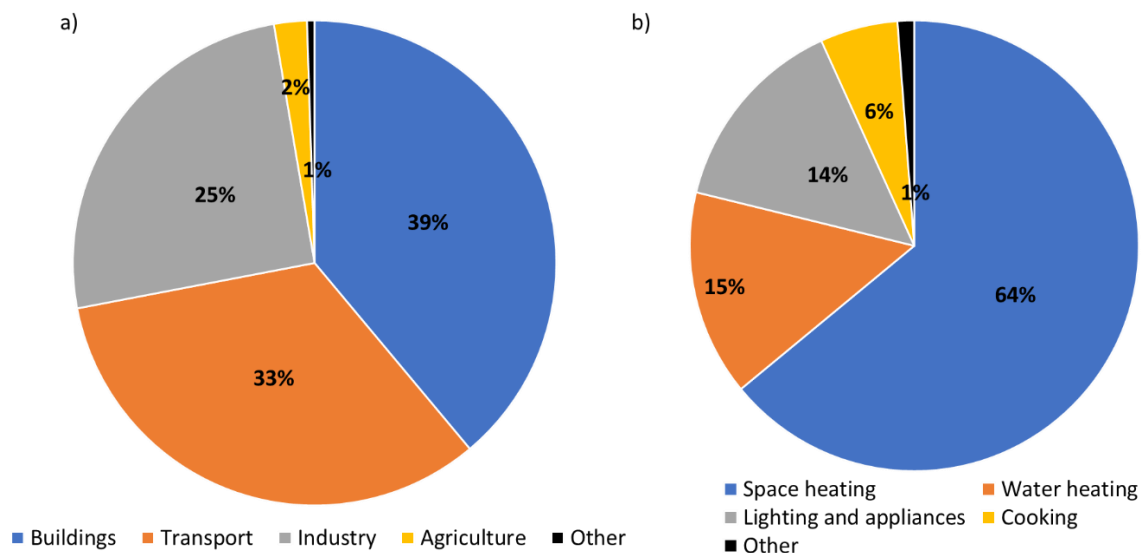


Figure 1-1 a) Final energy consumption per sector in Europe (2015). b) Final energy consumption in the residential sector in Europe (2017) [3]

Therefore, the integration of renewable energy systems on buildings can provide essential help to the reduction of CO₂ emissions. Solar systems are the most preferable energy systems for residential areas (PV modules and solar collectors) mostly installed on the roof. However, a significant amount of area is not utilised, and this is the façade of the building. The ratio between roof and façade is in average 0.33 and M. C. Brito et al [4] stated that PV modules on facades can be an important contributor to zero energy buildings. In addition, they stated that in the winter, PV modules installed on facades can double the solar energy due to better alignment with winter sun paths. Moreover, other energy systems that can be installed on facades are solar chimneys and Trombe walls which provide thermal energy and ventilation to the building from solar energy[5][6].

Consequently, PV modules combined with solar chimney would be an optimum configuration for ventilation and generation of electrical and thermal energy. Juan Camilo Ortiz and Sander Wapperom already developed in 2019 a thermal model for a solar chimney combined with PV modules and

validated it with experimental results[7][8]. The model is based on 2D transient finite difference method. The primary goal was to estimate the energetic performance of a naturally ventilated façade combined with PV modules. They optimized the geometry and configuration of the system by placing the PV modules in the front and inside cavity of the solar chimney, but also by adjusting the depth of the cavity and the distance between the PV modules and the wall. The main conclusion was that the system provides more than the necessary ventilation for a room in a building, but it could not provide thermal energy because of the low quality of heat generated due to low temperature differences. In addition, when the PV modules are inside, the thermal energy is more than when the PV modules are in the front, but the electrical yield is reduced. The optimum place for PV modules inside the solar chimney cavity is in the middle. When PV modules act as front layer of the façade, the optimum cavity depth is 0.2m.

The current thesis is a sequel of the work mentioned above and therefore it is highly recommended for the reader to revise it. The main goal of this thesis is the improvement of the thermal energy performance from the previous work. To achieve that, the design of the system must be reconfigured by combining a solar chimney with PV/T. In addition, new strategies must be introduced for utilisation of the thermal energy and ventilation. Lastly, an improved thermal model must be developed for high accuracy and low computational time. Therefore, below are the main objectives of the current thesis

- Design two configurations of PV/T with solar chimney. PV/T with fins and PV/T with water pipes are the main designs.
- Optimize the door openings of the solar chimney for each time step to achieve the highest energy yields. In addition, optimize the water mass flow of the PV/T with water pipes system for each time step to achieve the highest efficiency of the thermal system.
- Develop a finite difference transient implicit method where the density of the control volumes is highly depended on the temperature gradients to achieve high accuracy and low computational time.
- Compare both design options between them and with standard PV façade systems.
- Develop a MATLAB code which is user friendly and the inputs are reconfigurable.

2 State of the art

2.1 Solar chimney/ Trombe wall

Solar chimney and Trombe wall are used to increase the energetic performance of a facade. By using a glazing cavity in front of the façade, a Trombe wall or a solar chimney is created. There is also an absorptive material installed inside the cavity and is heated due to radiation. Therefore, the air inside the cavity is also heated. A different density is created between the air inside the cavity and the outlet environment. Consequently, buoyancy forces are acting on the air particles inside the cavity and mass flow is created. A solar chimney is combining the building and ambient environment as inlets and outlets for ventilation, heating and cooling [5]. Whereas, the Trombe wall has as inputs and outputs the building environment and therefore is used only for heating [6]. However, solar chimney and Trombe wall most of the times are referred for similar configurations of openings and therefore there is no difference between them. Figure 2-1 illustrates these two technologies for more clarification. In this document the chosen term is “solar chimney” even though there is a part of Trombe wall configuration.

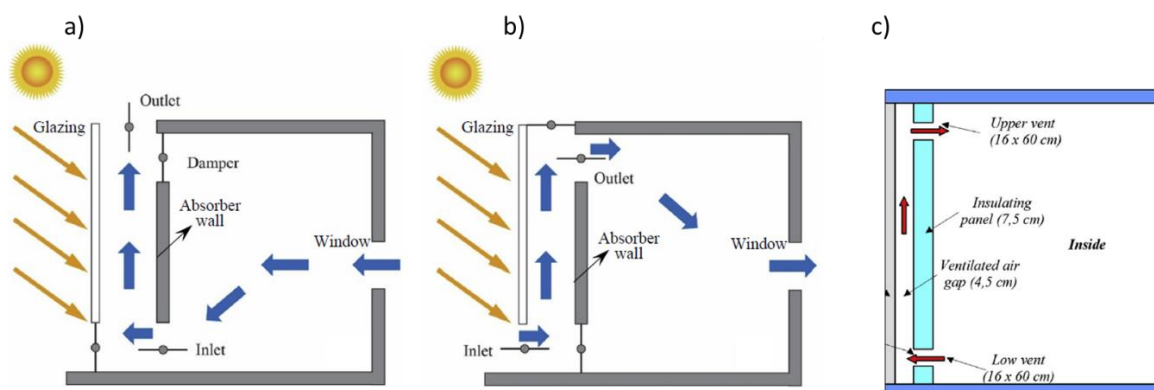


Figure 2-1 Solar chimney for a) cooling, b) Heating and ventilation[9]. c) Trombe wall for heating[10]

There are several studies published about Trombe walls and solar chimneys in the last decade. K. Sergei et al [10] pointed out the most important key findings of Trombe wall structure. The glazing has to be double and the wall has to be thick with insulation for better thermal resistance. In addition, the thickness of the air gap is recommended to be between 29-35cm and external fans are recommended for better automation. M. Raghieb Shakeel et al[11] investigated the performance of solar chimney. They indicated that heat losses from the glazing are essential for a thermal model because the air mass flow errors are reduced. In addition, it was found that the optimum air gap is at 0.3m. L. Shi [9] compared different configurations of solar chimney/ Trombe wall (see Figure 2-1). It was concluded that the chosen configuration has significant performance effects. In addition the configuration where the inlet of the cavity is the ambient environment (Figure 2-1-b) gives the highest volumetric rate.

2.2 Building integrated photovoltaic

Building integrated photovoltaic (BIPV) technology is an integration of PV modules at the building envelope. There are several BIPV product technologies aiming for aesthetic and efficient ways to use unused area at the external of a building.

A. K. Shukla et al [12] provides information about recent advancements of BIPV technologies. It is more efficient to place BIPV modules on the roof rather than the façade because of the better angle of the PV modules. However, the façade area is most of the times more than the roof area and therefore more potential energy yield is available. In addition, m-Si BIPV have the highest energy payback time and thin film BIPV have the lowest energy payback time. Lastly, 80% of BIPV technologies are installed on roofs and 20% on façades as can be seen from Figure 2-2.

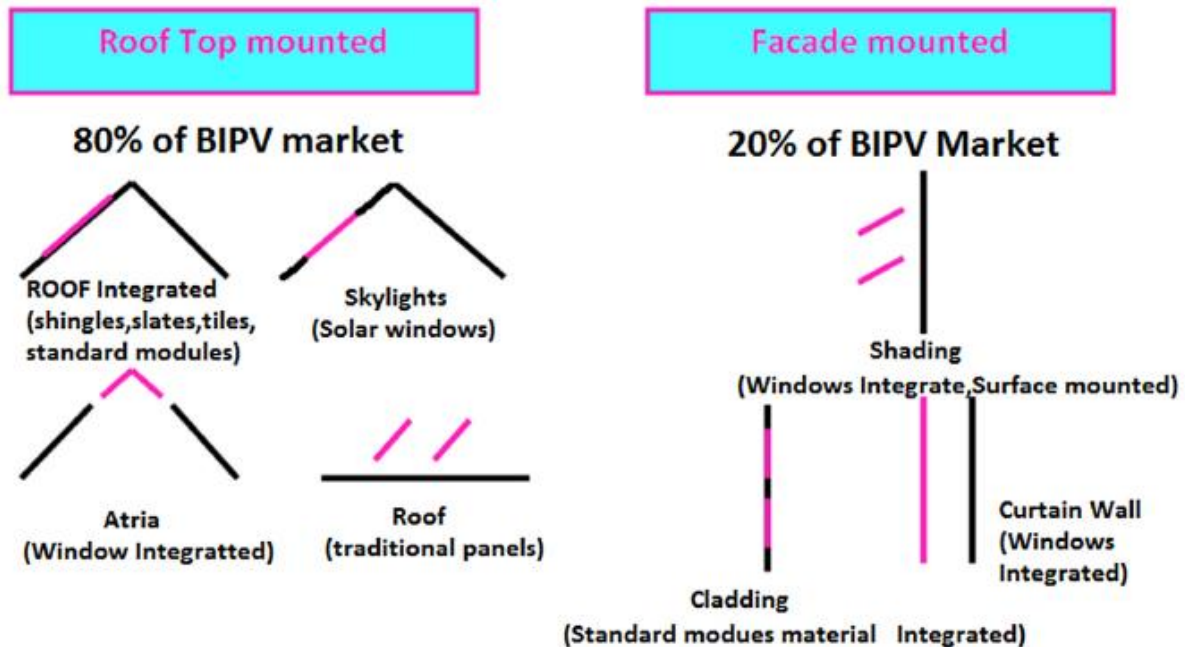


Figure 2-2 BIPV market[12]

2.3 Photovoltaic thermal

The term Solar systems is known as either the photoelectric type (PV modules) or the thermal type (for example solar collectors). However, the combination of those two systems creates the hybrid solar systems which are known as Photovoltaic Thermal (PV/T). A. H. A. Al-Waeli et al [13] provided status and future prospects of PV/T. The research of PV/T started 50 years ago, although there is a need of more development and improvements. One advantage of PV/T compared to standard PV modules is that they use a wider spectrum of radiation. The reason is that, only part of the visible light is converted to electricity but most of the solar spectrum is converted to thermal energy. In addition, the installation cost is less when using PV/T and the used area is less. A drawback of these systems is that the heat is low or medium and consequently the applications are limited (building air heating or domestic water heating). Lastly, A. H. A. Al-Waeli et al [13] concluded that most common fluids used for PV/T are water and air. An overview of all the PV/T can be seen in Figure 2-3. However only water and air-based PV/T will be introduced which are the ones used in this work.

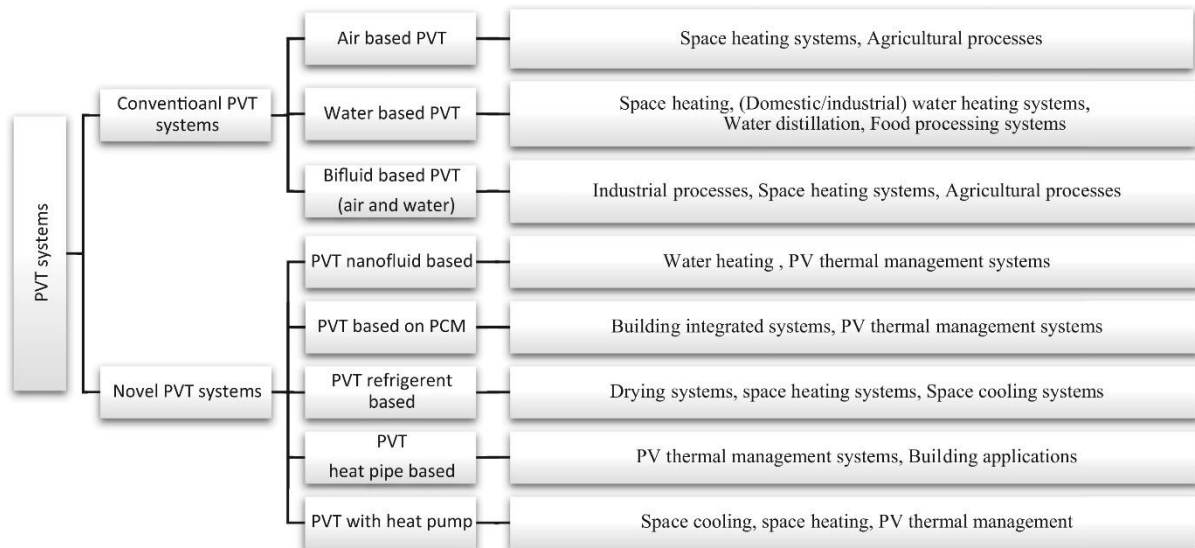


Figure 2-3 An overview of the PV/T technologies[14]

2.3.1 PV/T water

Water is a fluid with high heat capacity and very accessible, which is why it is widely used for PV/T applications. S. Dubey et al [15] analysed the performance of PV/T solar collectors. It was confirmed that PV/T solar collectors will provide great help in the reduction of carbon dioxide if they are used in residential areas. This is because the hot water can be used for heating the building and for domestic hot water, and also the PV modules can provide electricity. In addition, they recommended that if the primary need is hot water, then solar collectors should be partially covered with PV modules. But if the primary need is electricity then the solar collectors should be fully covered with PV modules. H. A. Zondag et al [16] investigated the thermal and electrical yield of a PV thermal collector shown in Figure 2-4. Three models (3D, 2D and 1D) are compared to experimental results and it was found that a 1D and a 2D models performed as good as the 3D model for the calculation of annual energy yield. T. T. Chow et al [17] also developed a model to calculate the performance of a PV thermal collector. It was suggested that using a steady state model is a wrong approach because the PV/T collector is inherently dynamic.

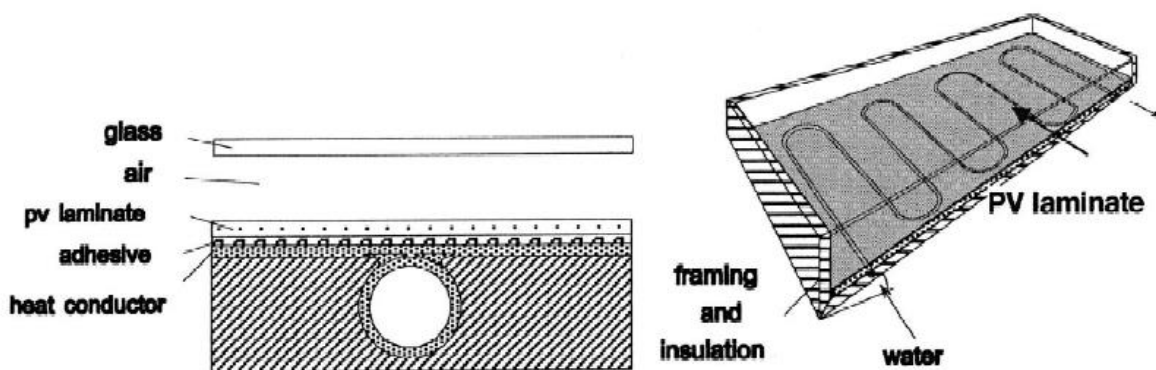


Figure 2-4 PV/T solar collector[16]

2.3.2 PV/T air

It is well known that the water as thermal collector is better than air, but air can be used directly for heating and ventilating the building or assist on other systems. In addition, air is more accessible than water. M. I. Sohel et al [18] investigated the performance of an air based PV system. There is a duct below the PV modules where forced air is passing through. The main conclusions of this model are that efficiencies are becoming less sensitive for air flow values of more than 300 l/s and that if the irradiance is less than 400 W/m² then there is not a significant thermal energy. J. K. Tonui et al [19] investigated the performance of improved PV/T air systems with installation of fins or suspended metal sheet inside the duct as can be seen from Figure 2-5-a. They found out that the fin system was better in both thermal and electrical performance than the other configurations. Also, the decrease of channel depth and increase of flow rate, increases both the thermal and electrical efficiencies. In addition, the fins can be easily installed on the system. J. C. Mojumder et al [20] also investigated the performance of PV/T air with fins (Figure 2-5-b). They also concluded that PV/T with fins increases the overall performance of the system. By installing fins the electrical and thermal efficiencies can increase by 0.81% and 18% respectively.

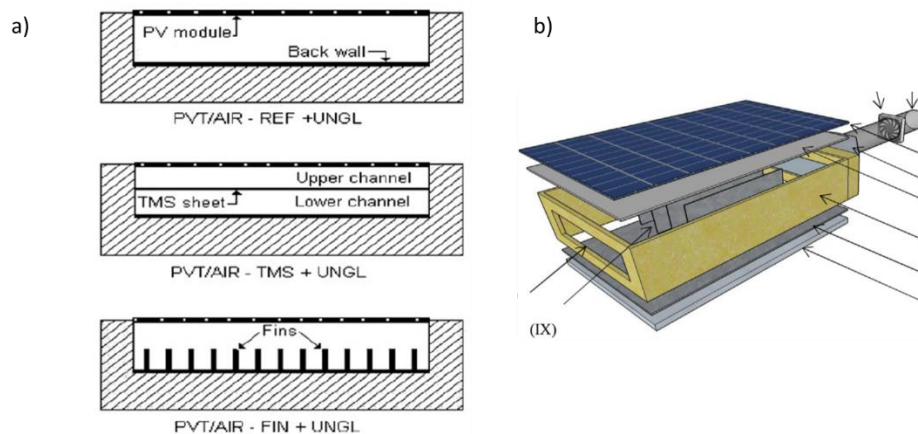


Figure 2-5 PV/T air configurations. a) the air flow direction is perpendicular to the page [19][20]

2.3.3 PV/T air and water

The combination of air and water at a PV/T system provides both the advantages of PV/T air and PV/T water. D. Su et al [21] investigated the performance of a PV/T with dual channels as can be illustrated in Figure 2-6. Water and air can pass through the channels and therefore 4 configurations are compared. Water-water PV/T was found to be the most efficient in both thermal and electrical energies. However, with water-air configuration, the water outlet had the highest temperatures. Lastly, the air-air configuration provides most thermal energy from air.

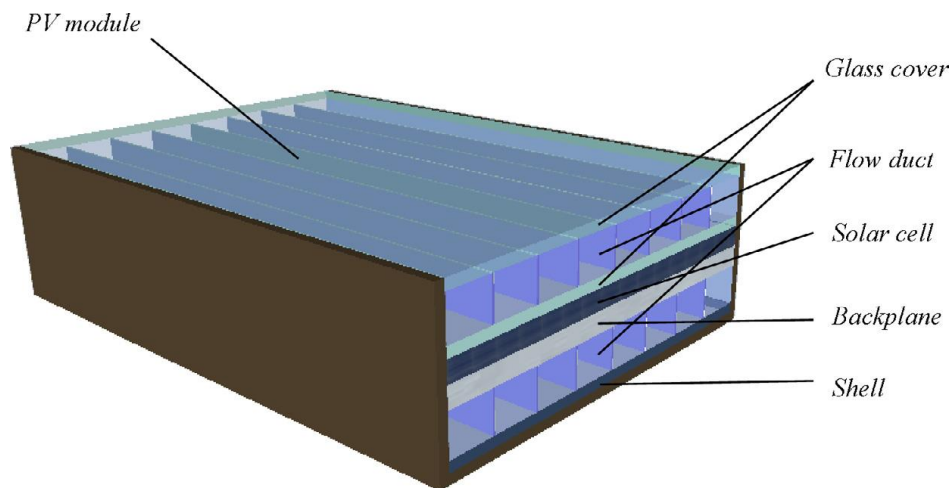


Figure 2-6 PV/T with two flow ducts for air and water combination[21]

2.4 Combinations

PV/T, BIPV and Solar chimney (Trombe wall) technologies can create combinations that provide essential energetic advantages and blend in with the aesthetics of the building. T. Yang et al[22] provided a review of building integrated PV thermal systems (BIPV/T). BIPV/T technology is a relatively new concept and therefore research and development are in need. The authors proposed BIPV/T systems with air, can be integrated to multiple building elements, like facades roofs and windows. Such systems could be Trombe walls and solar chimneys with PV modules which are also providing fresh air to the building. They also suggested that the system is most efficient when PV modules are the first layer. However, because air has low heat capacity the systems are not very efficient. Therefore BIPV/T with water are an alternative for better efficiency.

J. Jie et al [23] developed a Trombe wall with PV cells in the front glass. By combining PV cells with the Trombe wall, the thermal efficiency of the system is decreasing. However, the overall efficiency is increasing because of the additional electrical energy generation. A. K. Athienitis et al[24] created a BIPV/T with PV installed on a transpired collector (Figure 2-7-a). With this design thermal energy, ventilation and electricity are generated. Compared to only the transpired collector, the system provides less thermal energy but because there is electricity generation the overall efficiency is higher. Lastly, the space that the PV modules are taking can be adjusted for the thermal and electrical needs of the consumer. T. T. Chow et al [25] investigated an experimental performance of BIPV/T with water installed on a façade and can be seen in Figure 2-7-b. They concluded that the system also provides thermal insulation for the inside of the building. It was also determined that the natural circulation performed as good as the forced circulation of water for a small system. In addition, it is recommended that the water tank to be investigated better because a bigger volume will provide a better performance.

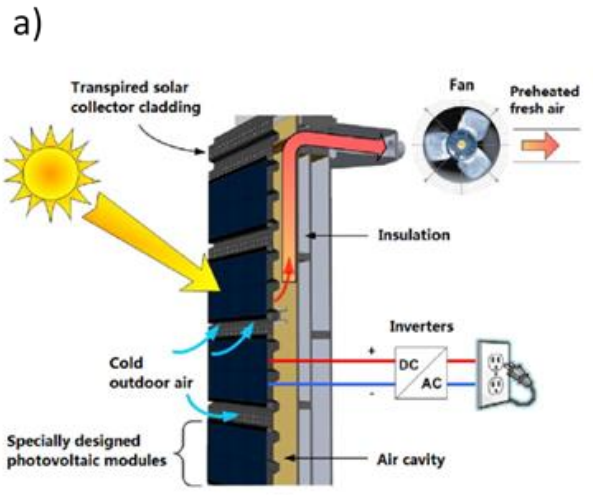


Figure 2-7a) BIPV/T with air. It is a combination of PV modules and a transpired collector [24]. b) BIPV/T with water. Solar collectors on façade combined with PV modules [25]

There are also several publications about BIPV/T with transparent PV modules, especially in combination with solar chimneys. However, this is not in the scope of this thesis. But, S.H.Wapperom [8] (thesis of similar topic in the previous year) already provided a detailed literature for this topic. The interested reader is referred to his work.

3 System designs and strategies

3.1 Designs

The choice of designs and configuration of the system is one of the most vital aspects of the model. Ortiz Lizcano et al [7] created a model with a PV/Solar-chimney design. Even though there were promising results of electricity, thermal energy and ventilation, the issue was that the thermal energy was not utilised due to the low quality of heat. In addition, the PV modules were reaching high temperatures because of the relatively high temperature (higher than environment) of the air inside the solar chimney. Consequently, the average efficiency of the PV modules was low. Therefore, new designs had to be introduced which with the combination of system components and strategies could lead to a system with higher and more utilised thermal energy and lower temperatures on the PV modules.

The designs therefore had to combine also a thermal system attached behind the PV modules. The combination of a conventional thermal system with PV modules is called PV/T, where T stands for thermal. There are several types of PV/T but in this model only water- and air-cooled PV/T are used. The chosen designs are shown in Figure 3-1. These two designs are chosen because they have some important advantages and can lead to substantial improvements from the design of Ortiz Lizcano et. al [7].

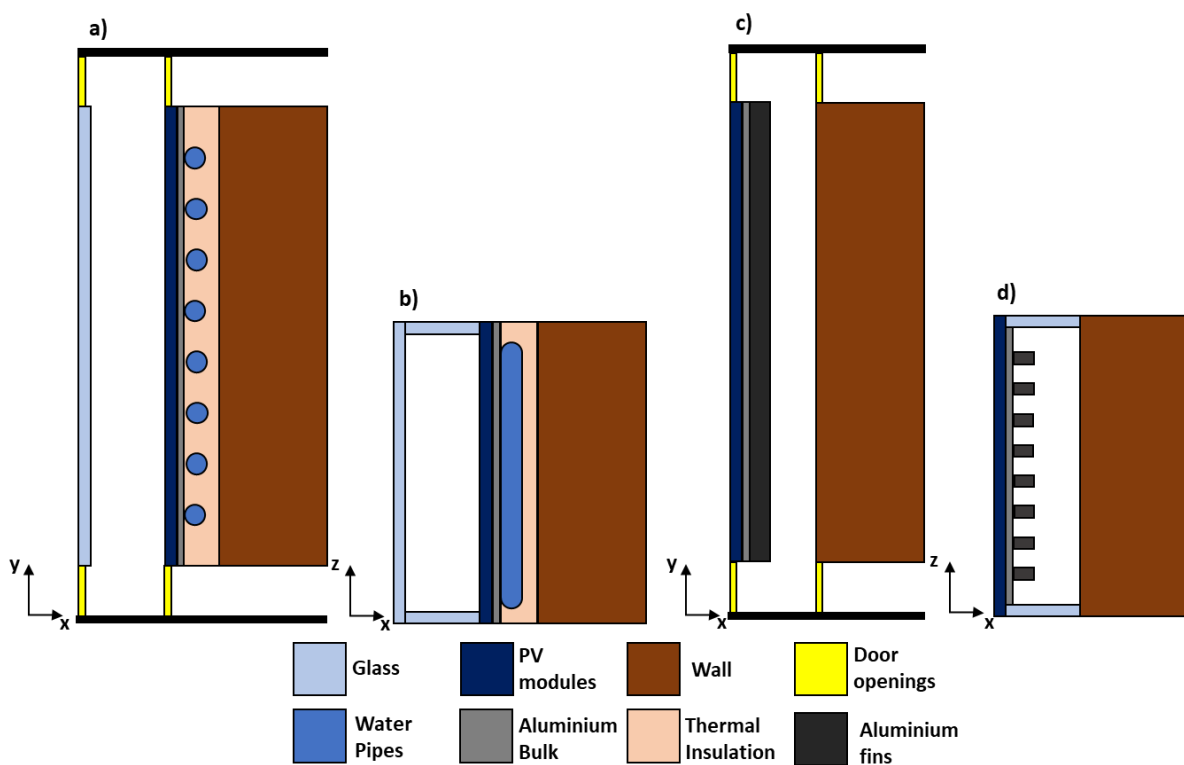


Figure 3-1 The chosen designs which combine a solar chimney with a PV/T. Environment is in the left and building in the right. a) Water pipe design seen from the side, b) Water pipe design cross-section, seen from above, c) Fin design seen from the side, d) Fin design cross-section seen from above

3.1.1 Water pipes design

The water pipe (Figure 3-1-a&b) design is the most common PV/T design, which is a solar collector where the absorber is replaced with the PV module which has high absorptivity. With this configuration the thermal energy of the PV module not only flows to the cavity and heats the air but also flows to the water pipes behind the PV module that heat up the water. Therefore, the benefits of this design are that electricity, ventilation and thermal energy of water/air, are utilised from one system. In addition, the temperature of the PV module is decreasing and can be monitored to avoid high fluctuations as the mass-flow of the water can change throughout time. Consequently, the efficiency of the PV modules will increase. A drawback of this configuration is that it is active because of the need of a water pump. Subsequently, a part of electrical energy generated from the system will be needed for the water pump. In addition, because the temperature of the water will increase as it flows through the system, the temperatures of the PV modules will not be uniform. Last disadvantage is the additional reflection losses due to the glazing in front of the PV modules for the configuration of the solar chimney.

3.1.2 Fin design

The second design is with fins (Figure 3-1-c&d). Aluminium fins are attached behind the PV module for more heat transfer to the air in the cavity. Equation 4.8 confirms that the heat transfer of a solid to the fluid is proportional to the area subjected to it. By implementing fins, the area factor increases because more area is exposed to the cavity. Therefore, the advantage of this design is that the temperature increase of the air inside the cavity will be higher. In addition, because of the temperature increase the mass flow will also increase with a consequence more heat flow and ventilation. The advantage of this design compared to the water pipe design is that is passive and consequently, there are no active parts. Furthermore, the design is simpler than the water pipe design with less parts and therefore less maintenance. Moreover, there is no additional reflection losses because the PV module is the first component subjected to the environment. However, this design will provide less thermal power than the water pipe design because thermal energy is lost in the environment and air has lower specific heat than the water.

3.2 System

The external system components are as important as the main system, because they are interacting continuously. External system components are the parts that are not installed on the solar chimney. These components can be seen in Figure 3-2.

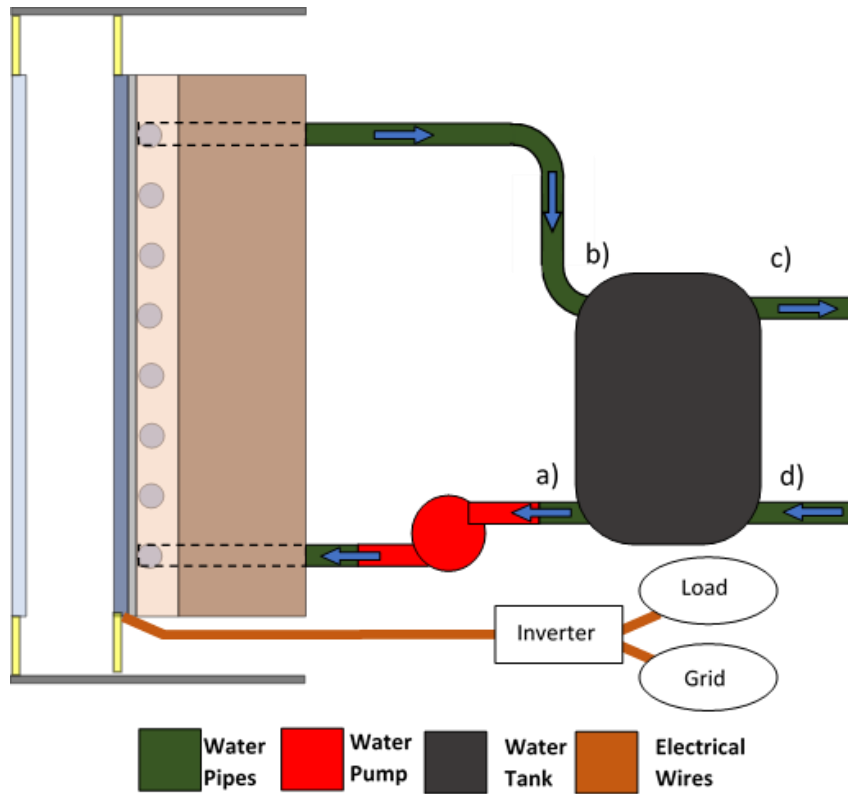


Figure 3-2 External components of the system for electricity and thermal energy from water. a) Water heading to the system b) Water heading back to the water tank from the system, c) Water heading to the load (Domestic or industrial), d) Water heading to the water tank from the mains

Both designs (fins/water pipes) have the electrical components which are electrical wirings and inverter. However, for simplicity of results the electrical energy given from the model is before the inverter. This is because the scale of the system in the model can be adjustable with respect of the user needs and therefore different inverter types might be needed for different scales which means different efficiencies of inverters.

The water pipe design has another external system which is for the water storage and the flow of the water. It consists a water tank, a water pump, and water pipes that pass also from the back of the PV modules as can be seen from Figure 3-2. Although, it is not exactly realistic because heat exchangers should be also in the system, nonetheless it is a reasonably accurate system. The design and methodology of the water tank were taken from E. M. Kleinbach et.al [26] which are explained in detail in a further chapter (4.6). As can be observed from Figure 3-2, there are four openings on the tank for the water to flow. The opening a is for the water that flows to the solar chimney which its temperature is equal to the temperature of the lowest-level water in the tank. The opening b is for the water that leaves the solar chimney and enters back to the water tank. This temperature is dependent from the amount of heat that is collected from the system. The opening c is for the water that goes to the load and its temperature is equal to the temperature of the highest-level water in the tank. Lastly, the opening d is for the water that comes from the mains to replace the water that went to the load. The temperature of that water is equal to the temperature of the mains.

3.3 Strategies

3.3.1 Door openings

The Door Openings Strategy (DOS) is essential to achieve optimum results of the system for all different weather scenarios. There are four doors installed on the system. Two are facing the ambient environment and the other two are facing the inside of the building. With these four openings, four configurations can be achieved as can be illustrated in the Figure 3-3. This strategy is inspired from M. Haase et.al [27] which introduces a similar approach. The left doors are facing the ambient environment and the right doors are facing the building.

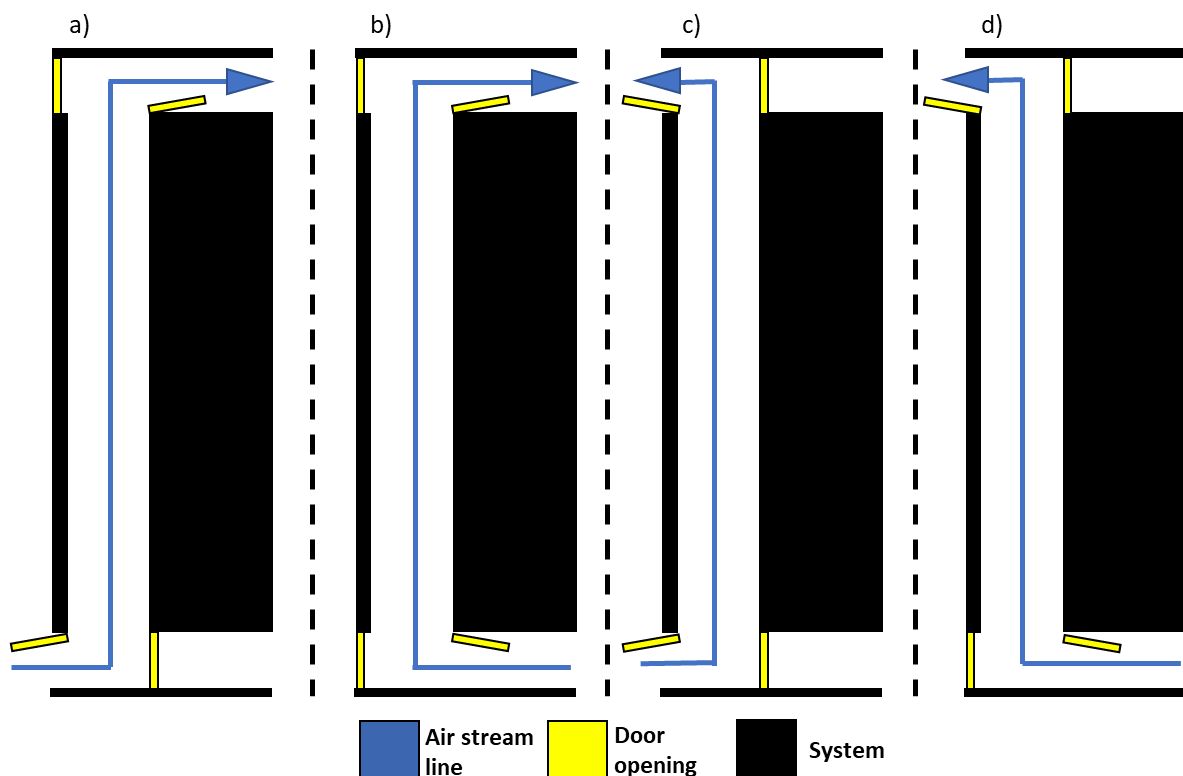


Figure 3-3 Four different strategies of door openings. Environment is in the left and building in the right. a) Bottom door environment and top door building, b) Bottom and top door building, c) Bottom and top door environment, d) Bottom door building and top door environment

A strategy has to be formed to decide which configuration must be used at each timestep. To create the strategy, the physics of massflow have to be considered. To have massflow, the temperature on the outlet of the cavity must be higher than the environment that is entering (Building or ambient) or else the opposite effect will occur. Massflow will flow downwards. This is something to avoid because it will have negative effect. For example, the configuration is the one illustrated in Figure 3-3-a, if the temperature of the air entering the building is not higher than the temperature of the building air then the opposite effect will happen and thermal energy will be extracted from the building which is not effective for this configuration. Because it is impossible to precisely predict the temperature of the air in the outlet, the strategy is formed accordingly as illustrated in Table 3-1.

Table 3-1 Strategy for door openings in respect of temperature differences

Bottom: Ambient Top:Building a)	$T_{Env} > T_{Building}$ & $T_{CellAvg} > T_{Env} + 1$ & $T_{Env} < 25^{\circ}C$
Bottom: Building Top:Building b)	$T_{Env} < T_{Building}$ & $T_{CellAvg} > T_{Building} + 1$
Bottom: Ambient Top:Ambient c)	$T_{Env} < T_{Building}$ & $T_{CellAvg} < T_{Building}$
Down: Building Up:Ambient d)	Never

For the first configuration (Figure 3-3 a), the temperature of the ambient environment must be higher than the temperature of the building and the reason is explained in the previous paragraph. In addition, it is required for the temperature of the PV modules to be higher than the temperature of the environment so the buoyancy forces can be applied and create mass-flow. Lastly, the temperature of the ambient environment must be less than 25°C because thermal energy is not needed (Hot day/Summer). Worth mentioning is that with this configuration there is also ventilation.

The second configuration (Figure 3-3 b) takes place when it is cold outside and no thermal energy from the environment can be used. Therefore, there is a circulation of the building air which is heated when is passing through the cavity. However, the average temperature of the cell is required to be higher than the temperature of the room, to heat the air and create a mass flow.

The third configuration (Figure 3-3 c) is applied when the ambient environment is cold, and the average temperature of the cells is lower than the temperature inside the building. With this configuration there is air mass flow, but it is not utilised because the air is entering and exiting the ambient environment. Although this mass flow keeps cool the PV system which is an important parameter.

The fourth configuration (Figure 3-3 d) unfortunately is never applied. This configuration is important in the summer where the building air can exit from the cavity and cooler air can enter from a different opening. However, because of the uncertainty what of the temperature value of the air in the exit of the cavity, it is not evident if this temperature is higher from the environmental temperature and therefore there is a risk of opposite results as explained above.

3.3.2 Water mass-flow variable speed

Another important strategy is the control of the water mass flow for the water pipe system. The control of the flow can be achieved with a variable speed water pump. Figure 3-4 Illustrates what is the difference if the water mass flow is low (a) or high (b) when passing through a hot plate. When the water mass flow is low, the temperature of a control volume moving through the system will increase rapidly during the flow because the lower the velocity the more time is passing through the hot plate. However, the lower the temperature difference between the water and the hot plate, the lower the thermal power is extracted (see equation 4.8).

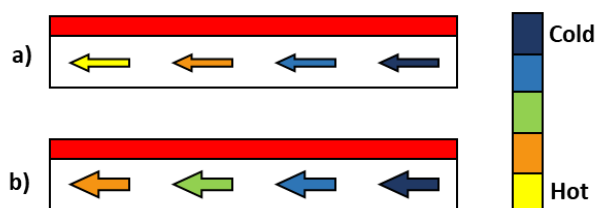


Figure 3-4 Example of water temperature in respect of space below a hot surface. a) Small Velocity, b) High velocity.

For example, if the temperature of the controlled water mass reaches almost the same temperature of the hot plate at a certain point, then there will not be a significant heat transfer from that point until the end. Therefore, higher mass-flow has better results because the temperature of the water will not increase significantly, and consequently more thermal power will be extracted. But the higher the mass-flow, the higher is the power needed from the water pump. As a result, regulation of the water mass-flow must take place for optimum outcome continuously. A suggested strategy is that when the temperature difference between the PV modules' (Tedlar for this model) back and the water in the inlet of the system (Figure 3-2-a) is higher than zero then there is a water mass-flow. If this difference increases, then the mass-flow increases.

$$\dot{m}_{Water} = \phi_s A \quad 3.1$$

Equation 3.1 proves that the water mass-flow is dependent from the specific flow rate (ϕ_s) and the area (A) of the PV modules. As a starting point of specific flow, R. Santbergen [28] suggested that ten kilograms per meter square per hour are enough for a good efficiency of the system. Figure 3-5 clearly illustrates the difference for different specific flow rates and it can be observed that for a specific flow rate from 10 kg/m²h and more, the temperature of the water does not rise substantially.

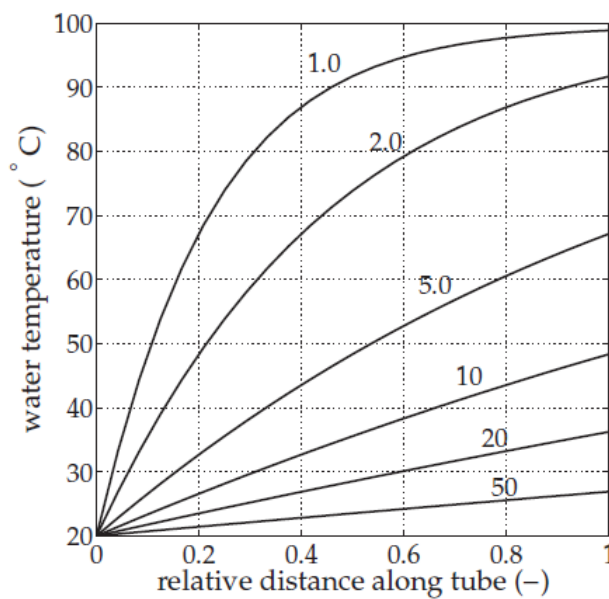


Figure 3-5 Temperature of the water along the tube for various specific flow rates (kg/m²h) (Temperature of the plate is equal to 100°C) [28]

Therefore, trial and error simulations were attempted to find the optimum specific flow rates for various temperature differences. Table 3-2 highlights all the specific flow rates for various temperature differences.

Table 3-2 Strategy of specific flow rate in respect of temperature differences

Temperature difference [°C]	Specific flow rate ϕ_s [kg/(m ² k)]
$T_{Avg\ Tedlar} < T_{Water\ Tank\ Down}$	0
$T_{Avg\ Tedlar} > T_{Water\ inlet}$ $T_{Avg\ Tedlar} < T_{Water\ inlet} + 3$	4
$T_{Avg\ Tedlar} > T_{Water\ inlet} + 3$ $T_{Avg\ Tedlar} < T_{Water\ inlet} + 6$	10
$T_{Avg\ Tedlar} > T_{Water\ inlet} + 6$ $T_{Avg\ Tedlar} < T_{Water\ inlet} + 9$	18
$T_{Avg\ Tedlar} > T_{Water\ inlet} + 9$ $T_{Avg\ Tedlar} < T_{Water\ inlet} + 12$	25
$T_{Avg\ Tedlar} > T_{Water\ inlet} + 12$	32

An important note is that the water tank is interacting with the system and therefore its average temperature will increase during the storage of hot water and the temperature of the PV modules will decrease. Consequently, the lower level temperature of the storage tank which is the temperature of the water inserting the system (Figure 3-2-a) will also have an increase. The result is that there is low possibility to have very high differences in temperature from the PV modules and the entering water. Hence, the probability of having 32 or 25 kg/(m²k) specific flow rate is small.

4 Methodology

4.1 Introduction

The model is a MATLAB software that provides as output the temperatures and energy yields (thermal and electrical) of the chosen design with respect to space and time for different scenarios, locations, dimensions and accuracy. The scenarios are, day with highest/ lowest irradiance on system, day with highest/lowest ambient temperature, average day of any month and results for the whole year. In addition, the dimensions of the design are variable for the needs of the user.

The model is divided to several main models that are interactive with each other for each timestep. In simple form, data are taken from software Meteronorm[29] and imported to the irradiance model to extract the irradiance on the PV for the chosen scenario. Then, the irradiance on PV is imported to the thermal model which interacts with the mass-flow model and electrical model for the calculation of the temperatures. The temperatures and power of the system then are imported to the energy model for the electrical and thermal energy yields. Worth mentioning, is that there are also numerous other secondary models that provide important data for the main models to run.

4.2 Irradiance model

To find the Irradiance on PV, the Direct Normal Irradiance (DNI), Diffused Horizontal Irradiance (DHI) and the orientation of the sun and the modules are needed. Thankfully, Meteonorm provides the two Irradiances as well as Global Horizontal Irradiance (GHI) which can be calculated from DNI and DHI . DNI is the non-scattered irradiance of the light arriving on a surface normal to the sun's path, DHI is the scattered irradiance arriving on a horizontal surface and GHI is the non-scattered and scattered Irradiances arriving on a horizontal surface.

The total Irradiance on PV is the sum of the direct irradiance (G^{dir}), the diffused irradiance (G^{dif}) and the Irradiance reflected from the ground (G^{ground}) to the PV as shown in Figure 4-1-a and equation 4.1. G^{dir} , G^{dif} and G^{ground} depend from DNI DHI and GHI respectively.

$$G^{PV} = G^{dir} + G^{dif} + G^{ground} \quad 4.1$$

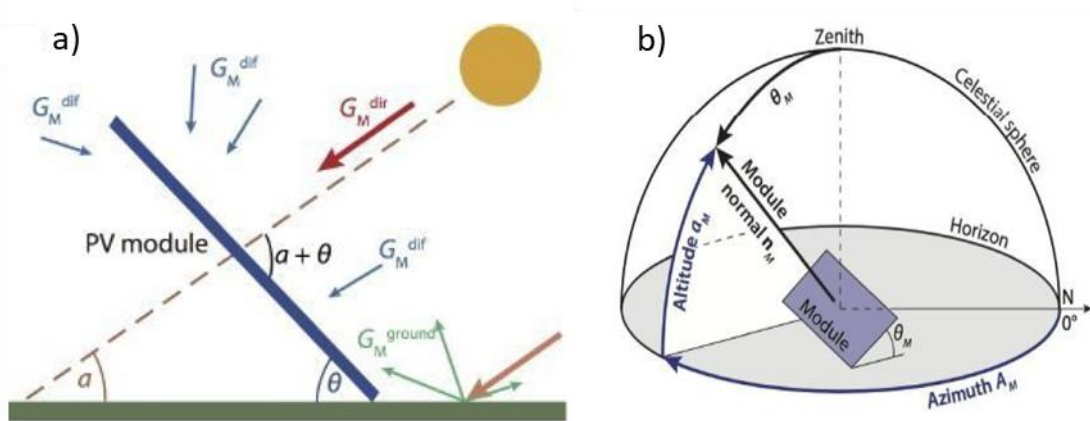


Figure 4-1 a) All the radiation on the PV module (Direct, Diffused, Ground) b) Azimuth and altitude of the PV module [30]

Equations 4.2, 4.3 and 4.4 calculate the direct, diffuse and ground irradiance on a PV module respectively. [30]

$$G^{dir} = (DNI)\cos(AOI) \quad 4.2$$

$$G^{dif} = (DHI)(SVF) \quad 4.3$$

$$G^{ground} = (GHI)(\alpha)(1 - SVF) \quad 4.4$$

Where AOI is the angle of incidence, SVF is the sky view factor and α is the albedo of the ground. AOI is the angle between the direct sunlight direction and the normal of the surface. This angle is depended from the azimuth (A_s)and altitude (a_s) of the sun as well as from the azimuth (A_M) and altitude(a_M) of the module as shown in Figure 4-1-b.

$$AOI = \cos^{-1}(\cos(a_M) \cos(a_s) \cos(A_M - A_s)) \quad 4.5$$

SVF is a factor that represents the actual percentage of diffused radiation that arrives on the PV surface. It is dependent on the module tilt angle (θ_M). The equation of SVF is 4.6.

$$SVF = \frac{1 + \cos(\theta_M)}{2} \quad 4.6$$

Because of the design limitations, θ_M/a_M will be always $90^\circ/0^\circ$ and therefore SVF will be always 0.5. A_s and a_s are given from Meteonorm. For albedo, it is assumed that the ground area is asphalt and 0.15 factor is chosen which is a representative number for urban areas [31].

With all the above considerations and assumptions, the Irradiance on PV can be calculated with very small errors.

After the calculation of the irradiance on PV modules, the next step is the irradiance that is absorbed (G_{Abs}). To find this type of irradiance, reflection losses must be considered. Two types of reflection losses are considered. The first reflection loss is the reflection of the glass of the PV module and the glass of the system. If the chosen design is the water pipe system, then the effect of glass reflection losses will be squared. The other reflection loss is due to the AOI of the sun on the PV module [32]. The higher the angle of incidence the higher the reflection losses.

4.3 Thermal model

4.3.1 Introduction to heat transfer

The thermal model has the three fundamental heat transfer methods. Conduction, convection and radiation which all must be implemented for accurate results. This chapter introduces these three heat transfer methods. To have heat flow, there must always be a temperature difference and this rule applies to all the heat transfer methods. An overview of the three heat flows can be seen in Figure 4-2 and is explained in more detailed below [33].

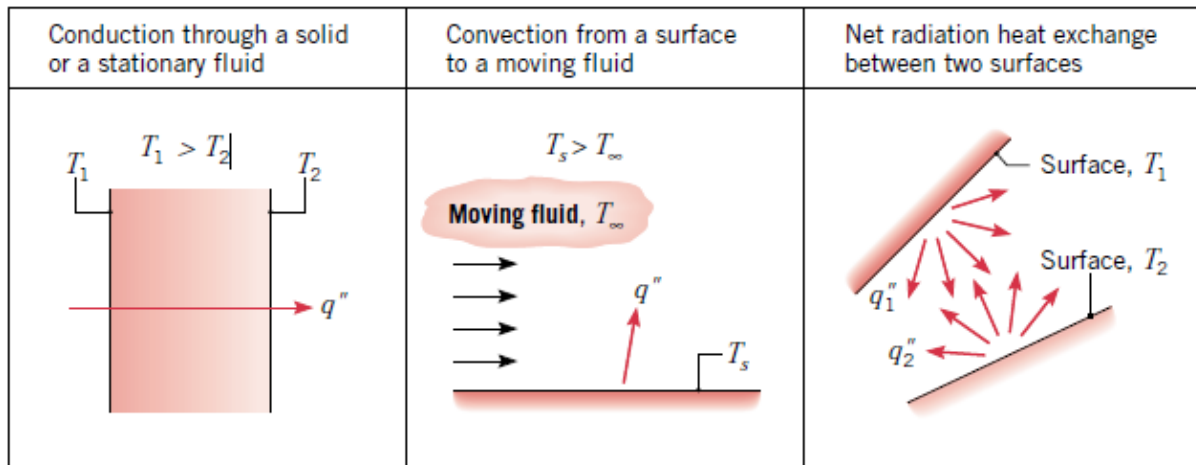


Figure 4-2 Examples of the three fundamental heat transfer methods. In the left is the conduction, in the middle is the convection and in the right is the radiation [33]

Conduction is the flow of heat inside a solid bulk. Therefore, conduction as an example, is the flow of heat inside the PV module (from high temperature to low temperature). In addition, conduction is occurring also when two materials are attached with each other and have different temperatures. The important parameter of conduction is conduction coefficient (k) which explains how easy a material can transfer heat and is different for each material. Equation 4.7 calculates the conduction. Where A is the cross-section area ΔT is the temperature difference and L the distance that heat travels.

$$q_{cond} = \frac{kA(\Delta T)}{L} \quad 4.7$$

Convection is the heat flow from or to a fluid that passes through or in contact with a surface. As an example of this, is heat flow that goes from the PV (high temperature) to the environmental air (low temperature) when there are high wind velocities. The important parameter of convection is the convection coefficient (h) which describes how easy the heat flows to or from the fluid. The two types of convection are forced and natural. Forced convection occurs when the fluid moves by an external mechanical force, for example a fan. Natural convection occurs because of buoyancy forces on the fluid (air inside solar chimney). The buoyancy forces are created due to the difference in temperatures of the fluid in different levels. These two types have different approaches for finding the convection coefficient which are derived in a later chapter (4.3.4). In general, forced convection coefficient is mainly dependent on the velocity of the fluid and natural convection coefficient is mainly dependent on the temperature difference between the surface and the fluid. In addition, the most common calculation of the convection coefficients is from experimental data. Therefore, convection coefficient is one of the most difficult values to be calculated in heat transfer, because for each different design,

experiments must be used for its calculation. Equation 4.8 calculates the convection. Where A is the exposed area.

$$q_{Conv} = hA(\Delta T) \quad 4.8$$

Radiation is the heat emission from a surface to another surface (or to the sky) due to radiation. As an example of this, is the increased temperature of the ground behind the PV module due to exchange radiation between the PV back and the ground. Important parameters of radiation are the emissivity (ϵ) and the view factor (F). The emissivity is a material property which explains how strong the radiation is. Emissivity can be found for all the materials. The higher the emissivity the more the radiation. The view factor represents a percentage of the radiation that travels from one surface to another and the derivation of it is explained in later chapter (4.3.5). Worth mentioning is also that radiation is becoming very important at high temperature differences because the temperatures in the equation are in the power of four. Equation 4.9 calculates the radiation. Where σ is the Stephan-Boltzmann constant.

$$q_{Rad} = \frac{A\sigma(T_1^4 - T_2^4)}{\frac{1}{\epsilon_1} + \frac{1}{\epsilon_2} + \frac{1}{F_{12}} - 2} \quad 4.9$$

4.3.2 Finite difference method

Several heat transfer models can be solved easily by analytical solutions. However, as the complexity of geometries and boundary conditions increase it is almost impossible to use analytical solutions. Therefore, a numerical technic can be used if the complexity is high. Such numerical techniques are finite difference, finite element and boundary element methods [33]. For simplicity only finite difference method will be explained because is the one used also for the model.

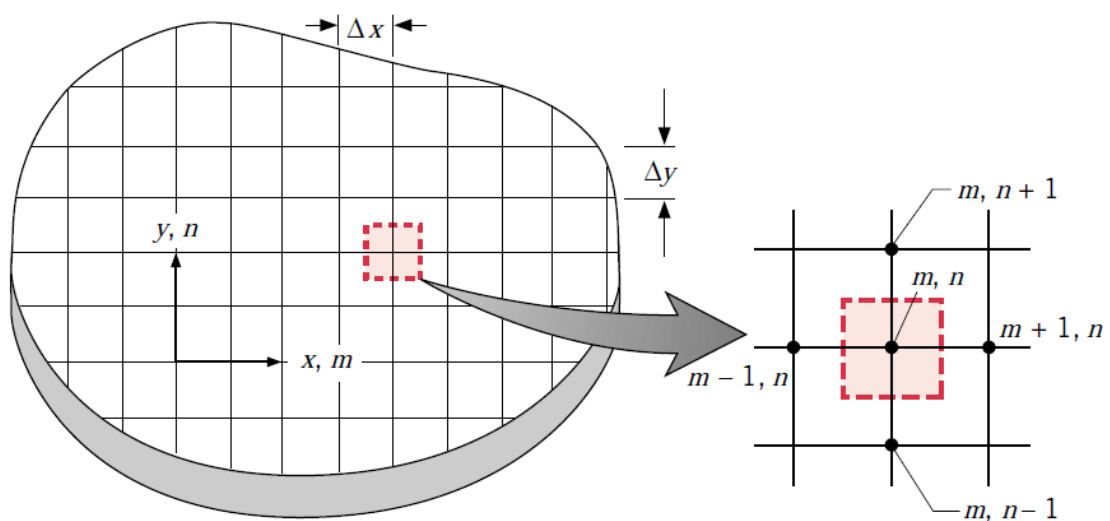


Figure 4-3 Example of a nodal network inside a bulk. In the right side there is a focus of a node and the neighbouring nodes [33]

As Figure 4-3 shows, to use numerical technique, the geometry must be divided into small control volumes. Each control volume has a nodal point in the centre which represents the temperature and properties of the volume.

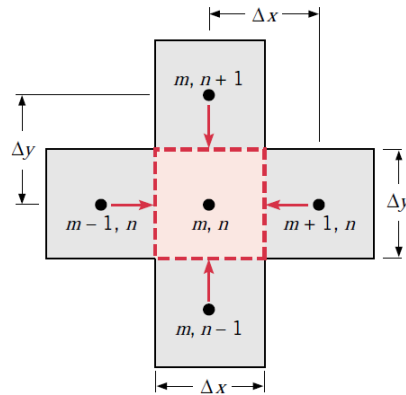


Figure 4-4 Example of finite difference method at a node and the conduction with the neighbouring nodes [33]

Every node depends of the neighbouring nodes or boundaries as can be seen from Figure 4-4. For each node, an energy balance equation can be derived which has as unknown, the temperature of the node and the neighbouring nodes for the next timestep. Energy balance equation is the conservation of energy (Energy stored= Delta Energy). Therefore, the temperatures can be calculated because there is the same number of equations as unknowns. Equation 4.10 represents the energy balance of centre node at Figure 4-4. The left side of the equation is the energy stored in the control volume at a timestep and the right side represents the energy transferred from or to the neighbouring nodes. Where C_p is the specific heat capacity and m the mass of the control volume.

$$\frac{m_{m,n} C_p \Delta T_{m,n}}{\Delta t} = \frac{\rho C_p \Delta x \Delta y W (T_{m,n}^{p+1} - T_{m,n}^p)}{\Delta t} = q_{m-1,n} + q_{m+1,n} + q_{m,n-1} + q_{m,n+1} \quad 4.10$$

There are two main methods to solve these equations, the explicit and implicit methods. The difference of these two methods is illustrated at equation 4.11. This equation represents the heat transferred from [m-1,n] node to [m,n] node, illustrated in Figure 4-4. The upper term in the right-hand side is explicit and the lower term is implicit. Consequently, the difference is that the right-hand side temperatures of equation 4.10 are from the previous timestep (known) if it is explicit and from the next timestep (unknown) if it is implicit. Where W is the width of the control volume

$$q_{m-1,n} = \begin{cases} \frac{k \Delta y W (T_{m-1,n}^p - T_{m,n}^p)}{\Delta x} & \text{Explicit} \\ \frac{k \Delta y W (T_{m-1,n}^{p+1} - T_{m,n}^{p+1})}{\Delta x} & \text{Implicit} \end{cases} \quad 4.11$$

The advantage for explicit method is that it offers computational conveniences compared to the implicit method. This is because the only unknown in the equations is the temperature of the node as opposed to implicit method where the unknowns are also neighbouring node temperatures. However, the explicit method has a limit of what Δt is chosen because the temperatures will be unstable and wrong if the limit is passed. In addition, due to this limit, there is a possibility that Δt must be very small with a consequence high computational time. Therefore, for this model the chosen method is implicit because low computational time is essential, and no limit will be necessary.

The energy balance equations are linear with one exception. The exception is the radiation because the temperatures are in the power of four as can be seen from equation 4.9. To eliminate this situation, the equation is transformed to equation 4.12.

$$q_{Rad} = \frac{A\sigma(T_1^2 + T_2^2)(T_1 + T_2)(\Delta T)}{\frac{1}{\varepsilon_1} + \frac{1}{\varepsilon_2} + \frac{1}{F_{12}} - 2} \quad 4.12$$

Where the temperature terms before ΔT are taken from the previous timestep. Therefore, the type of equations that must be resolved if the chosen method is implicit are illustrated at equation 4.13.

$$\begin{aligned} a_{11}T_1 + a_{12}T_2 + a_{13}T_3 + \dots + a_{1N}T_N &= C_1 \\ a_{21}T_1 + a_{22}T_2 + a_{23}T_3 + \dots + a_{2N}T_N &= C_2 \\ &\vdots \\ a_{N1}T_1 + a_{N2}T_2 + a_{N3}T_3 + \dots + a_{NN}T_N &= C_N \end{aligned} \quad 4.13$$

There are several methods of solving these equations, however the best method for this model is matrix inversion because the software used is MATLAB and it is very effective with the handling of matrices. To solve the equations with matrix inversion, the equations must be translated to matrix and vectors (4.14 & 4.15).

$$[A][T] = [C] \quad 4.14$$

$$A \equiv \begin{bmatrix} a_{11} & a_{12} & a_{13} & \dots & a_{1N} \\ a_{21} & a_{22} & a_{23} & \dots & a_{2N} \\ & & \cdot & & \\ & & \cdot & & \\ a_{N1} & a_{N2} & a_{N3} & \dots & a_{NN} \end{bmatrix} \quad T \equiv \begin{bmatrix} T_1 \\ T_2 \\ \cdot \\ \cdot \\ T_N \end{bmatrix} \quad C \equiv \begin{bmatrix} C_1 \\ C_2 \\ \cdot \\ \cdot \\ C_N \end{bmatrix} \quad 4.15$$

Then the inverse of matrix A can be easily calculated, and the equations can be solved (4.16, 4.17 and 4.18)

$$[T] = [A^{-1}][C] \quad 4.16$$

$$A^{-1} \equiv \begin{bmatrix} b_{11} & b_{12} & b_{13} & \dots & b_{1N} \\ b_{21} & b_{22} & b_{23} & \dots & b_{2N} \\ & & \cdot & & \\ & & \cdot & & \\ b_{N1} & b_{N2} & b_{N3} & \dots & b_{NN} \end{bmatrix} \quad 4.17$$

$$\begin{aligned} T_1 &= b_{11}C_1 + b_{12}C_2 + b_{13}C_3 + \dots + b_{1N}C_N \\ T_2 &= b_{21}C_1 + b_{22}C_2 + b_{23}C_3 + \dots + b_{2N}C_N \\ &\vdots \\ T_N &= b_{N1}C_1 + b_{N2}C_2 + b_{N3}C_3 + \dots + b_{NN}C_N \end{aligned} \quad 4.18$$

4.3.3 Thermal model approach

Before the explanation of the approach, the main criteria must be introduced. The first criterion is that distances between the nodes (Δx , Δy) are not constant throughout the whole system and change in respect of temperature gradients. This can be seen in the closeup of Figure 4-5.

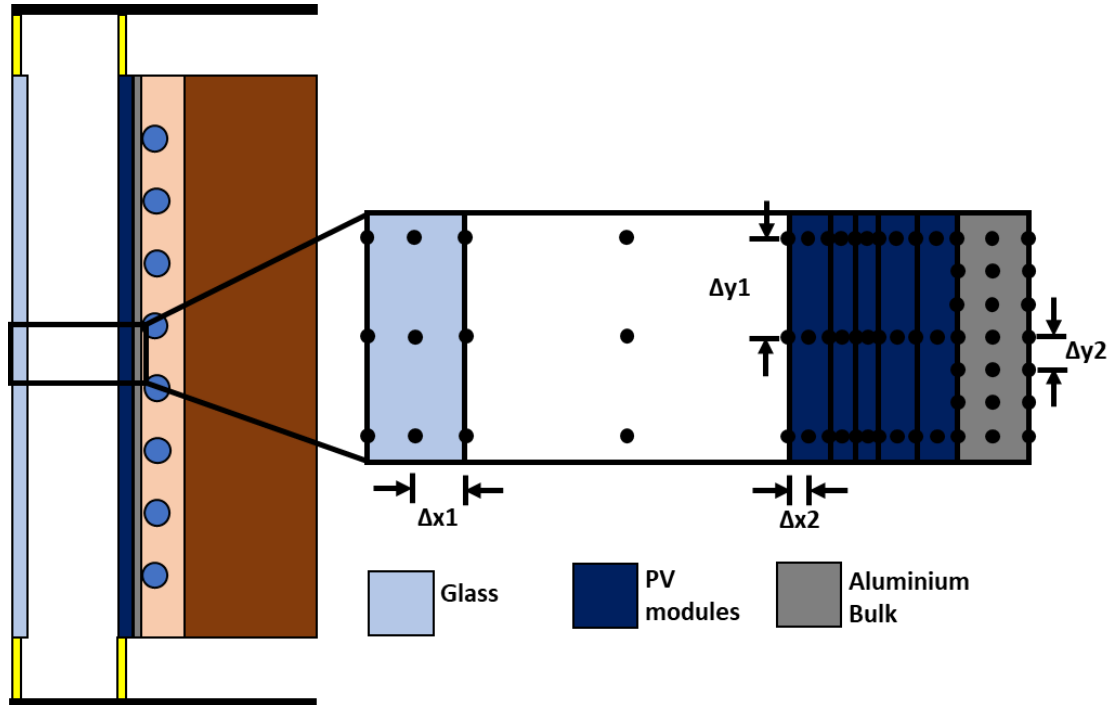


Figure 4-5 Focus on a small area of the water pipe design for the demonstration of flexible Δx and Δy

For example, Δx at PV module is magnitudes smaller than Δx at the front façade glass, because there are larger temperature gradients in the x-axis at the zone of PV modules rather than the zone of front glass. In addition, the Δy at the water-cooling system is smaller than the Δy at other areas of the system. The reason is that at the water-cooling system there are water pipes that are small and therefore the temperature gradients in the y-axis are high.

Another important criterion is that the dimensions of the model are only 2. It is assumed that in the x-axis (depth) and y-axis (height) (see figure) there are changes of temperature. In the x-axis the changes are because of the heat flow due to different temperatures of materials (For example PV modules and wall). In the y-axis the changes are because of the chimney effect and the water cooling. The temperatures of the air and water change in respect of height and therefore all the materials are influenced from these changes. However, it is assumed that in the z-axis (width) there are no temperature changes. This assumption is not going to influence the results because there are no important causes that change the temperature in the z-axis throughout time.

For the derivation of each node equation, two important conditions are considered. The first condition is the type of material. This condition is important because each material has different properties. The second condition is the type of node. Type of node is a title of each node that has different boundaries. For example, there are surface nodes, inside nodes, corner nodes and a lot more that are displayed in Figure 4-7.

Therefore, equations for each type of node are derived and then different factors are used depending from the material. For an easier formation of the code and better programming, numerous factors (Fourier, Biot and combinations) are used. An example of an equation derivation is shown below. The example represents a node inside the PV module which receives also heat from irradiance shown in Figure 4-6.

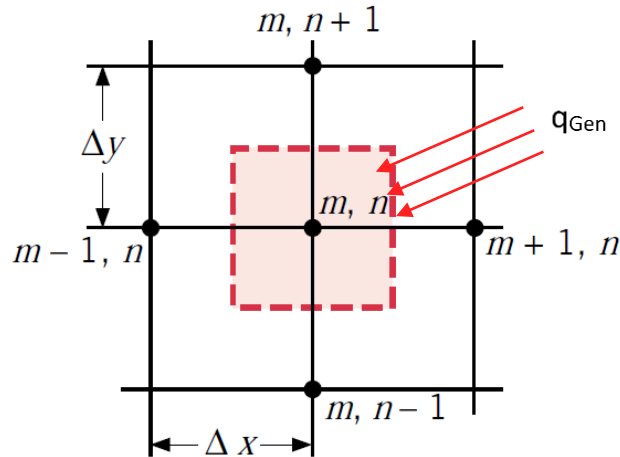


Figure 4-6 Example of a node inside the solar cell. This node has conduction with neighbouring nodes and is subjected to radiation from the sun [33]

The starting point is equation 4.10. Where each component is converted, and the result is equation 4.19. Where G_{PV} is the incident irradiance n_{el} the electrical efficiency and $refl$ the reflection coefficient

$$\begin{aligned} & \frac{\rho C_p \Delta x \Delta y W (T_{m,n}^{p+1} - T_{m,n}^p)}{\Delta t} \\ &= \frac{k \Delta y W (T_{m-1,n}^{p+1} - T_{m,n}^{p+1})}{\Delta x} + \frac{k \Delta y W (T_{m+1,n}^{p+1} - T_{m,n}^{p+1})}{\Delta x} \\ &+ \frac{k \Delta x W (T_{m,n-1}^{p+1} - T_{m,n}^{p+1})}{\Delta y} + \frac{k \Delta x W (T_{m,n+1}^{p+1} - T_{m,n}^{p+1})}{\Delta y} \\ &+ G_{PV} \Delta y W (1 - n_{el}) (1 - refl) \end{aligned} \quad 4.19$$

By introducing the factors needed (4.20) the equation is rewritten to equation 4.21. Where, α is the thermal diffusivity and Fo_x/Fo_y is the Fourier number.

$$a = \frac{k}{\rho C_p} \quad Fo_x = \frac{a \Delta t}{\Delta x^2} \quad Fo_y = \frac{a \Delta t}{\Delta y^2} \quad 4.20$$

$$\begin{aligned} T_{m,n}^{p+1} - T_{m,n}^p &= Fo_x (T_{m-1,n}^{p+1} - T_{m,n}^{p+1}) + Fo_x (T_{m+1,n}^{p+1} - T_{m,n}^{p+1}) + Fo_y (T_{m,n-1}^{p+1} - T_{m,n}^{p+1}) \\ &+ Fo_y (T_{m,n+1}^{p+1} - T_{m,n}^{p+1}) + \frac{G_{PV} (1 - n_{el}) (1 - refl) \Delta t}{\rho C_p \Delta x} \end{aligned} \quad 4.21$$

Continuing by rearranging the components of equation 4.21, the final version is equation 4.22.

$$\begin{aligned} (1 + 2Fo_x + 2Fo_y) T_{m,n}^{p+1} - Fo_x T_{m-1,n}^{p+1} - Fo_x T_{m+1,n}^{p+1} - Fo_y T_{m,n-1}^{p+1} - Fo_y T_{m,n+1}^{p+1} \\ = T_{m,n}^p + \frac{G_{PV} (1 - n_{el}) (1 - refl) \Delta t}{\rho C_p \Delta x} \end{aligned} \quad 4.22$$

The factors of each temperature in the left side are imported in the matrix A and the right side is imported in the vector c. The above derivation is the simplest and this is done for each type of node. Below you can see all the different types of nodes used in this model (Figure 4-7).

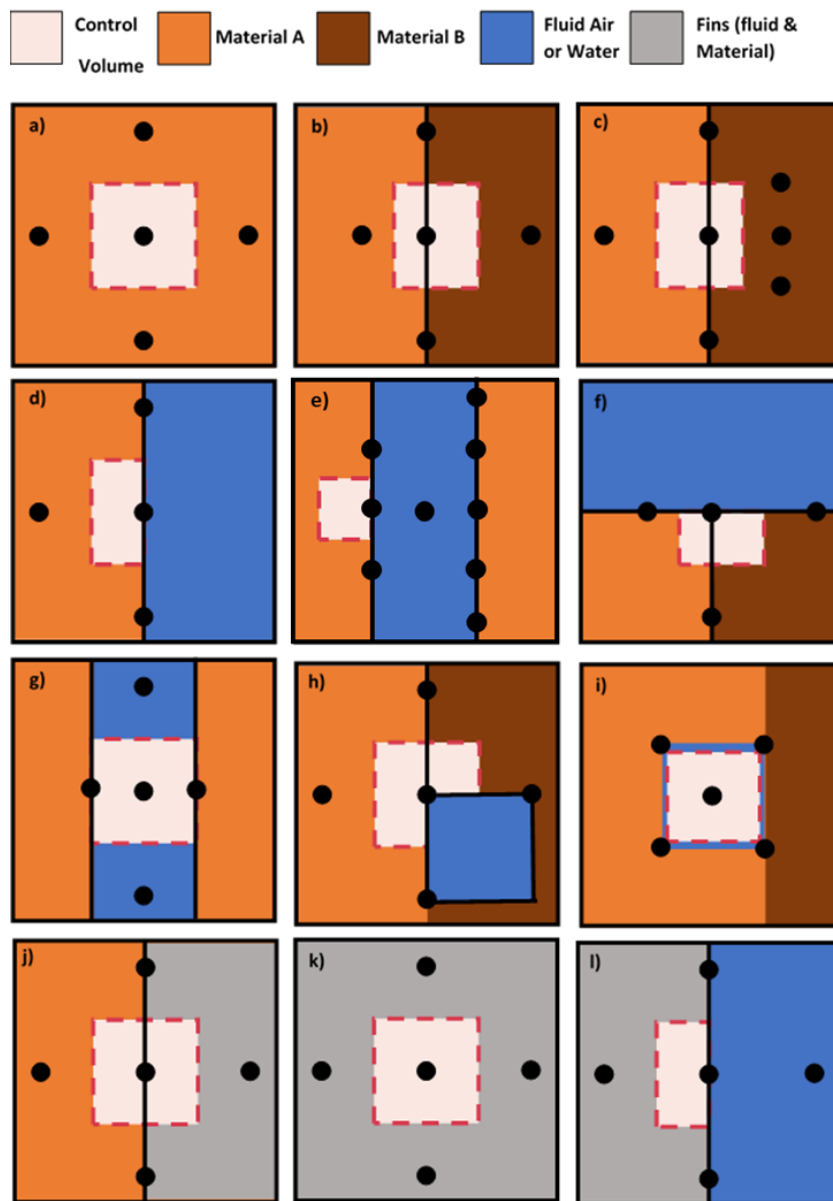


Figure 4-7 Type of nodes which have different equations. The nodes that are outside the control volume are affecting the node in the control volume. a) Node inside a material, b) Node in the intersection between two materials, c) Node in the intersection between two materials where material B has more dense nodes in the y-axis, d) Surface node facing the environment, e) Surface node facing the cavity (radiation with nodes in the other side), f) Node in the intersection between two materials which is also on a surface, g) Node inside the cavity, h) Water pipe corner node in the intersection of two materials, i) Node inside water pipe, j) Surface node in the cavity that also has conduction with the fins, k) Node inside the fins which are also have convection with the cavity. l) Surface node on fins.

4.3.4 Convection coefficients

Convection coefficients are significant parameters for this model because numerous materials are exposed to fluids (air or water). In addition, most of the type of nodes shown in Figure 4-7 are exposed

to a fluid (d, e, f, g, h, i, j, k and l). Therefore, there is no room for error and the convection coefficients must be accurate enough.

There are four convection coefficients in this model. There is the convection coefficient of the environment, the convection coefficient in the cavity at the hot side (PV modules), the convection coefficient in the cavity at the cold side (wall or glass) and the convection coefficient at the water pipes. All convection coefficients are averaged. The meaning of averaged is that all the nodes in the y-axis for an x, will have the same convection coefficients. Local coefficients would give more accurate results, but in the same time the computational time would substantially increase and therefore it will be implemented in future works.

The environment convection coefficient is taken from J. A. Palyvos et.al [34] where a thorough research was performed for the best convection coefficients of a facade. Two type of convection coefficients are used for the environment (equation 4.23). These convection coefficients are averaged from numerous equations derived from different publications. Where V_{Wind} is the velocity of the wind.

$$\bar{h}_{Env} = \begin{cases} 7.4 + 4.0V_{Wind} & \text{Windward} \\ 4.2 + 3.5V_{Wind} & \text{Leeward} \end{cases} \quad 4.23$$

To find out which of the two equations is used at a certain time, the wind direction must be known. Fortunately, Meteororm provides this information. Windward equation is applied when the angle of incidence between the direction of air with the normal of the façade is less than $\pm 90^\circ$. Leeward equation is applied when the angle of incidence is more than $\pm 90^\circ$. For example, if the systems normal is facing south, then, when the wind direction is in the north-east or north-west the windward equation is applied.

To find the convection coefficients inside the cavity it was quite a challenge because of lack of research in that field. Convection coefficients are directly proportional to the Nusselt number (Nu) as can be seen from equation 4.24.

$$\bar{h} = \frac{\overline{Nu}k}{L} \quad 4.24$$

Where k is the conduction coefficient of the fluid and L is the height of this material. The only unknown in equation 4.24 is the Nusselt number. The Nusselt number depends of dimensionless parameters. If the convection is forced, then the Nusselt number depends on the Reynolds and Prandtl number and if the convection is natural, then is derived from Rayleigh and Prandtl number.

As it was mentioned before, the literature for convection coefficient in cavity is limited and after a detailed research, it was concluded that convection for a vertical wall is going to be used. There are some publications that give convection coefficients for a cavity, but they are very limited in their boundaries. There are equations for symmetric isothermal plates, symmetric isoflux plates and adiabatic plates [35]. However, the case for this model is not in match with these boundaries. The reason is that the only surface that is heated is the surface with the PV modules and the other surface is heated in much lower levels (radiation from surface of PV modules and convection with hot air in the cavity). Therefore, the convection coefficients used for both surfaces (hot and cold) are well known and used equations for convection on vertical plates. For the heated area (PV module surface) there is natural convection and due to natural convection, there is air mass-flow parallel with the walls inside the cavity. Due to this mass-flow there is also forced convection at the other surface of the cavity. This other surface could be the wall if the design is with the fins or glass if the design is with water pipes.

The Nusselt number for the surface with the PV modules (natural convection) can be calculated from equation 4.25. [36]

$$\overline{Nu_{L_{Nat}}} = \left(0.825 + \frac{0.387 Ra_L^{1/6}}{(1 + (0.492/Pr)^{9/16})^{8/27}} \right)^2 \quad 4.25$$

Where Rayleigh (Ra_L) and Prandtl (Pr) number equations are 4.26 and 4.27 respectively.

$$Ra_L = \frac{g\beta(T_s - T_{air})L^3}{\nu a} \quad 4.26$$

$$Pr = \frac{\nu}{a} \quad 4.27$$

Where, g is the gravity and β is the volumetric thermal expansion coefficient. The Nusselt number for the surface of the wall or the glass (forced convection) is calculated from equation 4.28. [33]

$$\overline{Nu_{L_{For}}} = 0.664 Re_L^{1/2} Pr^{1/3} \quad 4.28$$

Where Reynolds number (Re_L) equation is equation 4.29.

$$Re_L = \frac{(\dot{m}_{air}/X_{cav}W_{cav}\rho)H}{\nu} \quad 4.29$$

Where, m_{air} is the air mass flow, X and W_{cav} are the cross-section dimensions of the cavity and H is the height of the cavity. For the water convection coefficient, an internal flow equation had to be considered. The pipes are assumed to have a circular cross section even though in the simulation of the pipes have square cross section for computational convenience (see Figure 4-7 h and i). The Nusselt equation used is 4.30 and the Reynolds number (Re_D) for this equation is calculated from equation 4.31. [37]

$$\overline{Nu_{LW}} = 3.66 + \frac{0.0668(D/L)Re_D Pr}{1 + 0.04((D/L)Re_D Pr)^{2/3}} \quad 4.30$$

$$Re_D = \frac{\dot{m}_{water}}{\mu \Delta y_{water}} \quad 4.31$$

Where, D and Δy_{water} are the diameter of the water pipe, L the length of the pipe and m_{water} is the water mass-flow. The calculation of the convection coefficients is determined for every timestep. The reason is that, the parameters that affect the Nusselt number are changing for every timestep. For example, the temperature difference of PV modules and air inside the cavity are affecting the Rayleigh number. In addition, the mass-flow of air inside the cavity and water affect the Reynolds of water and air respectively.

4.3.5 View factor of radiation

View factor is a percentage of radiation that travels to another surface or sky/ground. For the designs used, there are three surfaces that have radiation. The first is the surface which faces the environment and the other two are the surfaces in the cavity.

Starting with the surface facing the environment, the calculations of the view factor for each node are relatively easy. The reason is that the surface is always vertical with respect to the ground. Therefore,

half of the radiation is exchanged with the sky and the other half with the ground. The reason is because, the radiation is diffused, and the intensity is uniform

To find the view factor of each node at the surfaces in the cavity is more complex. This is because the node is exchanging radiation with more than one node at the opposite surface and the view factor for each node is different as can be seen from Figure 4-8.

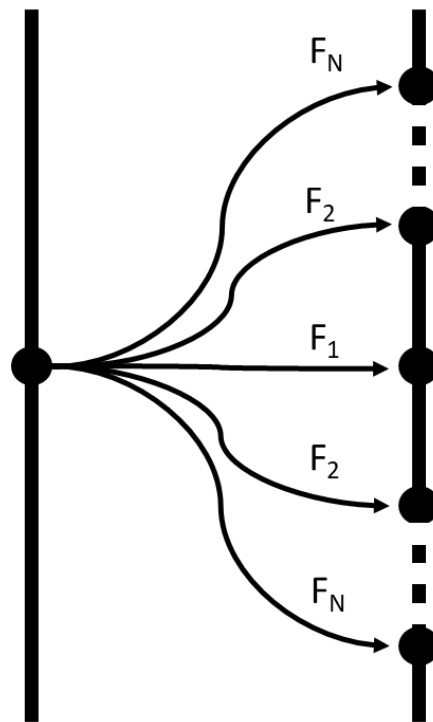


Figure 4-8 View factor of the cavity surface node and nodes on the other side.

M. Isidoro [38] developed an equation for the view factor of long surfaces for very small areas dA_1 and dA_2 as shown in Figure 4-9-a. However, for the model used, there is no third dimension and therefore dA_1 and dA_2 are becoming the whole area of the long surfaces. Figure 4-9-b also illustrates the nodes of the model.

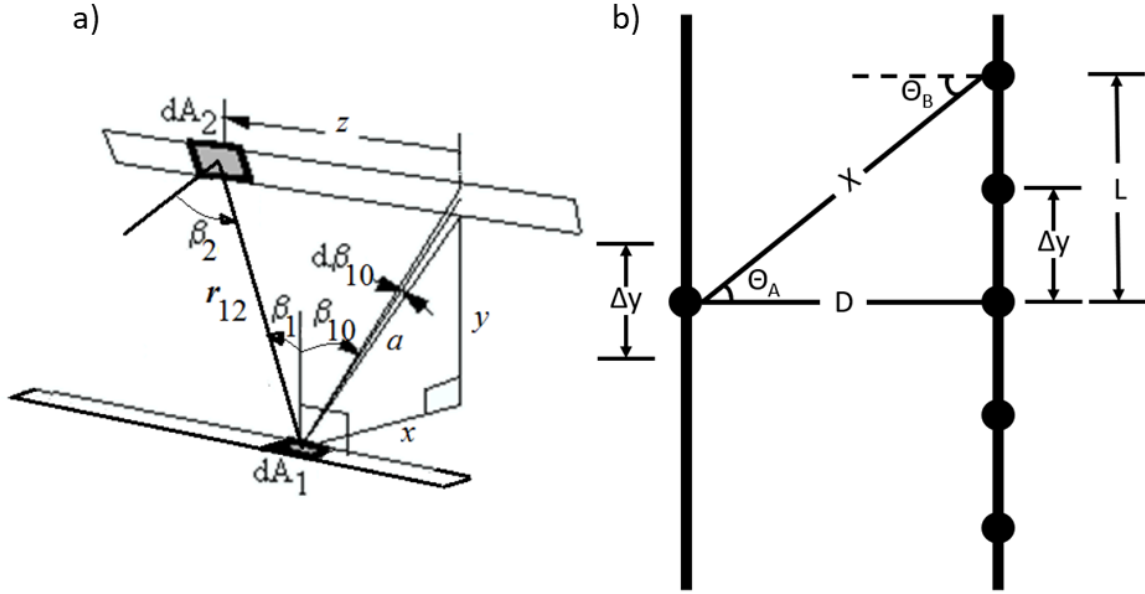


Figure 4-9 a) Schematic of two long narrow surfaces that exchange radiation in 3D [38] b) Translation of the schematic to the design used for this model in 2D

The equation taken from M. Isidoro [38] is 4.32 where the parameters are shown in Figure 4-9-b

$$F = \frac{\cos(\theta_A) \cos(\theta_B) \Delta y}{2X} \quad 4.32$$

The factor Δy shown in the equation above represents the height of the node's control volume and D the depth of the cavity. By replacing the unknown factors with the equations 4.33-4.35

$$\cos(\theta_A) = \cos(\theta_B) = \frac{D}{X} \quad 4.33$$

$$X = \sqrt{D^2 + L^2} \quad 4.34$$

$$L = n\Delta y \quad 4.35$$

the equation rearranges to 4.36 which is the final.

$$F = \frac{D^2 \Delta y}{2(D^2 + (n\Delta y)^2)^{3/2}} \quad 4.36$$

Where, n is the absolute difference of the y-axis digit between the two nodes exchanging the radiation. For example, in Figure 4-9-b, n is equal to 2.

The equation derived above has the assumption that there is no radiation escape to the sky from the sides of the cavity. The reason is that the equation is correct for infinite long surfaces. However, because the depth/width ratio of the cavity is very small there is no important error. Worth mentioning, is that there is view factor for all the nodes in the opposite surface if the above equation is applied. Therefore, there is a limit in the model which exchanges radiation with nodes until the view factor will reach 99% (Usually no more than 10 nodes). In addition, if the node is near the ceiling or ground of the system, then a percentage is exchanged with the sky.

For better understanding, Table 4-1 displays the view factors for the neighbouring nodes when Δy is 0.15m and the depth (D) is also 0.15m. Except the view factor F_1 which is in the same height as the inspected node, the other view factors are implemented to two nodes mirrored between F_1 due to symmetry (see Figure 4-8).

Table 4-1 View factors for $\Delta y=0.15m$ and $D=0.15m$

F_1	F_2	F_3	F_4	F_5	F_6	F_{All}
0.5	0.177	0.045	0.016	0.007	0.003	0.996

Worth mentioning, is that if the Δy is very big (0.5m), then there is a possibility of view factor more than 1 for F_1 . Therefore, a limit is put to view factor equal to 1 if this is the case, and the node is exchanging all the radiation only with the opposite node.

4.4 Air mass-flow model choice

The aim of a solar chimney is to create air mass flow for ventilation and heating of a building. Due to the heat of a high absorptive material inside or in the front of the solar chimney (in this case PV modules), also the air inside the solar chimney is heated. Consequently, there is density difference between the air inside the solar chimney and the air in the outlet. This density difference is creating buoyancy forces which are acting on the air particles inside the chimney and therefore movement is generated.

There are several publications for a solar chimney models [10]. However, the chosen model is taken from [39]. In this article, three mass-flow models for a solar chimney were explained and compared. These three models are, single zone model, stratification model and plume model and they are illustrated in Figure 4-10.

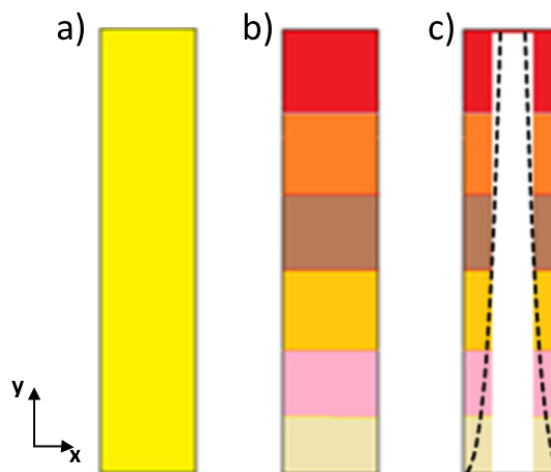


Figure 4-10 Different methods of solar chimney model. a) Single zone model, b) Stratified method c) plume model [39]

In the single zone model (Figure 4-10-a) it is assumed that the temperature inside the cavity is uniform and there is no variation with height. In the stratified model it is assumed that the temperature changes throughout the height as can be also seen from Figure 4-10-b. Lastly in the plume model a

boundary layer is also taken into account and therefore there is also variation of temperature in the x direction (alongside the cavity).

Ortiz Lizcano et.al [7] chose the plume model because it is the most accurate and can provide the optimum depth inside the solar chimney. However, the plume model needs more computational time compared to the other models because iterations must be established at each time step for the calculation of the discharge coefficient (C_d). In addition, if the mass-flow inside the cavity is relatively high (0.05kg/s and above) the boundary is eliminated because the air becomes turbulent and therefore the plume model is becoming the stratified model.

Figure 4-11 provides results for the comparison between the models and experimental results. For low mass flows (Figure 4-11-a) the plume model has the least error, while the stratified and single zone models have large deviations and overpredict the mass flow. However, for high mass flows (b) the stratified model performs very well with very small deviations. It can also be seen that the plume model underpredicts the mass flow, but with provided correction factors these errors can be eliminated.

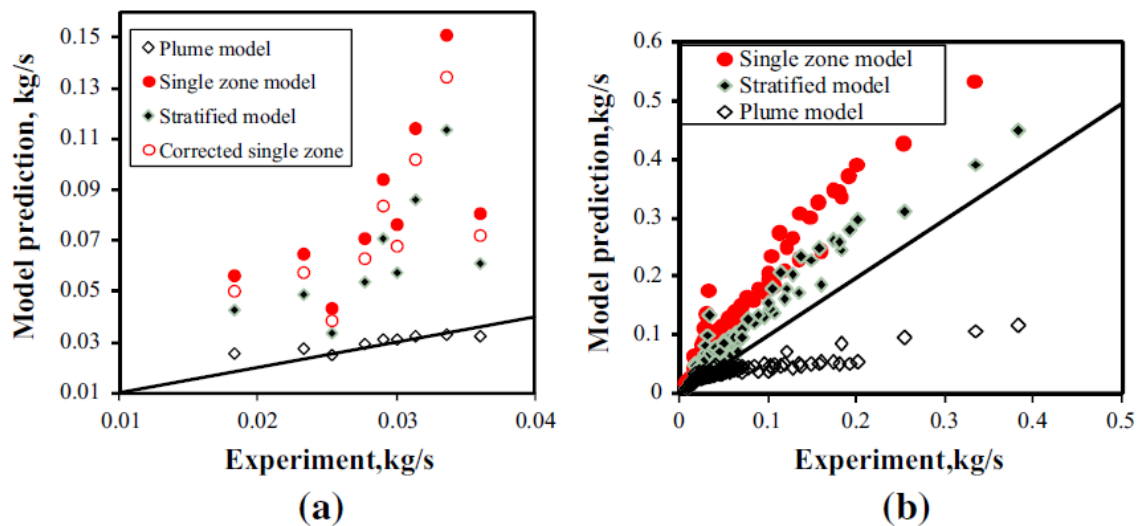


Figure 4-11 Comparison of models with experimental results. a) Experiment for low mass flows b) Experiments with high mass flows.

Considering the results presented in [7], the air change per hour (ACH) is 78% of the time in a year more than 2. The mass flow of ACH equal to 2 for the chosen reference room (720m³) is 0.49kg/s which is very high. Therefore, the stratified model is chosen because is accurate for high mass flows and needs less computational time than the plume model. One drawback is that with the stratified model is impossible to get optimum depth results. However, [7] the authors already calculated the optimum depth (0.2m) and it will be taken as reference.

Therefore, to find the mass-flow for each time step, equation 4.37 is used.

$$\dot{m}_{air} = C_d \rho_i A \sqrt{\frac{2gH(T_i - T_r)}{T_i}} \quad 4.37$$

Where the lower-case letter i represents the average properties of the air inside the cavity and r represents the properties of the referenced air entering the cavity (environment or building). For the calculation of the density inside the cavity equation 4.38 was used.

$$\rho_i = \frac{\rho_r T_r}{T_H - T_r} \ln\left(\frac{T_H}{T_r}\right) \quad 4.38$$

Where T_H is the temperature in the outlet of the cavity. Worth mentioning also is that the discharge coefficient (C_D) which depends on the overall friction of the cavity is most of the times in between 0.56-0.8 and therefore a number in that range is taken.

4.5 Electrical model

The electrical model is an important parameter for the accuracy of the overall model. Fortunately, Andres Calcabrini (PVMD group of TU Delft) provided an electrical model which is based on the two-diode model. This model can provide in great accuracy the I-V curves of a cell (or a module) for different combinations of temperature and absorbed irradiance.

This is very important because the temperature change influences in great matter the voltage. As the temperature increases, the open circuit voltage (V_{OC}) of the cell decreases and the short circuit current (I_{SC}) increases by a smaller factor. In addition, the irradiance mostly affects the I_{SC} . When the irradiance is increasing, the I_{SC} is increasing but also the V_{OC} is increasing in a smaller factor. Lastly, the fill factor is also affected by the temperature and irradiance. Therefore, the maximum power point is affected by these two parameters and consequently the electrical power [30]. The maximum power point is the point in the IV-curve where the maximum electrical power can be generated. The effects of temperature and irradiance on IV curves are illustrated in Figure 4-12.

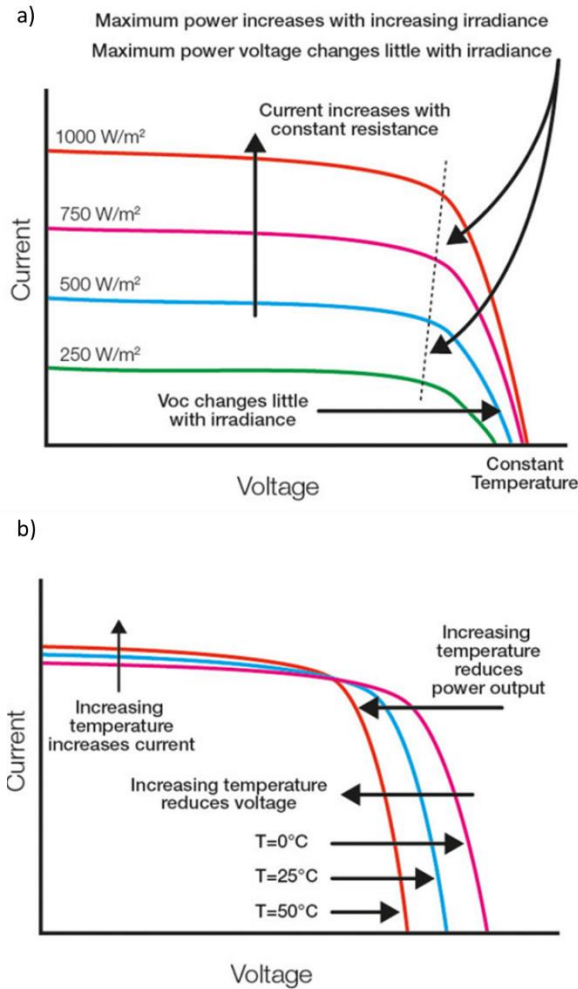


Figure 4-12 IV-curve of a cell and the effect of a)irradiance and b)temperature[40]

After extracting all the IV-curves for each combination of temperature and irradiance, the maximum power point of each configuration is taken. As a result, a 2D table is created with the power density for each absorbed irradiance and temperature configuration. This table then is imported in the model, and for each timestep the electrical power of the system is determined. Therefore, there is a correction and recalculation of the efficiency for each timestep.

4.6 Water tank model

The water tank is an important component in the water pipe design. It is essential to develop an accurate model for it. After an extensive research it was decided that, a similar as the one used by R. Santbergen [28] will be considered. This approach was taken from E. M. Kleinbach et.al [26] which provides three different methods for a storage tank model. The name of the method taken is stratified storage tank model.

Stratified storage tank model is a method to calculate the temperatures of a storage tank that provides water to the system and to the load. Because there is stratification in the storage tank, it must be divided into several volumes. The stratification is occurred because there are different levels of

temperatures in the tank with lower temperatures at the bottom and higher temperatures at the top. Consequently, it is a wrong approach to take one temperature for the whole tank. For this model the storage tank is divided into three volumes as can be seen from Figure 4-13(Top, Middle and Bottom). Three volumes will give a good estimation of the water tank average temperature. One disadvantage of this method as opposed to the other methods, is that it does not consider mixing of the temperatures due to turbulence. Nevertheless, is a suitable approach.

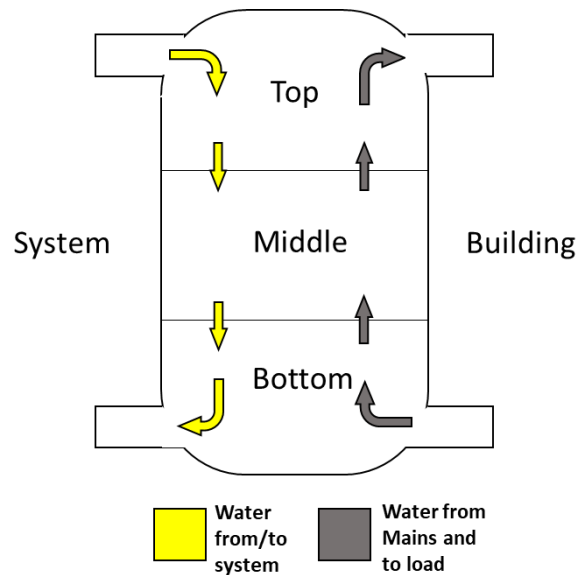


Figure 4-13 Storage water tank. The tilted arrows represent the mass flow coming and leaving from the tank and the straight arrows represent the mass flow movement between the volumes

The calculation of the temperature at each volume for each timestep in the simulation, is similar to the calculations of the temperatures for the system nodes which is explained in chapter 4.3.3. Every volume has an energy balance equation which depends on the boundaries and the neighbouring volumes.

However, there is a complexity with the inputs and outputs of water coming from the system and from the mains. When the temperature passes through the system and is heated up, then it is returning to the water tank (look yellow arrow Figure 4-13). But, if the temperature is not higher than the temperature of the Top volume, then it is stored either in the Middle volume or in the Bottom volume. Similarly, when the temperature coming from mains (look grey arrow Figure 4-13) is lower than the temperature of the Bottom volume then it will be stored either in the Middle volume or the Top volume. Consequently, the input water mass-flows are stored to a volume with the nearest temperature.

Another complexity of this model is that conservation of mass must be considered. This means that if input water mass-flow is stored in one of the volumes then water from this volume will move to the neighbouring volume (straight arrows Figure 4-13). Similarly, if water mass-flow is extracted from a volume either to the system or to the load, then mass-flow will come from a neighbouring volume. This leads to energy moved to another volume. The equation used for each node is 4.39.

$$\frac{m_{Volume} C_{p_{water}} \Delta T_{Volume}}{\Delta t} = Energy\ in - Energy\ out \pm Convection \quad 4.39$$

Where energy in and energy out are related to the mass-flows entering and leaving the volume and convection is happening with the environment outside of the tank.

The storage tank, load profile and water mass-flow that goes to the system are related to the systems scale (PV modules area).Worth mentioning, is that the equations of the approach where derived with the explicit method from E. M. Kleinbach et.al [26], and therefore they are adapted to the implicit method used in this model.

4.7 Energy yield model

4.7.1 Electrical energies

There are two electrical energies that are consider in this model. The electrical energy extracted from the PV modules is the main because it is used in both designs. In addition, if the design is with water pipes then there is also the electrical energy needed for the pump.

To calculate the electrical energy yield it is a simple process. The power density (P_{PV}) calculated from the electrical model is saved for each timestep and multiplied by the area (A) taken from the PV modules. Then the energy for each step is calculated by multiplying the power with the time (Δt) of each timestep. Lastly all the timestep energies are added for the calculation of the yearly electrical energy yield. However, if the design is with water pipes, then the energy needed for the water pump (E_{pump}) is removed from the PV modules energy. This assumption was considered so the system will provide results for energy that can be used outside of the system. Equation 4.40 represents the energy yield (E_{PV}) for the simulated period.

$$E_{PV} = \sum_{i=1}^{timesteps} P_{PV}^i A \Delta t - E_{pump} \quad 4.40$$

To calculate the energy needed from the pump, the hydraulic power equation was considered [41]. The hydraulic power depends on the height difference of the water transfer, from the mass-flow and from the friction of the pipes. Because it is assumed that the water is leaving and entering the same water tank, there is no dependence from the height. Therefore, only friction and water mass-flow are considered for the calculation of the hydraulic power as can be seen from equation 4.41.

$$P_{Pump\ Hydraulic} = m_{water} \dot{g} Head \quad 4.41$$

Where $Head$, is calculated from the friction of the pipe and is derived from the overall loss coefficient (K_{All}) and the velocity of the water: the overall loss coefficient relates to three factors. The length of the pipe, the inlets/outlets types and the type/number of bends in the system. The equations of the Head and loss coefficients are 4.42 and 4.43 respectively.

$$Head = \frac{K_{All} V_w^2}{2g} \quad 4.42$$

$$K_{All} = K_{Pipe} + K_{Inlet} + K_{Outlet} + K_{Bend} \quad 4.43$$

The inlet/outlet (K_{Inlet} and K_{Outlet}) and bend loss (K_{Bend}) coefficients are taken from literature [41]. For the bends, loss coefficient for 90° bend is considered. Although, this loss coefficient is multiplied with the number of bends in the system which are related to the height of it. There are two 90° bends every

0.1 meters height at the system. Therefore, if the system height is 10 meters then the bend loss coefficient is multiplied by 200.

The loss coefficient of pipe length (K_{pipe}) is given by the friction coefficient (f), the length (L_{pipe}) and the diameter (D_{pipe}) of the pipe as can be seen from equation 4.44.

$$K_{pipe} = \frac{fL_{pipe}}{D_{pipe}} \quad 4.44$$

Where the friction coefficient is depended from the roughness (r), diameter of the pipe and the Reynolds number (Re) of the water (equation 4.45).

$$f = \frac{0.25}{\left(\log\left(\frac{r}{3.7D_w} + \frac{5.74}{Re^{0.9}}\right)\right)^2} \quad 4.45$$

After calculating the hydraulic power, the mechanical and electrical losses (n_{mech} and n_{el}) are considered for the calculation of the required electrical power (equation 4.46). Then a similar approach as the electrical energy from PV is taken to calculate the electrical energy yield of the pump. Therefore, the overall equation for the energy yield needed for the water pump is defined 4.47.

$$P_{pump} = \frac{P_{pump\ Hydraulic}}{n_{mech}n_{el}} \quad 4.46$$

$$E_{pump} = \sum_{i=1}^{timesteps} P_{pump}^i \Delta t \quad 4.47$$

4.7.2 Thermal energies

Because of the configuration of the system, there will be also thermal energy coming from the air in the solar chimney for both designs. However, there is also thermal energy coming from water if the design is with the water pipes.

For the calculation of thermal energy of air, the inlet and outlet temperature difference of the air inside the cavity is considered ($T_{air\ outlet}$ and $T_{air\ inlet}$). In addition, because of the door opening strategy, there is a possibility of having temperature difference, but the thermal energy is not utilised (see Figure 3-3-c). Therefore, thermal energy of air is modified with regards of the type of door openings. The statement is, if the building door in the top of the system is open then there is thermal energy and if not, the thermal energy is zero. The equation that gives the thermal energy of air is 4.48.

$$E_{Air} = \sum_{i=1}^{timesteps} \dot{m}_{air}^i C_{p_{air}} \Delta t (T_{air\ outlet}^i - T_{air\ inlet}^i) Door_{status}^i \quad 4.48$$

For the calculation of water thermal energy, the same approach is taken. However, there is no additional term for strategy as before, because the strategy of water is already implemented in the water mass-flow (see equation 4.49).

$$E_{water} = \sum_{i=1}^{timesteps} \dot{m}_{water}^i C_{p_{water}} \Delta t (T_{water\ outlet}^i - T_{water\ inlet}^i) \quad 4.49$$

5 Results and discussion

5.1 Introduction

5.1.1 General description of results

The configurations introduced in chapter 3.1, will be also compared with the same designs but without the thermal systems. This means without the water pipe system and without the fins. These designs and their configuration are illustrated in Figure A 1 located in the appendices. With this comparison, the advantages (or disadvantages) of each thermal system will be clearer. The four design names are Water pipes (Figure 3-1-a), No water pipes (Figure A 1-a), Fins (Figure 3-1-c) and No fins (Figure A 1-c).

The results are divided into two sections. The one section is extreme weather conditions scenario results and the other section is yearly results. The scenario results are illustrated in a three-day period and the scenario day is in the middle (second). Both sections focus more on the water pipe configuration because of the additional results (water temperatures/thermal energies). However, all the configurations are compared between them in respect of energy, temperatures and strategies.

Worth mentioning is that the calculated energy of the water pump is relatively very small compared to the energy extracted from the PV modules for the water pipe system. More precisely the yearly energy yield of the pump is less than 0.5% fraction of the yearly energy yield of the PV modules. Therefore, the pump energy is excluded from the plots. The low energy consumption of the water pump was also discovered from other PV/T solar collector simulations in other publications [42]. Therefore, this hypothesis is expected to be valid. However, a more thorough look for the pipe diameter in respect of water mass flow is recommended for future work

5.1.2 Main Inputs and parameters

The model software is developed in such a way that everything is reconfigurable and can be changed easily from the user. However, for the results of this thesis, the parameters and inputs are introduced in the tables below. Table 5-1 shows the main inputs of the system and the location which is Delft, Netherlands. This location is ideal for solar chimney PV/T configuration due to the weather conditions. Table 5-2 provides the thermal properties and thickness about the PV and non-PV materials that are used. Table 5-3 provides the main information about the thermal systems (fins and water pipes). Worth mentioning is that the fin inputs are not optimized. The reason is that to optimize the fins, a new mass flow model must be developed because the fins influence the friction inside the cavity. However, this is not the aim of this thesis and it is recommended for future work. Table 5-4 shows the chosen accuracies for the two result sections. The Δx depends on each material and the number of x-nodes it has. For example, all the PV materials have each 3-xnodes, but the front glass and wall have each 5 x-nodes. Therefore, the smallest Δx 's are located at the PV materials due to their small thicknesses. In addition, the number of nodes for each configuration are shown. This number also represents the number of equations that must be resolved for each timestep. Lastly from the electrical model, a 2D matrix was extracted which calculates the electrical power of the chosen modules (see Table 5-5) in respect of their temperature and absorbed irradiance (see Figure 5-1).

Table 5-1 Inputs and system dimensions

Location	Delft, Netherlands
Orientation	South
Weather data	Meteonorm TMY
Height [m]	10
Width [m]	1
Depth [m]	0.2

Table 5-2 Materials, thermal properties and thicknesses[43][7][28]

PV Materials	PV glass	EVA1	C-si	Al	EVA2	Tedlar
k [W/mK]	1.8	0.32	149	237	0.32	0.56
ρ [kg/m³]	2700	960	2300	2700	960	1370
C_p [J/kgK]	750	2090	838	900	2090	1176
Thickness[mm]	4	1	0.16	0.1	1	1
Other materials	Front glass	Wall (brick masonry & insulation)	Insulation	Aluminium bulk		
k [W/mK]	1.58	0.61	0.038	237		
ρ [kg/m³]	2700	1922	2100	2700		
C_p [J/kgK]	750	900	160	900		
Thickness[cm]	2	20	5	1		

Table 5-3 Fin and water pipe design parameters

Fin Design			
Number of fins	Fin thickness [cm]	Fin height [cm]	Material
90	0.5	2	Aluminium
Water pipe design			
Diameter of pipe [cm]	Distance between pipes [cm]	Number of bends	Water Tank volume[L]
2	10	200	1000

Table 5-4 Accuracy parameters

Accuracy parameters		Scenarios	Yearly
Δt[s]		900	3600
Δy[m]		0.25	0.50
Δy near pipes[m]		0.02	0.02
Δx		Different for each material	
Number of Nodes	Water pipes	3257	2879
	Fins	1025	525
	No water pipes	943	483
	No Fins	779	399

Table 5-5 General information about the PV modules

Cell type	C-Si with surface texturing and optimized anti reflection coating
Cell Area [cm²]	253
Cell thickness [mm]	7.26
Configuration of module	4x4 in series

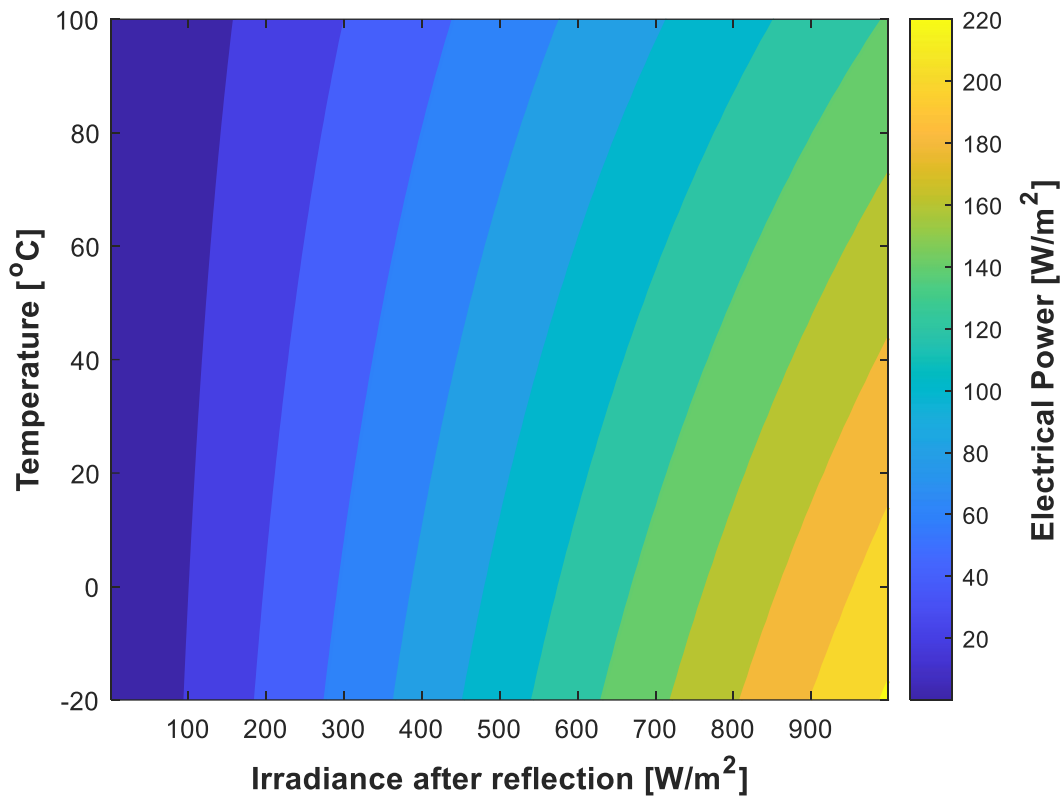


Figure 5-1 Electrical power density in respect of absorbed irradiance and temperature of the cell

5.2 Yearly results

5.2.1 Energies

This chapter provides information about the yearly results of the four designs. Figure 5-2 illustrates the monthly energy yields of the Water pipe design compared to the monthly Irradiance on the system. The thermal energy of water is the highest for all the months electricity being the second. The thermal energy of the air is almost negligible compared to the other energies and it is occurring mainly in summer. In addition, most of the irradiance is utilised due to the high energy extracted from the water.

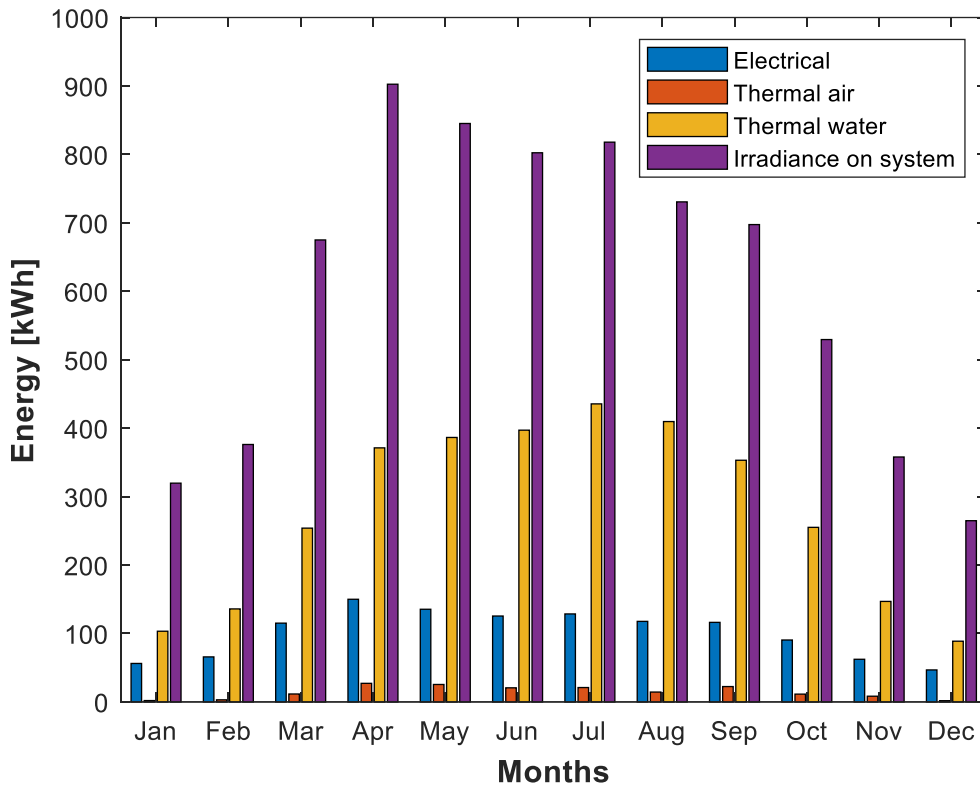


Figure 5-2 Monthly Irradiance on the system and energies of water pipe design for a year

Figure 5-3 compares the monthly electrical energy gained from each configuration. Fins design generates the most electrical energy each month. The electrical energy of Fins design is slightly higher from the No fins design since Fins design has lower temperatures at the cells (Figure 5-10) and consequently higher efficiency. Water pipe and No water pipe designs provide lower electrical energy than Fins and No fins designs because of the additional reflection losses occurring from the front glass of the system. Lastly, the Water pipe design provides more electrical energy compared to the No water pipe design even though a fraction of energy is taken from the water pump. The reason is that the temperature of the No water pipes design cells is overall much higher than the Water pipe design cell temperatures.

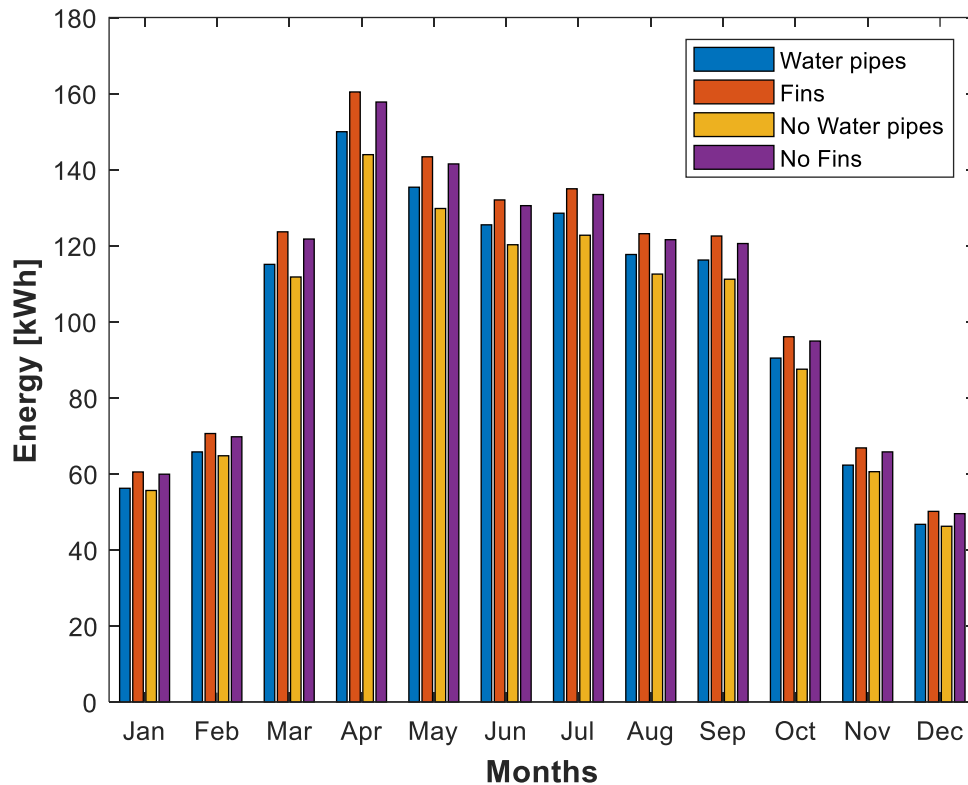


Figure 5-3 Monthly electrical energies of each configuration for a year

Figure 5-4 provides the monthly thermal energies of air for each configuration. The air thermal energies are relatively high, and this is thanks to the door openings strategy, where there is thermal energy usage also when the ambient temperature is low. The thermal energy of the No water pipes design is magnitudes larger than the thermal energies of the other configurations. The reason is that the PV modules provide most of their thermal energy to the air inside the cavity as opposed to the other configurations that provide a fraction of thermal energy to the environment (Fins and No fins) or to the water (Water pipes design). In addition, the thermal energy gained from Fins design is almost double the amount compared to the No fins design in the summer. The reason is that more thermal energy is provided inside the cavity because of the fins. Worth mentioning is that the thermal energy of Water pipes design is slightly higher than the thermal energy of Fins in the winter but is magnitudes smaller in the summer.

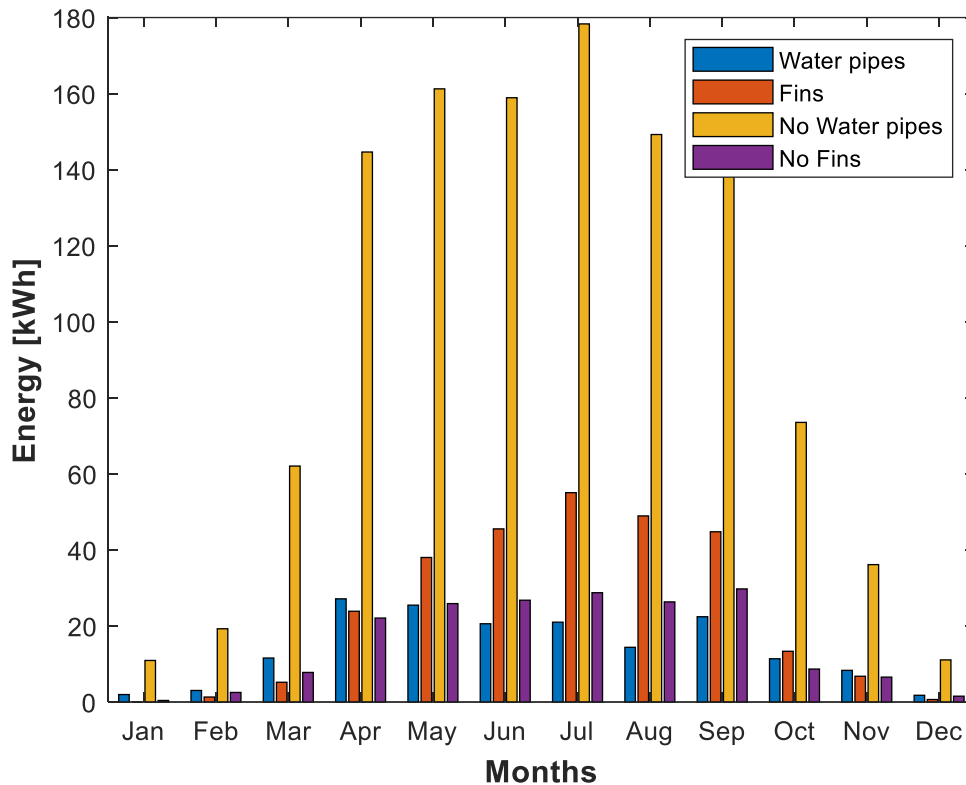


Figure 5-4 Monthly air thermal energies of each configuration for a year

Table 5-6 provides information about the yearly energy yields for each configuration. The best electrical performance is given by the Fins design, the best air-thermal performance is given by the No water pipes design and the best thermal energy of water performance is given by the Water pipes design (The only one with this energy). Overall, the best performance is given by the Water pipes design due to the high thermal energy that water provides.

Table 5-6 Yearly electrical and thermal energy yields with the highest energies highlighted.

Designs	Electrical [kWh]	Air thermal [kWh]	Water Thermal[kWh]	Overall [kWh]
Water pipes	1203	169	3336	4708
Fins	1284	283	-	1567
No water pipes	1168	1147	-	2315
No fins	1267	187	-	1454

5.2.2 Ventilation

The chose designs can also provide ventilation if the air in the cavity enters from the environment and exits into the building. However, this door opening strategy has as a condition for the temperature of the environment to be higher than the temperature of the room (explanation in chapter 3.3.1). Therefore, the most ventilation is occurring in the summer (see Figure 5-5). Figure 5-6 is a zoom-in of Figure 5-5 during the summer for better clarification of the differences between each configuration. The No water pipes design has higher daily ventilation than the other configurations because the temperature of the air inside the cavity is higher due to the high temperature of the cells(Figure 5-10) and therefore more mass flow is occurring. Worth mentioning is that the daily ventilation of Fins design is higher than the No fins design because more thermal energy is provided to the air inside the cavity and therefore more mass flow is created. Table 5-7 provides information about the yearly

ventilation in metric tonnes. The highest yearly ventilation is occurring from the No water pipes system and the second highest from Fins design. Lastly, if the ventilation is zero it does not mean that there is no heating because the inlet air to the cavity might be from the building, forming a closed loop.

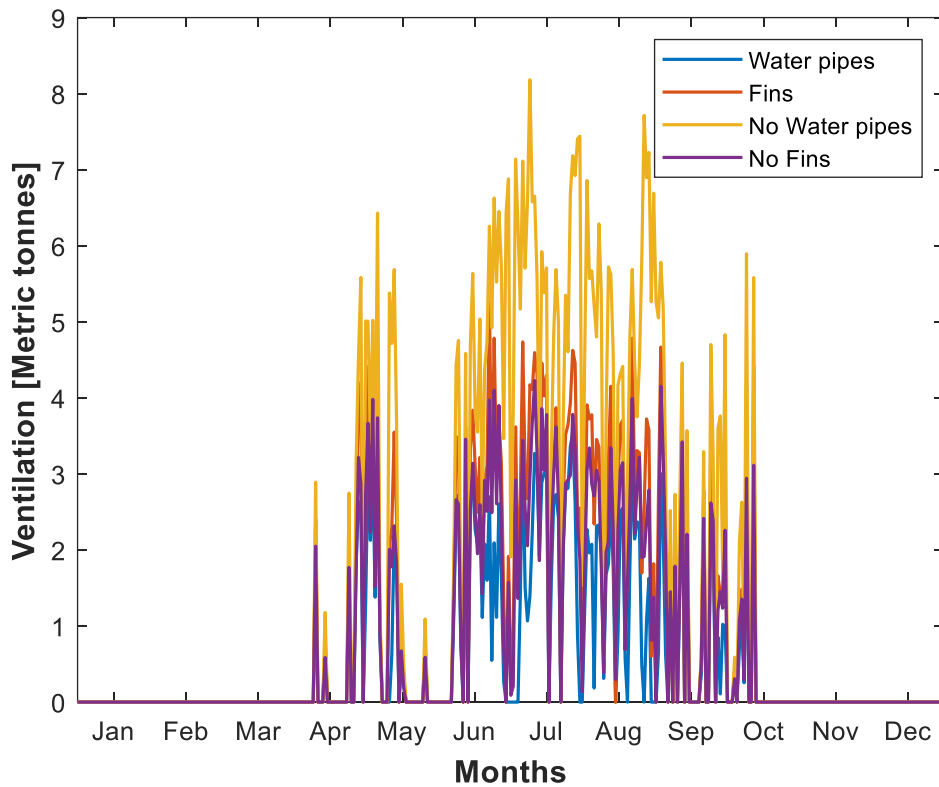


Figure 5-5 Daily ventilation of four configurations for a year

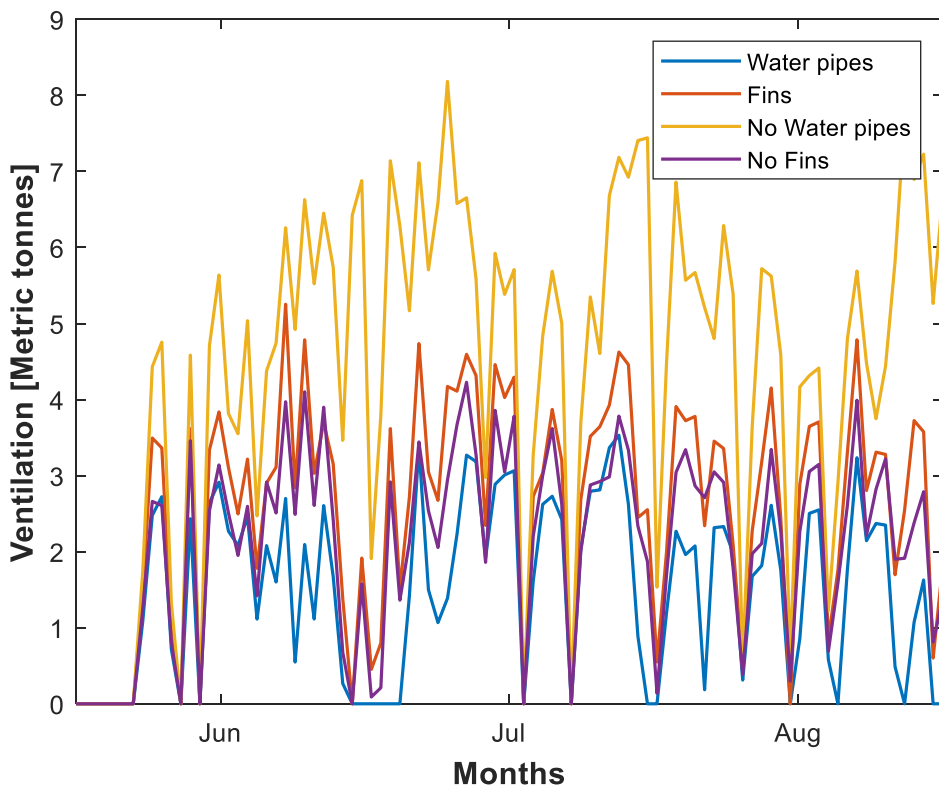


Figure 5-6 Daily ventilation of four configurations for three months in the summer

Table 5-7 Yearly ventilation of air with the highest ventilation highlighted

	Water pipes	Fins	No water pipes	No fins
Ventilation [Metric tonnes]	204	343	564	281

5.2.3 Efficiencies

The efficiency of the system can determine how much of the irradiance is utilised from each energy. Starting with the water pipe design, Figure 5-7 demonstrates the daily efficiencies of electricity, thermal energy of air and thermal energy of water in respect of solar energy subjected on the system. The highest efficiency is from the water thermal energy which was expected due to the high heat capacity and density of the water. In addition, there are several days where the water thermal energy efficiency is very high and reaches or even surpasses the 100%. There are two scenarios for this unusual situation. The first scenario is a situation where there is no high irradiance for a day but at the previous day the irradiance was high. Therefore, thermal energy was stored in the PV modules and was extracted slowly from the water passing from behind with a consequence this gain of energy to continue after midnight which is the next day. Subsequently, the thermal energy taken from the previous day is compared to the solar energy of the current day. The second scenario is that there is very high temperature but not high irradiance. Because the temperature of the water that comes from the mains is assumed to be always 10°C, there is a possibility that thermal energy of water is gained from the high ambient temperatures and not from the solar energy. The second scenario is a bias to the simulation and therefore it is recommended for future work to implement a variable temperature of the water that comes from the mains. Most probably the temperature of the water coming from the mains is heavily relies on the ambient temperature.

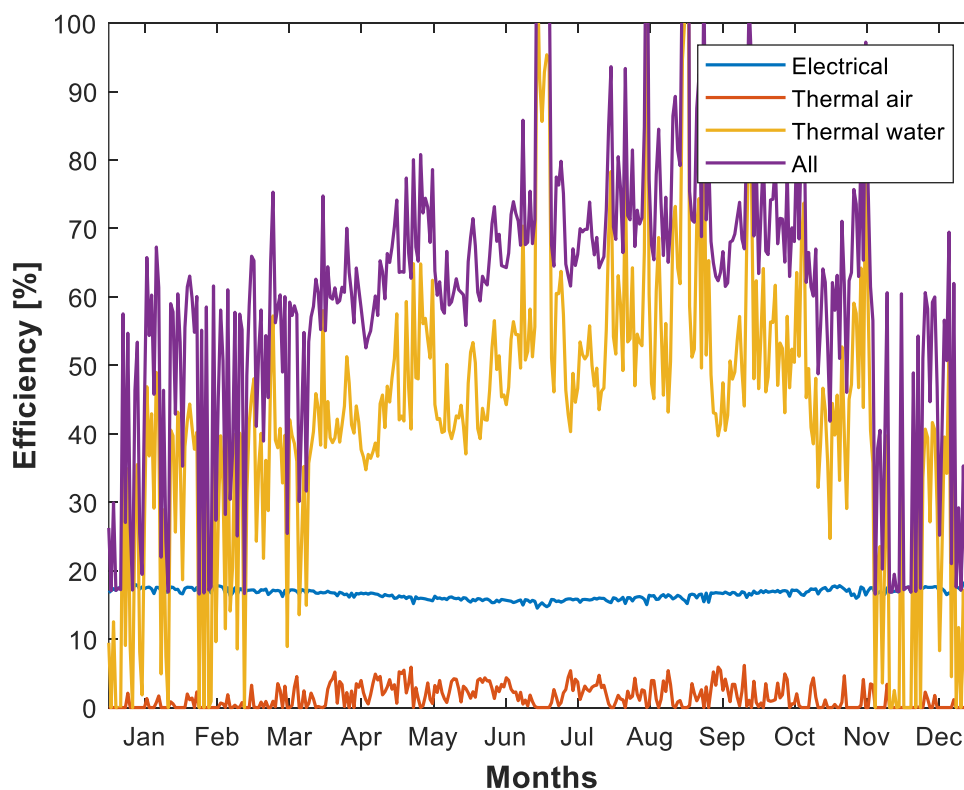


Figure 5-7 Daily efficiencies of water pipe design for a year

Figure 5-8 illustrates the daily electrical efficiencies of each configuration for a year. There is a linear decrease from winter to the summer and the opposite for all configurations. The reason is that the efficiency decreases with the increase of cell temperature. The cell temperatures in the summer are much higher compared to the winter (Figure 5-10). The highest daily electrical efficiencies are found for the Fins design. The reason is that fins design has lower temperatures compared to the No fins design and less reflection losses compared to the Water pipes and No water pipes design. The worst electrical efficiencies are occurred for the No water pipes design because the cell temperatures of this design are also very high compared to the Water pipe design.

Continuing with Figure 5-9, the highest daily thermal efficiencies are occurred from the No water pipe design which was expected because of the high temperatures of the PV module. Worth mentioning, is that the Fins design has higher thermal efficiencies of air from both the No fins and Water pipes designs because it provides more thermal energy to the system due to the larger contact area provided by the fins.

Table 5-8 provides information about the yearly efficiencies of the energies for each configuration in respect of incident solar energy throughout a year. The best efficiency is from the Water pipe design which utilises more than half of the overall solar energy. The No water pipes design utilises also a large amount of the incident solar energy.

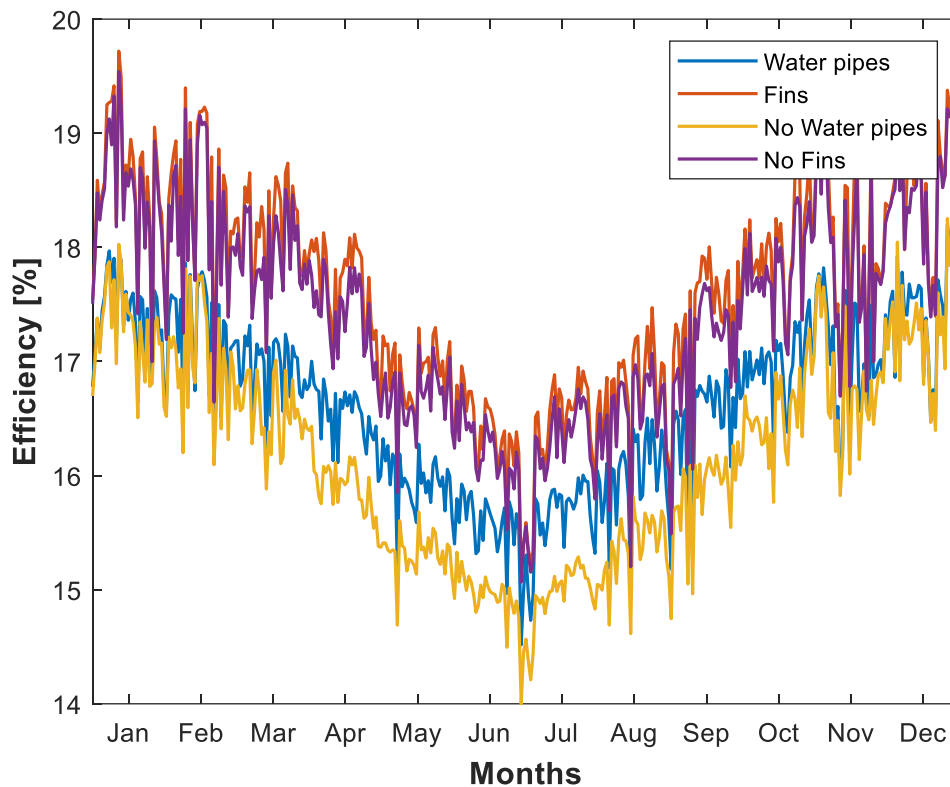


Figure 5-8 Daily electrical efficiencies of each configurations for a year

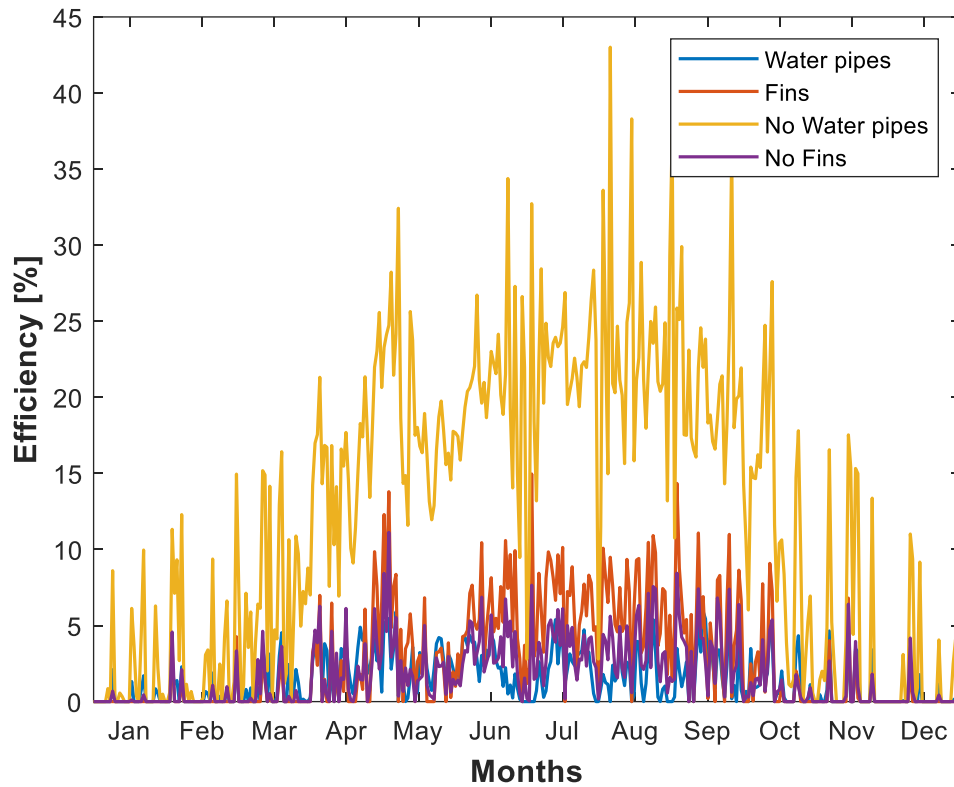


Figure 5-9 Daily air thermal efficiencies of each configuration for a year

Table 5-8 Yearly electrical and thermal efficiencies with the highest highlighted for each energy

Designs	Electrical [%]	Air thermal [%]	Water Thermal [%]	Overall [%]
Water pipes	16.4	2.3	45.6	64.3
Fins	17.5	3.8	-	21.3
No water pipes	15.9	15.7	-	31.36
No fins	17.3	2.5	-	19.8

5.2.4 Temperatures

The operational temperatures of the PV modules on the system are very important because it is a parameter that significantly affects all the energies. Figure 5-10 illustrates the daily maximum average temperatures of cells for each configuration throughout a year. The No water pipe design has the highest maximum temperatures which was expected because it is not providing thermal energies to the environment or to the water pipes. The No fins design has the second highest temperatures of cells and the Fins and Water pipe designs have similar temperature patterns.

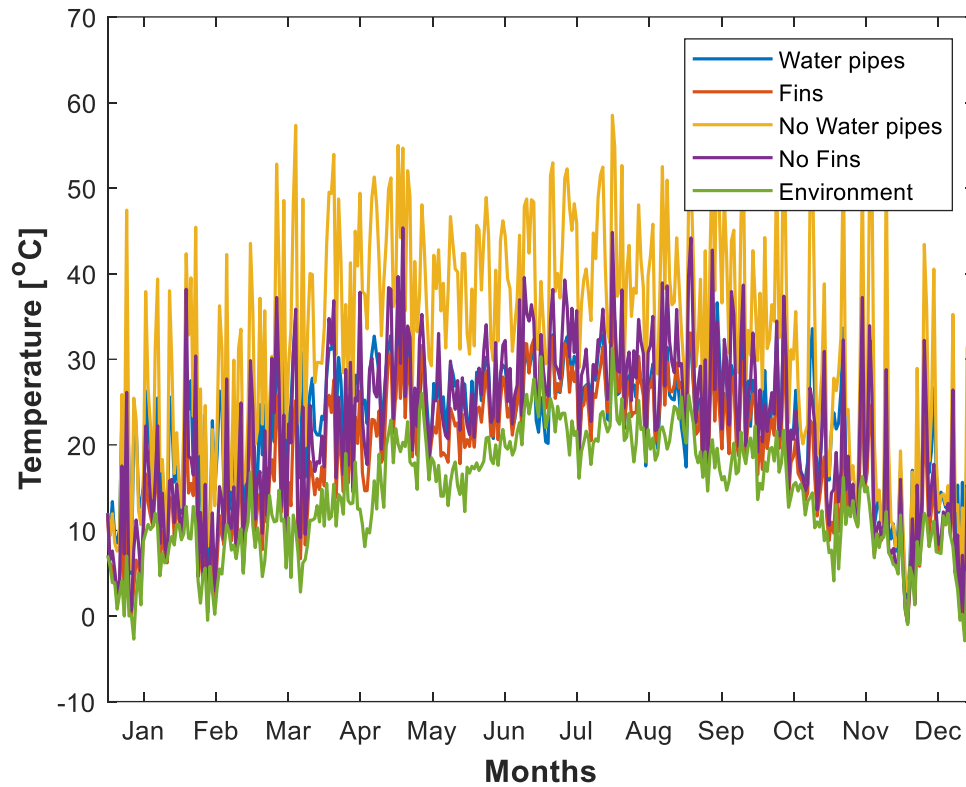


Figure 5-10 Maximum daily cell average temperatures of each configuration for a year

Figure 5-11 illustrates the maximum daily temperatures of the tank levels. The top-level temperatures have relatively high temperatures throughout the year compared to the mains temperature which is 10°C. In addition, the difference of the temperatures in the tank levels proves that is important to take a stratified model for the tank. In the scenario chapters the behaviour of the tank temperatures is clearer.

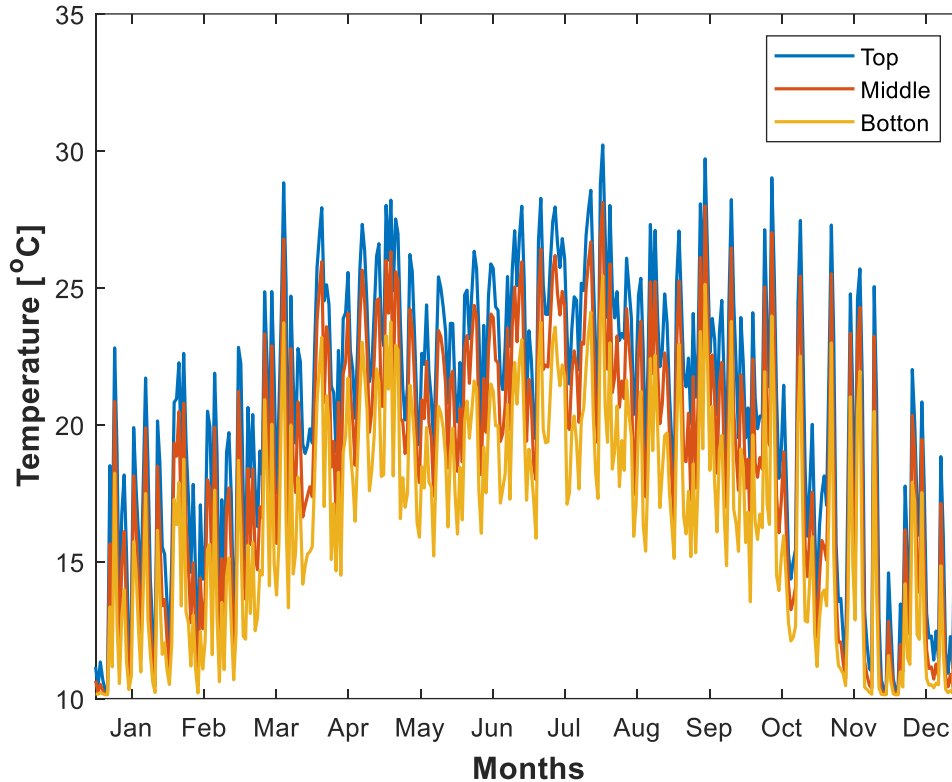


Figure 5-11 Maximum daily tank level temperatures for a year

These temperatures although are slightly underestimated. The reason is that the accuracy (see Table 5-4) for the yearly results is not so high compared to the scenarios results in order to have a small computational time.

5.3 Scenario results

This chapter explains the energetic behaviour of the system in extreme weather scenarios. The chosen scenarios are based on extreme values of irradiance and ambient temperature. The scenarios are shown in Table 5-9. The figures provide information for three days, but the discussions are only for the middle day which is the day with the extreme condition. The figures are for three days to show how the performance of the previous or day affect the next day.

Table 5-9 Scenarios and their dates

Scenarios	Date
Highest incident Irradiance	15/09/2005
Lowest incident Irradiance	23/11/2005
Highest ambient temperature	03/07/2005
Lowest ambient temperature	12/01/2005

5.3.1 Highest Irradiance

The highest irradiance on the system is a very important scenario to show how the temperatures change throughout the day and how much power can be extracted in such conditions. Starting with

the performance analysis of water pipe configuration, Figure 5-12 illustrates the electrical and thermal (air and water) performances for the day with highest irradiance. The thermal energy of water is the highest compared to other energies and second highest is the electrical energy. In addition, more than half of the irradiance is utilised if all the energies are added together. Lastly, thermal energy of water is extracted also at the evening where there is no irradiance.

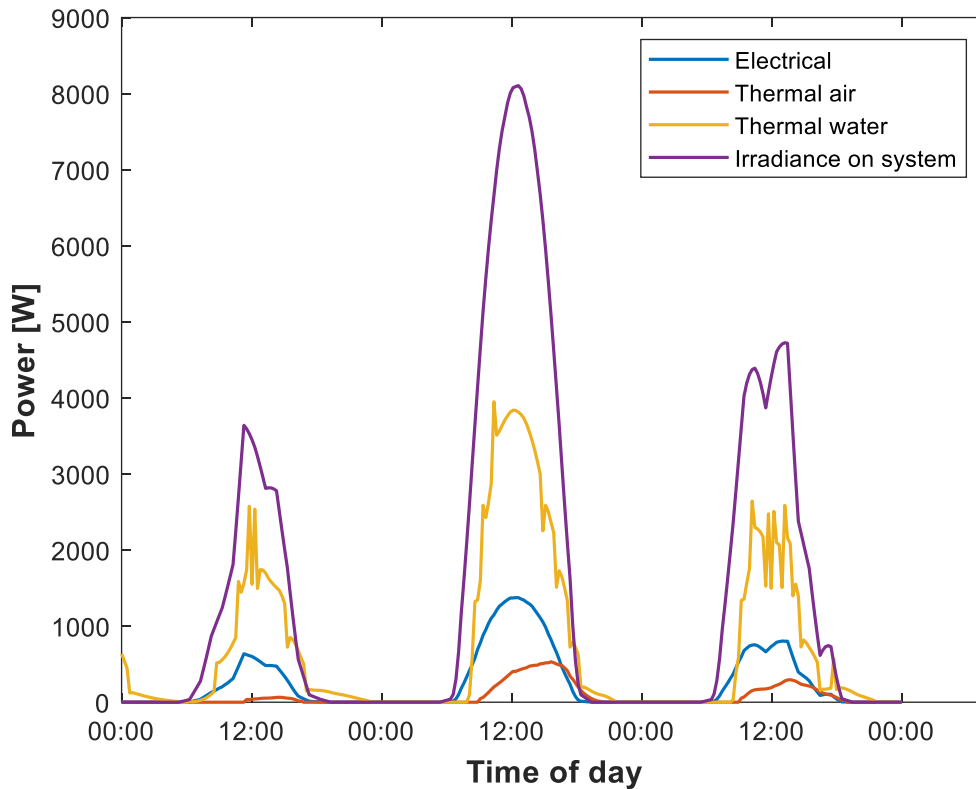


Figure 5-12 Incident Irradiance and powers from water pipe design for highest irradiance day (Middle day)

Continuing with the main temperatures of the water pipe configuration (see Figure 5-13), the average maximum cell temperature (about 38 °C) is relatively low for such high irradiance. The reason is that the water behind the PV modules extracts most of the thermal energy and cools down the cells. The highest temperature difference of inlet and outlet of the water reaches almost 10 °C. In addition, there is air temperature increase inside the cavity which provides thermal energy and sometimes ventilation. The yellow line of Figure 5-13 represents the air inlet in the cavity and the different strategies are observed. When the air inlet is constant at 18°C, it means that the inlet air is from the building and if not then is coming from the ambient environment.

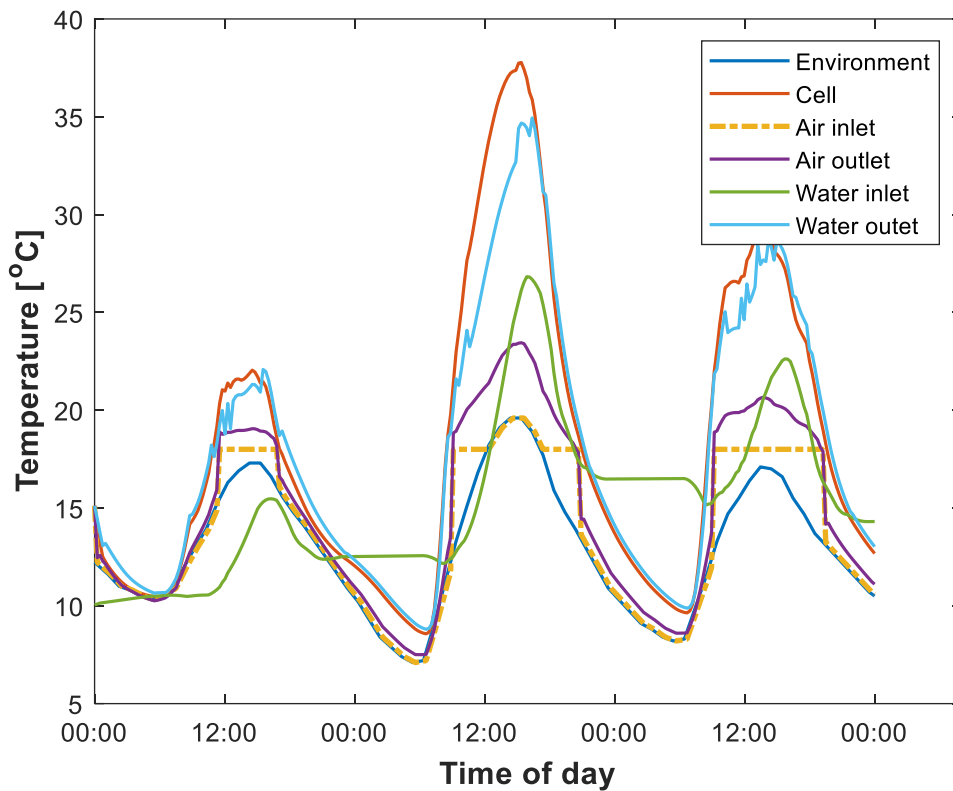


Figure 5-13 Temperatures of water pipe design for highest irradiance day (Middle day)

Figure 5-14 illustrates the air and water mass flows of water pipe configuration. In addition, the water mass flow of the load is shown, which relates to the scale of the system. It can be seen that the water mass flow strategy is working perfectly and increases as the temperature difference of the PV modules and inlet water increases (see Figure 5-13).

Figure 5-15 shows the temperature distribution of the water tank throughout the day. The temperature increase of the water stored in the tank changes with the thermal energy gained from the system. On the contrary, the temperature increase of the water stored in the tank is depends on the water load. The highest and lowest temperatures inside the tank are in the range of 10-35°C. Lastly the tank temperatures can influence behaviour of the system for the next day because every night the temperatures are different.

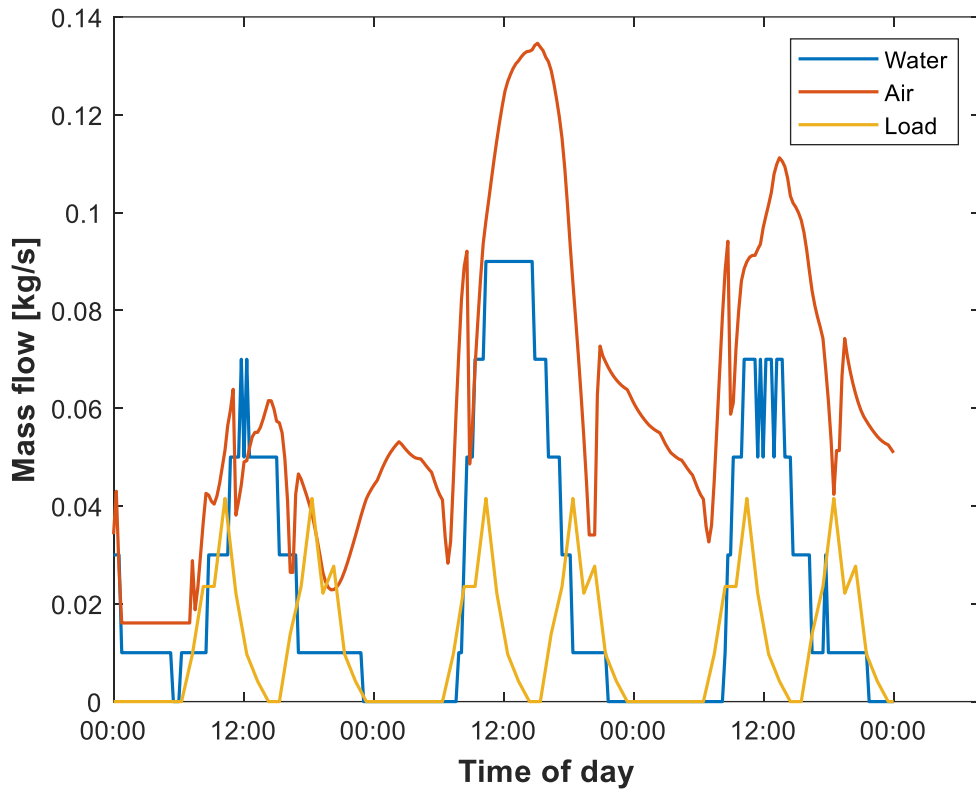


Figure 5-14 Water/air mass flows and water load of water pipe design for highest irradiance day (Middle day)

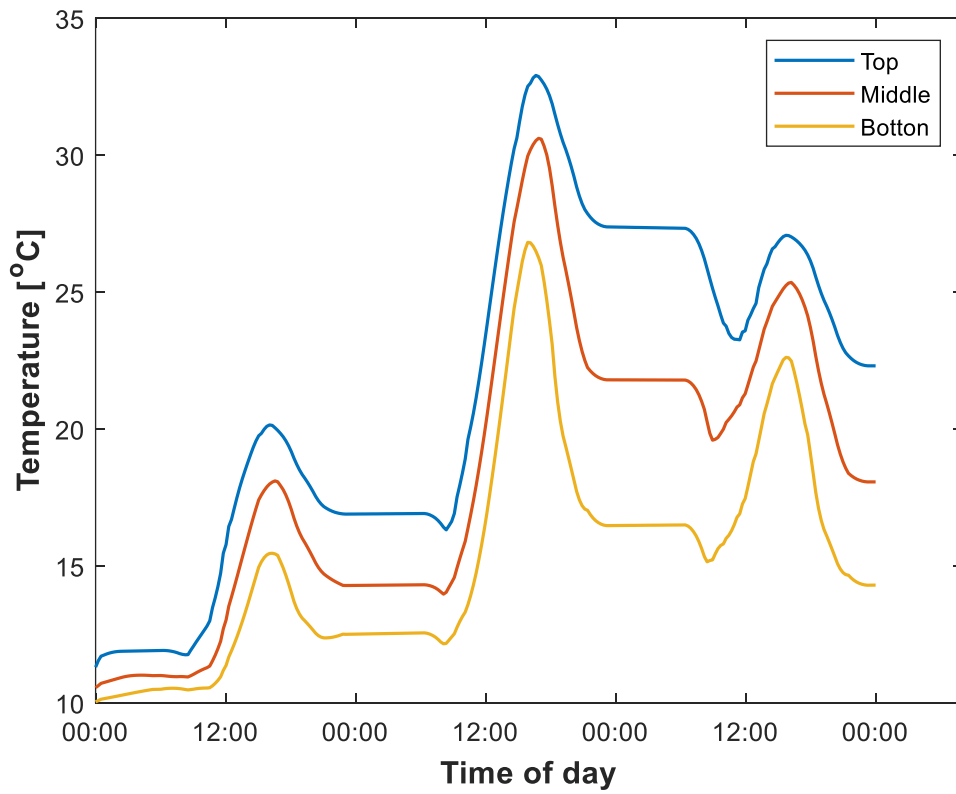


Figure 5-15 Temperatures of water tank levels for highest irradiance day (Middle day)

The figures below show the differences of each configuration. Starting with Figure 5-16, the electrical energy of each configuration is illustrated. The configurations where the PV modules are in the front (Fins, No fins) give more electrical power compared to the configuration of PV in the back (Water pipes, No water pipes). This is because when the PV modules are in the back there is an additional reflection from the glass and if the design is Water pipes then there is also electrical power loss for the pump. The highest electrical power is generated from the Fins design because the PV modules are in the front and also their temperature is lower than the No fins design (see Figure 5-18) which will give higher efficiency (see Figure 5-1 for efficiency dependence). In addition, the No water pipes design provides the lowest electrical power because the module temperature is very high compared to the Water pipes design as can be seen from Figure 5-18.

Continuing with air thermal power Figure 5-17, the highest air thermal power is extracted from the No water pipes design. The reason is the high temperature of the PV modules because it is not providing thermal energy to the environment or to the water as opposed to the other designs. The second highest air thermal energy is extracted from the Fins design. The reason is that the fins provide more thermal energy to the cavity.

Comparing the cell temperatures (Figure 5-18), the lowest temperature is from the Fins design because a big amount of thermal energy is extracted from the environment (due to convection) but also from the cavity due to the fins. The highest temperature is from the No water pipes design. However, these results are heavily influenced from the high wind speeds (Figure B 1-d). If the wind speeds are lower, the lowest temperature profile might be observed from the Water pipe design (see Figure 5-18 first day)

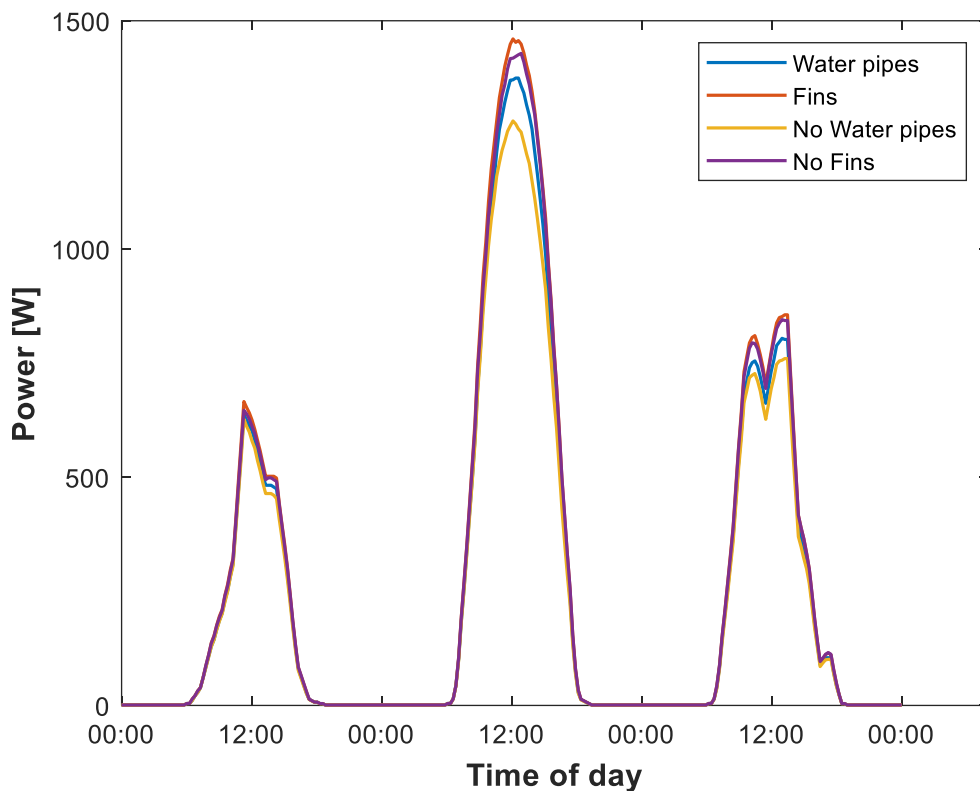


Figure 5-16 Electrical power of each configuration for highest irradiance day (Middle day)

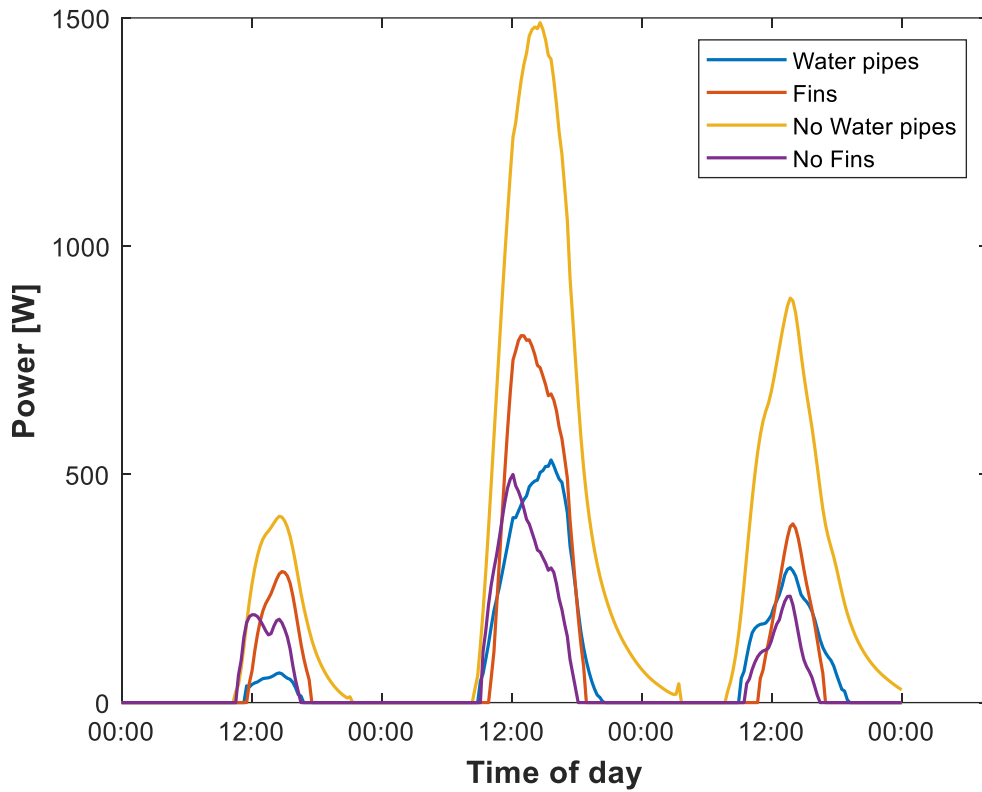


Figure 5-17 Air thermal power of each configuration for highest irradiance day (Middle day)

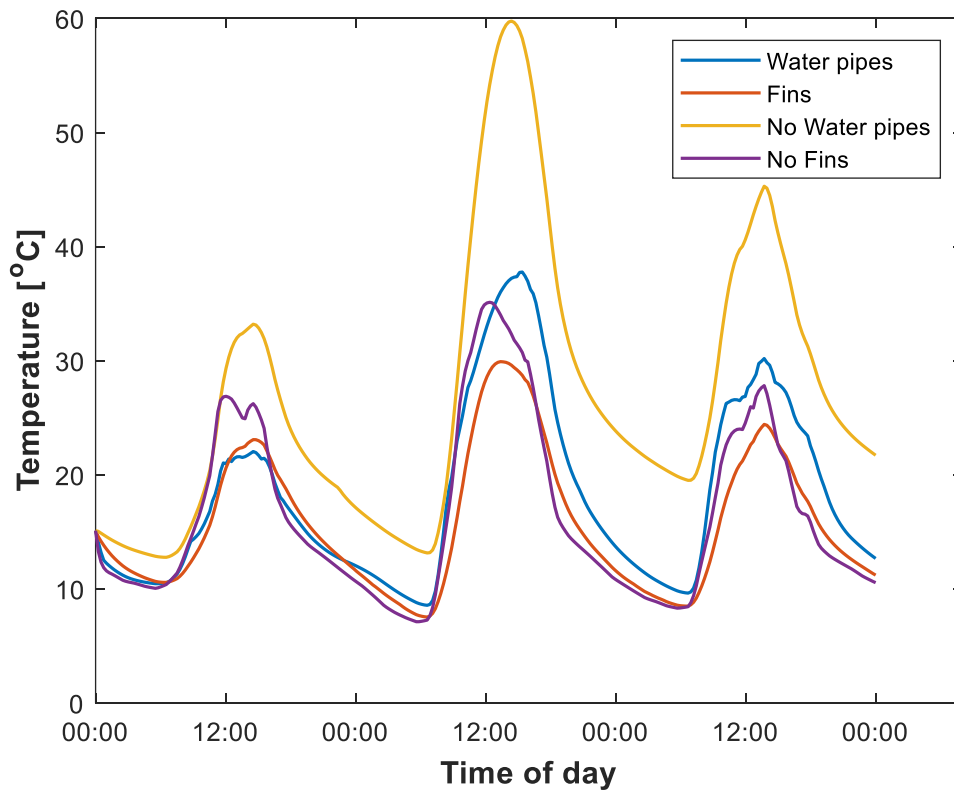


Figure 5-18 Average PV cell temperatures of each configuration for highest irradiance day

Figure 5-19 Illustrates the temperature distribution of the cells in respect of height for the time with the maximum temperature. All configurations show an increase in temperature with respect of

increase in height. The reason is that, the air temperature inside the cavity is increasing with height and therefore is influencing the temperature of the cells. However, the Water pipe design has a very high increase in temperature with respect of height which is almost 8°C. The reason is that the Water pipe design has also water behind the PV modules which has also increasing temperatures with height like the air. However, the water temperature has higher increase (Figure 5-13 see water inlet and outlet temperatures). Therefore, the influence is essential on the PV modules.

Figure 5-20 illustrates the ventilation and heating status of the four configurations in respect of time. Ventilation is on only during the day for a small period for all configurations, where the temperature of the environment is high enough. However, heating is On, more hours because the building air is entering the cavity and heated without ventilation. Worth mentioning is that the heating for the Water pipe and No water pipe designs is On, more hours than the other configurations. This is because the cell from the other configurations are cooled down from the environment. Lastly, the heating status of the No water pipe design show that there is heating throughout the whole night and this is because of the high temperatures of the PV modules.

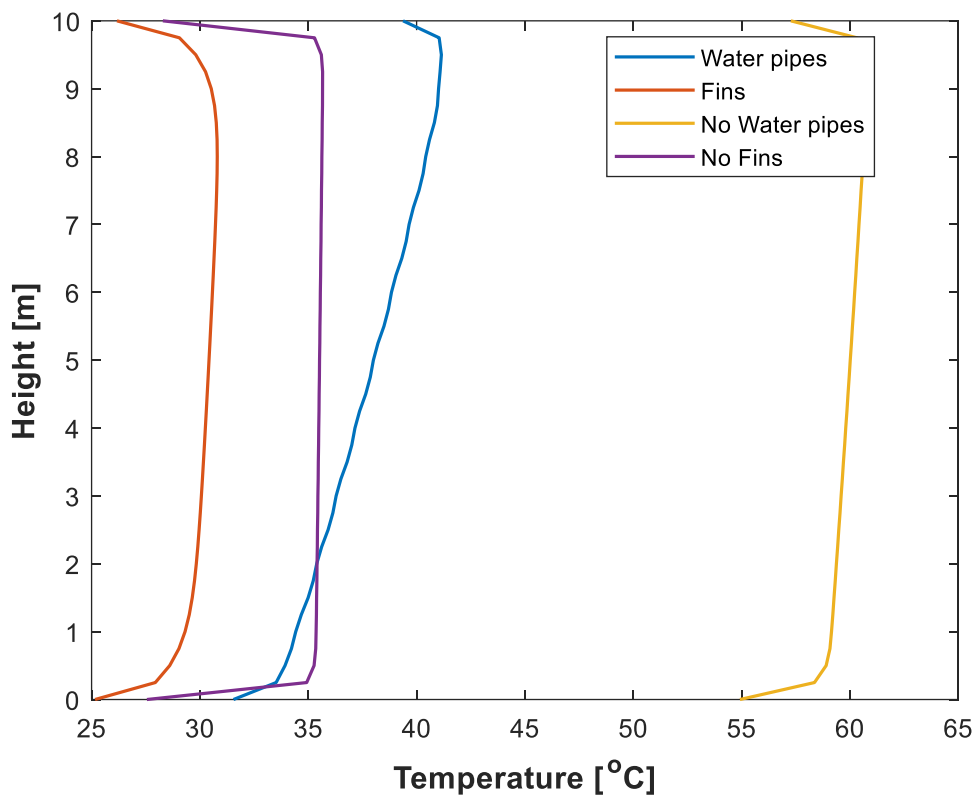


Figure 5-19 Maximum temperature distribution of PV cells in respect of height for each configuration for highest irradiance day

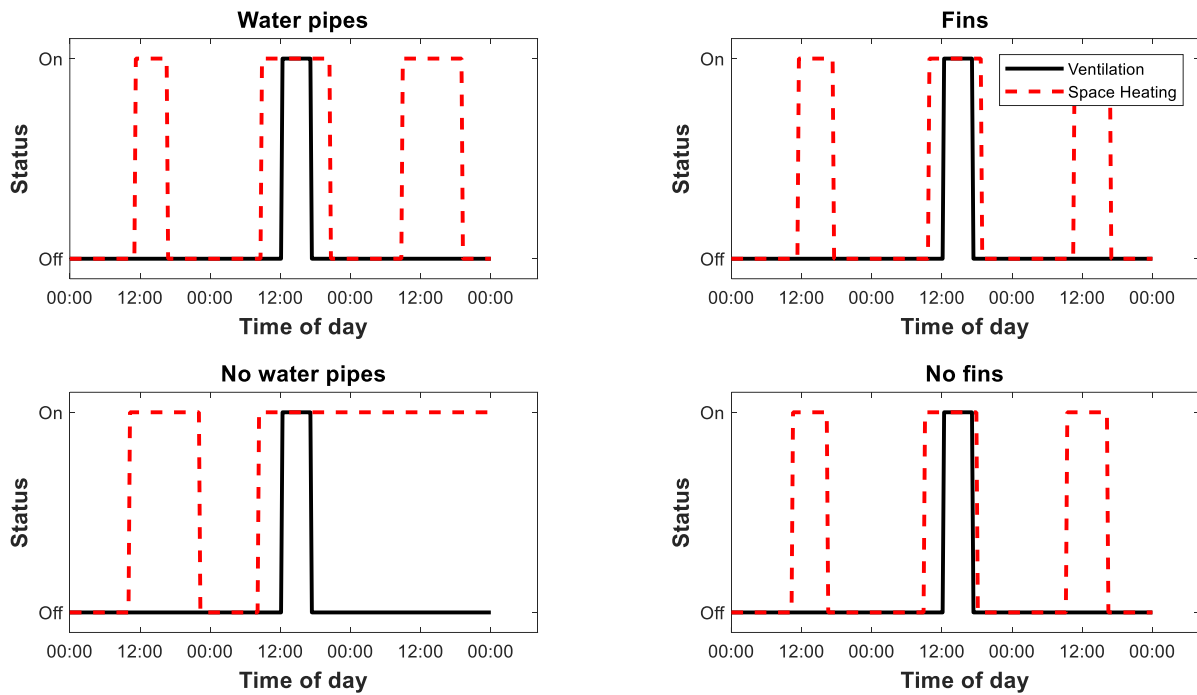


Figure 5-20 Ventilation and heating status (strategy) of each configuration for the highest irradiance day

5.3.2 Lowest Irradiance

The scenario with lowest irradiance day can determine the performance of the systems in such conditions. Figure 5-21 illustrates all the power profiles of Water pipe design. There is no air thermal energy extracted that day and very little water thermal energy only during the afternoon. In addition, the electricity has very low levels. Despite the low irradiance, also the ambient temperature is very low (Figure 5-22) and therefore there is no source of solar or thermal energy.

Figure 5-22 shows various temperatures of the Water pipe design. The temperature of the cell is a bit higher than the temperature of the environment and therefore the air inside the cavity is not heated enough for ventilation or heat. However, there is an air mass flow inside the cavity but the air is escaping in the environment (Figure 5-23). Figure 5-23 also shows that there is a little mass flow from the water and therefore a small fraction of water thermal energy is extracted.

The water tank temperatures are in very low levels but it can be seen that also in such extreme scenario the top level water temperature is higher compared to the temperature of the water coming from the mains (10°C) (Figure 5-24). The reason is that, heat is stored from previous days which had higher irradiance.

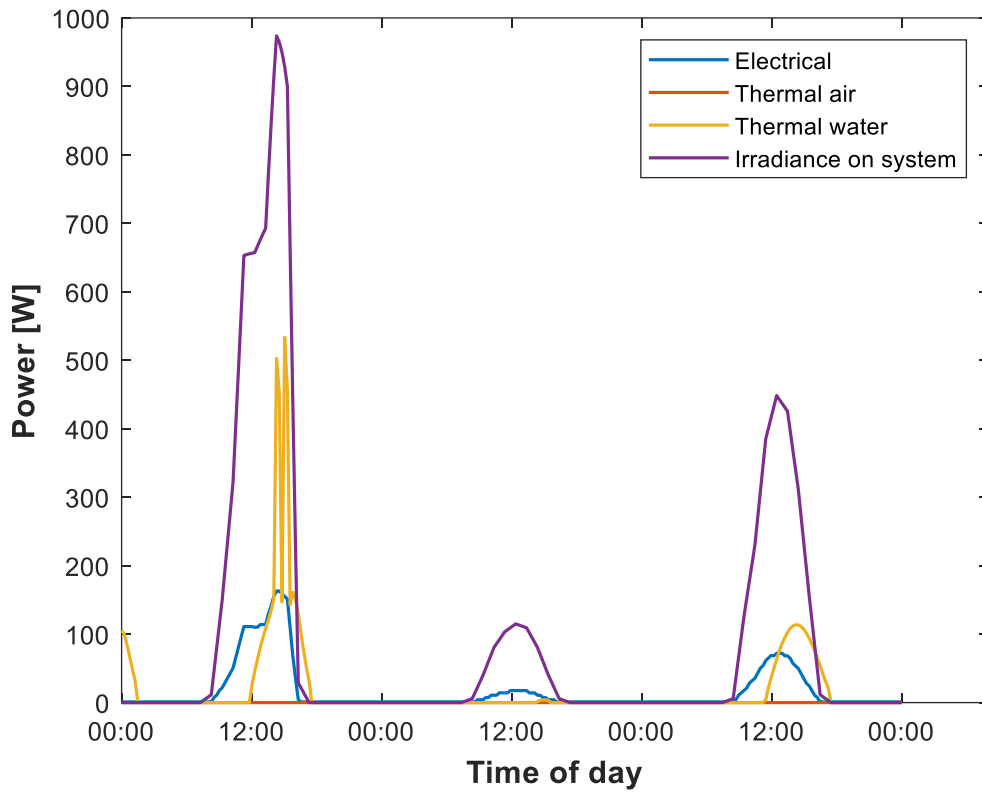


Figure 5-21 Irradiance on system and powers from water pipe design for lowest irradiance day (Middle day)

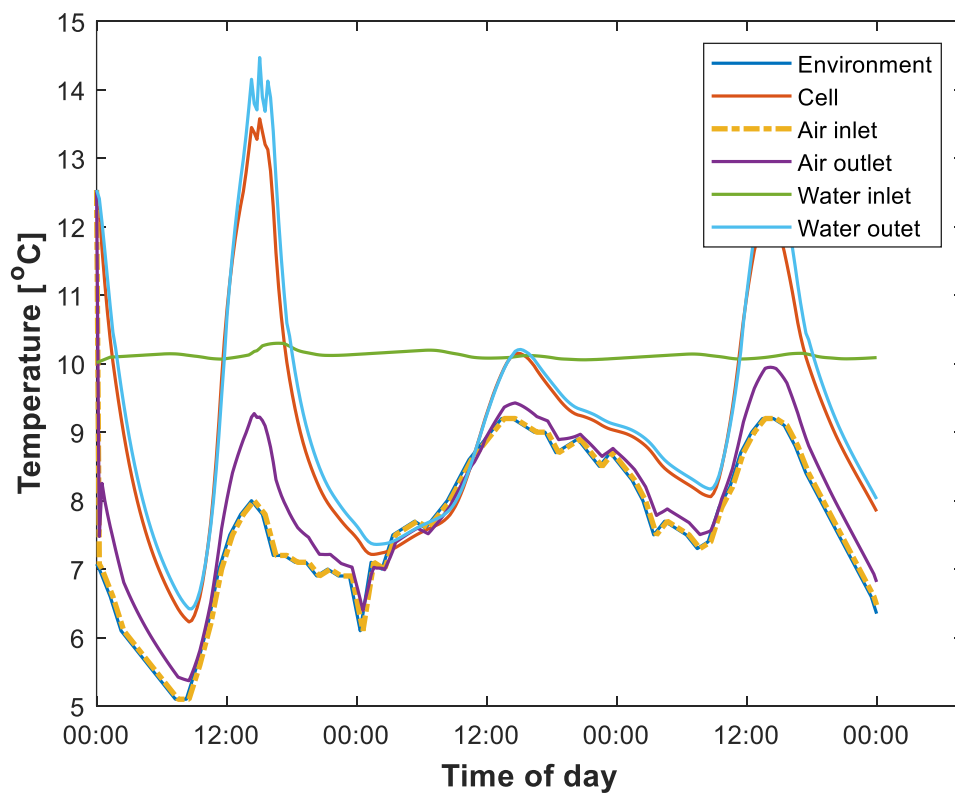


Figure 5-22 Temperatures of water pipe design for lowest irradiance day (Middle day)

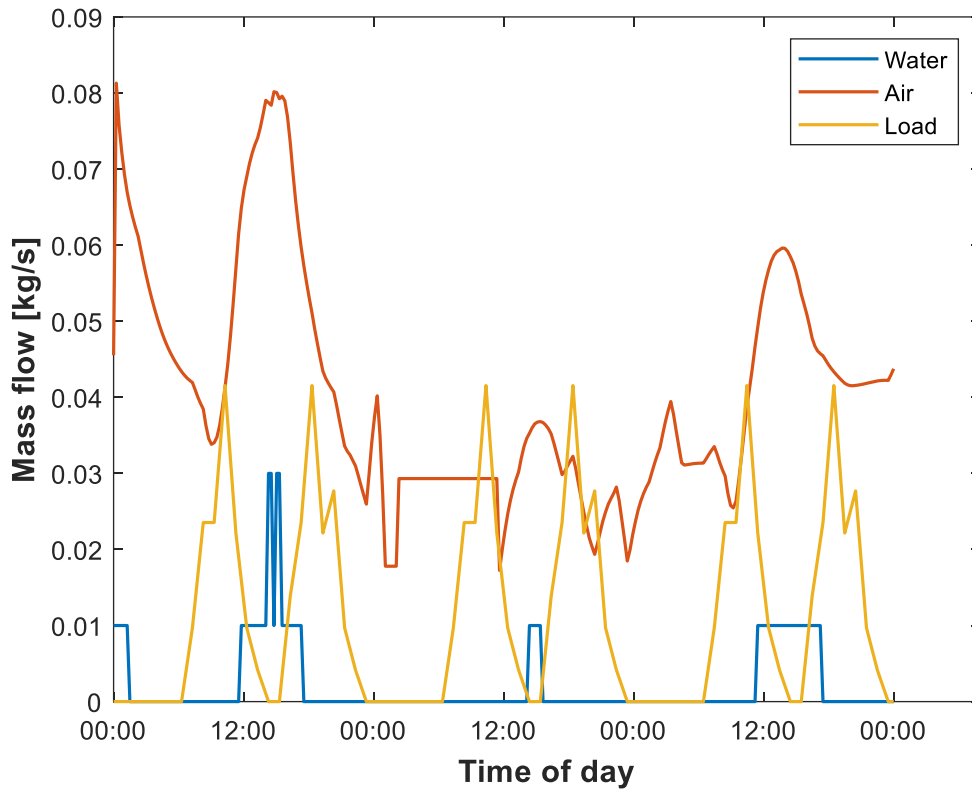


Figure 5-23 Water/air mass flows and water load of water pipe design for lowest irradiance (Middle day)

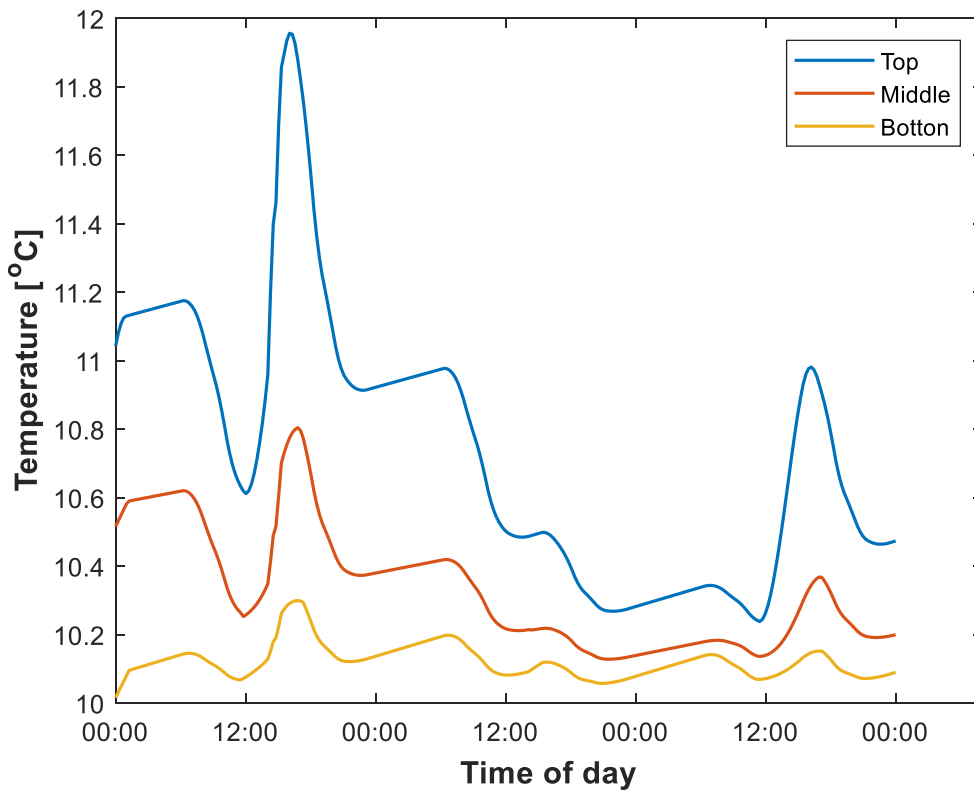


Figure 5-24 Temperatures of water tank levels for lowest irradiance day (Middle day)

Because of the low irradiance, there are no significant differences between the four configurations. Figure 5-25 illustrates the electrical power of the four configurations but there is almost no difference because of the low irradiance and low cell temperatures. In addition, there is no air thermal energy from all designs and therefore also the ventilation and heating status are continuously off. As can be seen from Figure 5-26 all designs have similar temperatures.

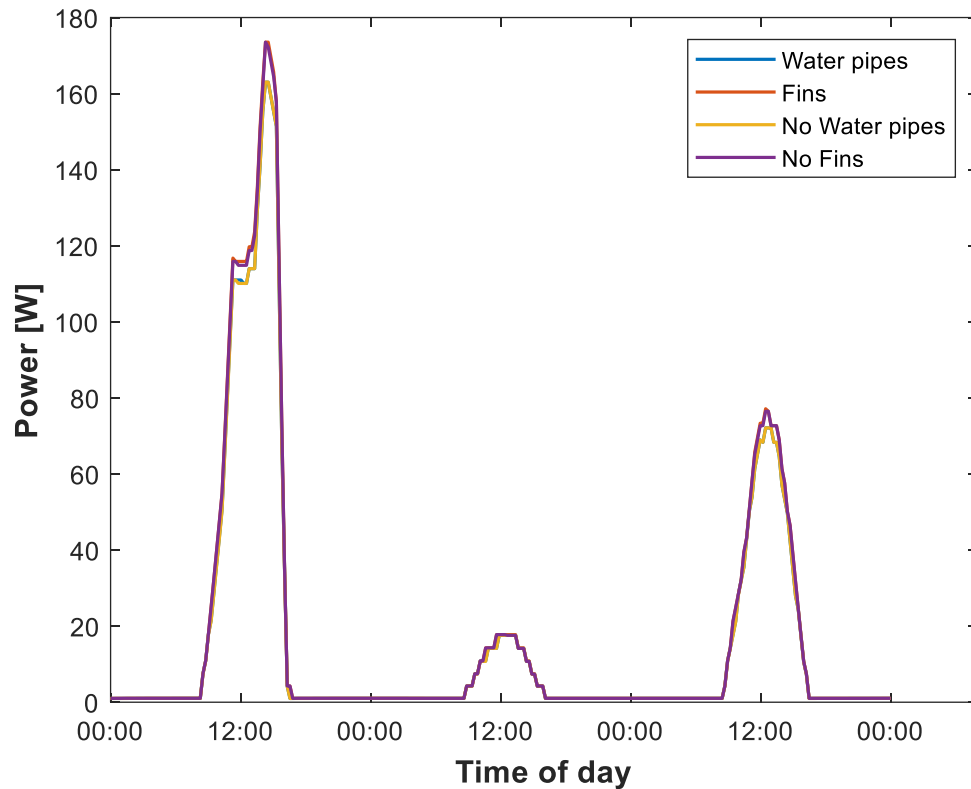


Figure 5-25 Electrical power of each configuration for lowest irradiance day (Middle day)

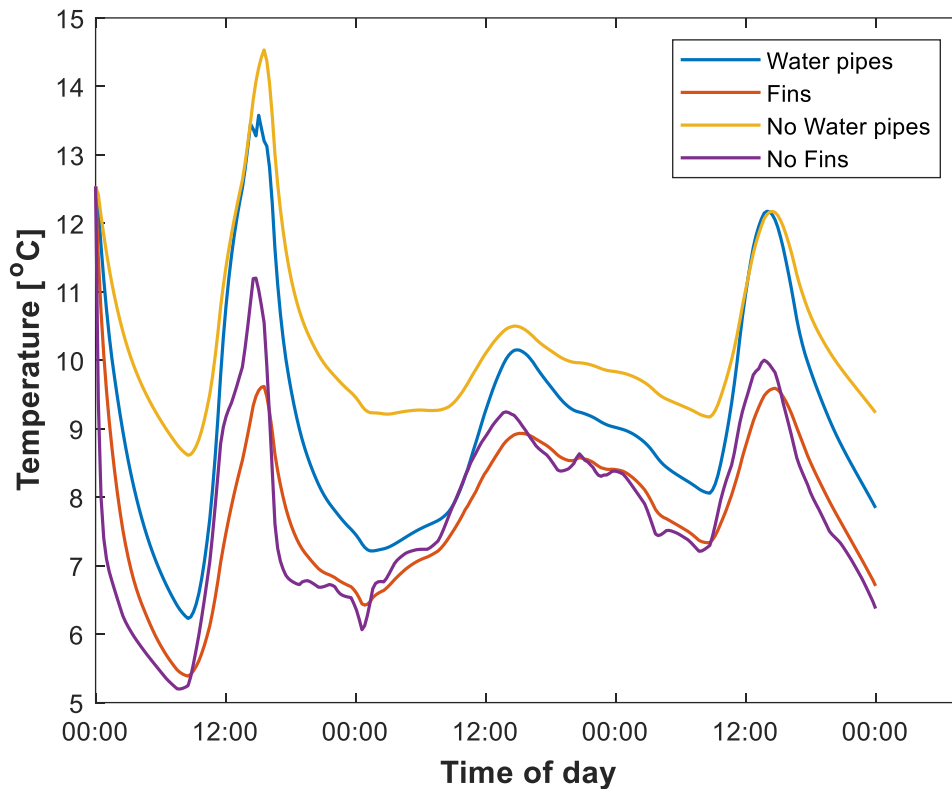


Figure 5-26 Average PV cell temperatures of each configuration for lowest irradiance day

5.3.3 Highest ambient temperature

This chapter shows the performance of the designs for the day with the highest ambient temperature. Figure 5-27 illustrates the powers of the Water pipe design. Despite the low irradiance levels, the thermal energy of the water is high. In addition, there is thermal energy of water during the night. The reason is that the temperature of the water coming from the mains is constant throughout the year at 10°C. This means that thermal energy is extracted because of the high temperatures and not because of the solar energy. Therefore, it is recommended in future work to implement a variable water temperature from the mains throughout the year. The reason of the spikes of thermal energy, is because the water mass flow has also spikes (Figure 5-29). This rapid increase and decrease of mass flow throughout the day is because of the strategy of the water mass flow. The mass flow is increasing and decreasing in respect of cell and water inlet temperature differences. Because the temperature gradient of the cells throughout the day is very small (not high irradiance), the mass flow increases in one timestep with consequence to significantly reduce the temperature of the cell but for the next timestep is decreasing due to the cell and water inlet temperature difference high decrease. Lastly, there is no thermal energy of air because the temperature of the cell is lower than the temperature of the environment and therefore it cannot heat the air (Figure 5-28).

Figure 5-28 illustrates the temperatures of Water pipe design. One important result is that the temperature of the cell is lower than the temperature of the environment because of the explanation given above for the water temperature from the mains.

The temperatures of the tank (Figure 5-30) are overall lower from the ambient temperature throughout the day and therefore there is a continues increase except the time when there is water mass flow load.

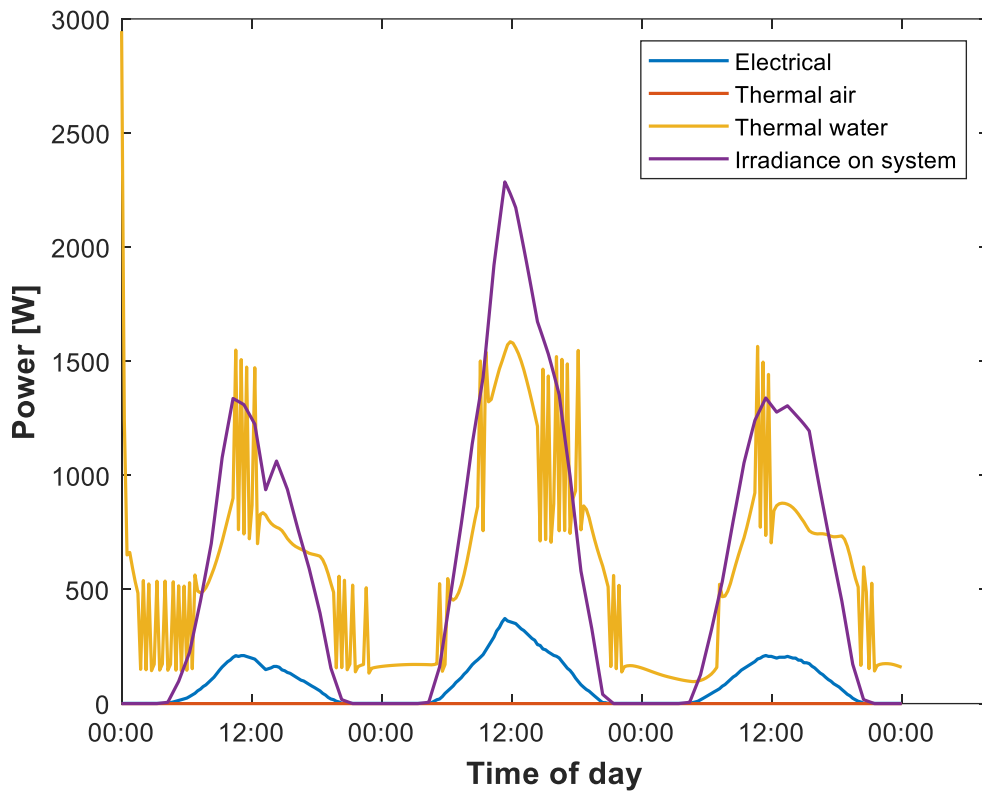


Figure 5-27 Irradiance on system and powers from water pipe design for highest ambient temperature day (Middle day)#

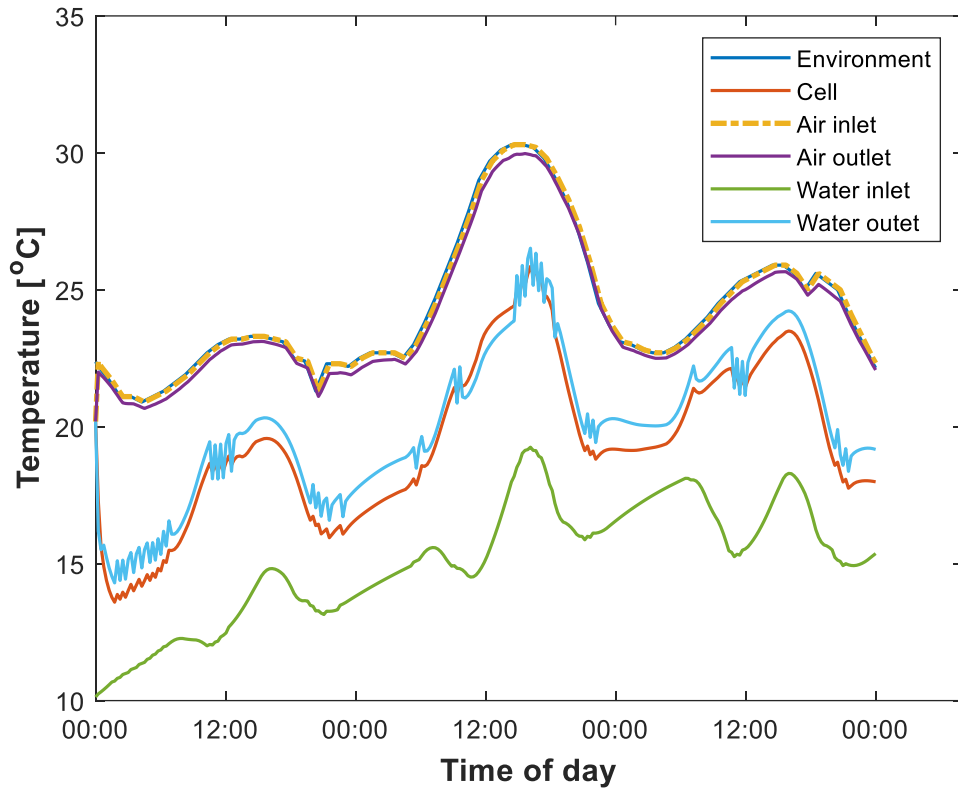


Figure 5-28 Temperatures of water pipe design for highest ambient temperature day (Middle day)

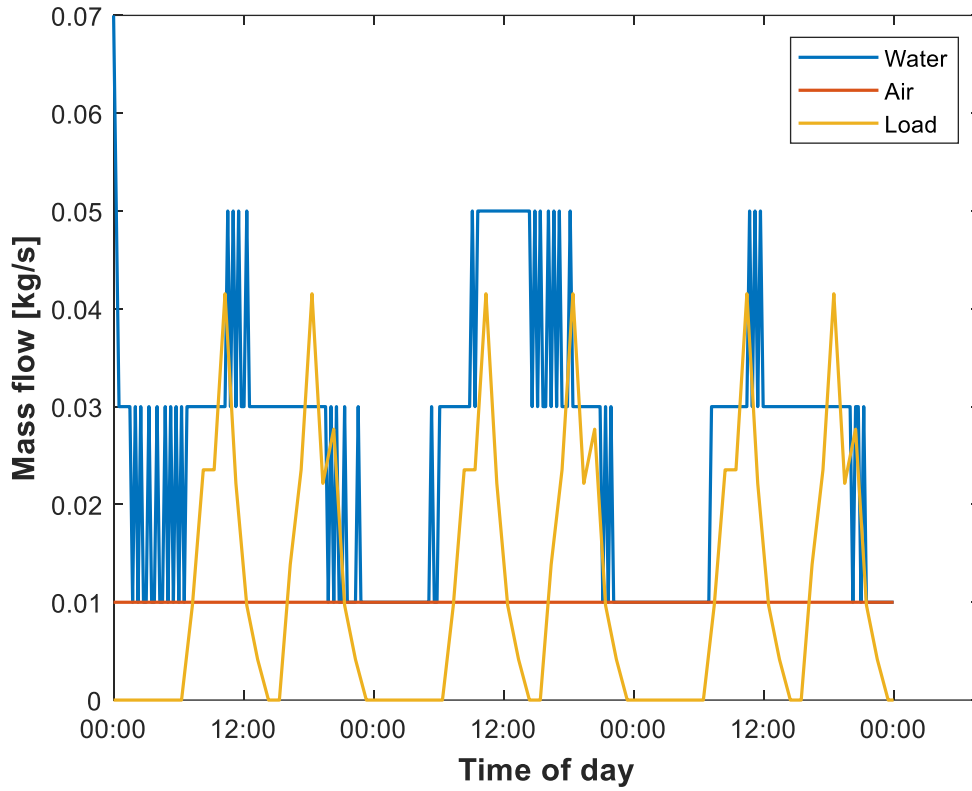


Figure 5-29 Water/air mass flows and water load of water pipe design for highest ambient temperature (Middle day)

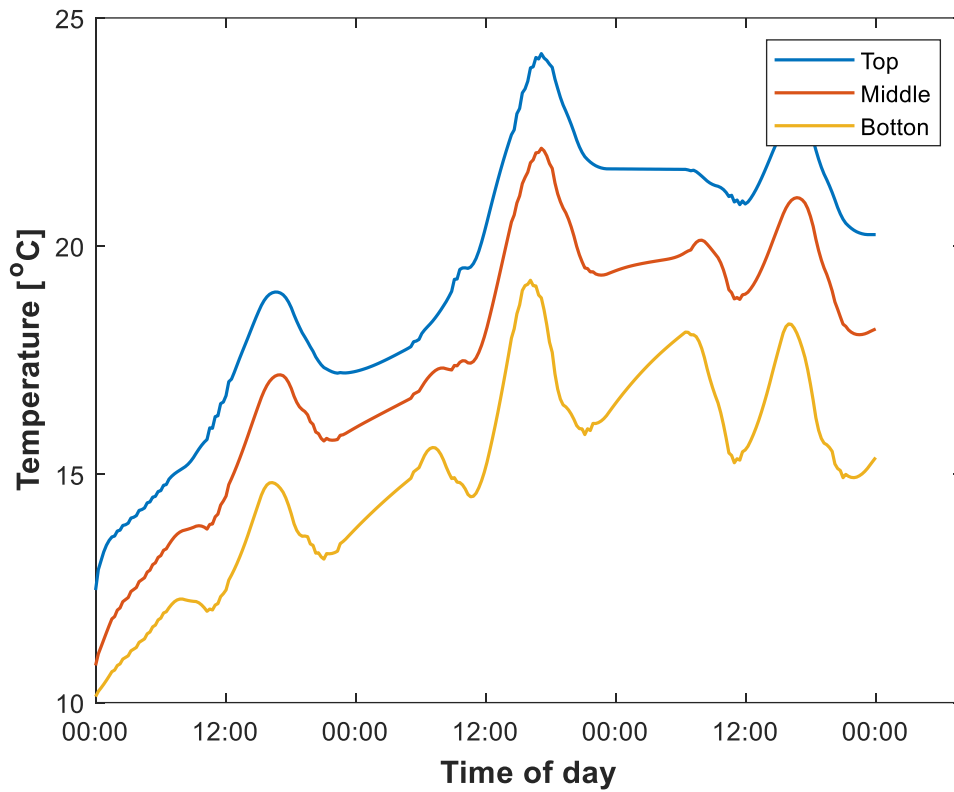


Figure 5-30 Temperatures of water tank levels for highest ambient temperature day (Middle day)

The electrical power (Figure 5-31) of the No water pipes design is the lowest compared to the other configurations because it has more reflection losses and higher temperature (Figure 5-33) than the Fins and No fins configuration. Despite that the Water pipes design has also additional reflection losses, it has similar electrical performance with the Fins and No fins configurations. The reason is that it has lower temperature than the other configurations and therefore its efficiency is increasing.

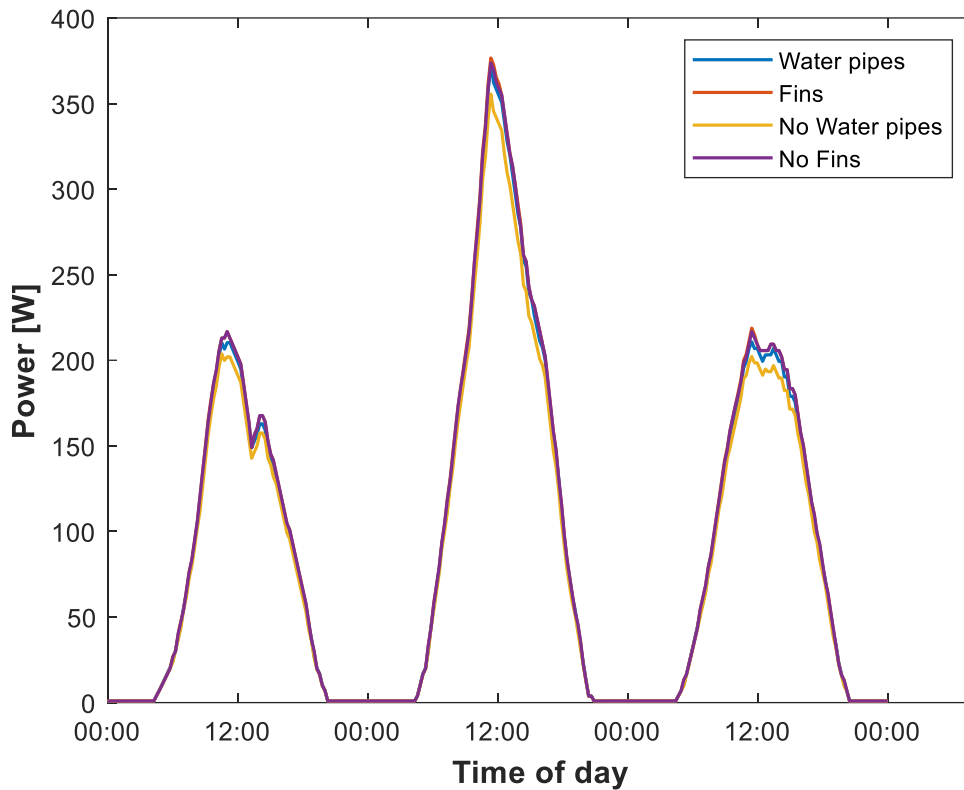


Figure 5-31 Electrical power of each configuration for highest ambient temperature day (Middle day)

Figure 5-32 illustrates the air thermal power for all configurations. There is no air thermal energy from the Water pipe design and negligible energy from the Fins and No fins design. The air thermal energy of the No water pipe design is occurring at the night. The reason is that in the day, the temperature of the environment is higher than 25°C which is the limit to stop the thermal energy. However, at night it drops below 25°C and the temperature of the cell is higher. Therefore, ventilation and thermal energy are occurring at the same time (see Figure 5-35).

Figure 5-34 shows the temperature distribution of PV cells in respect with the height. Again, the Water Pipe cells have this gradient that is explained also in chapter 5.3.1.

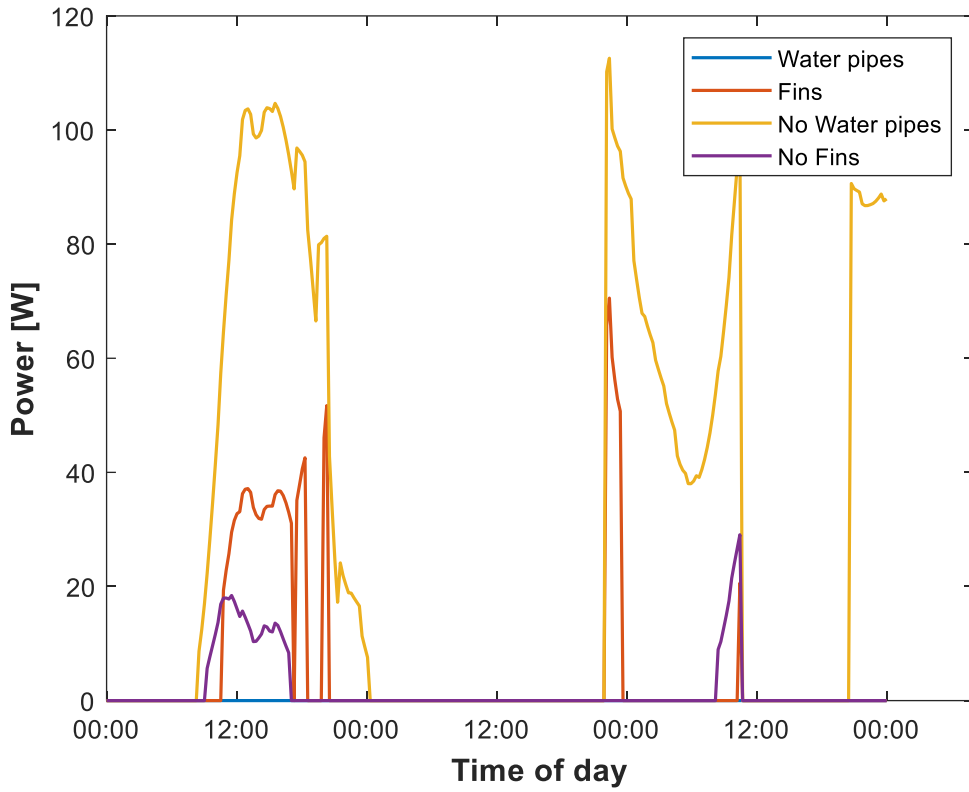


Figure 5-32 Air thermal power of each configuration for lowest ambient temperature day (Middle day)

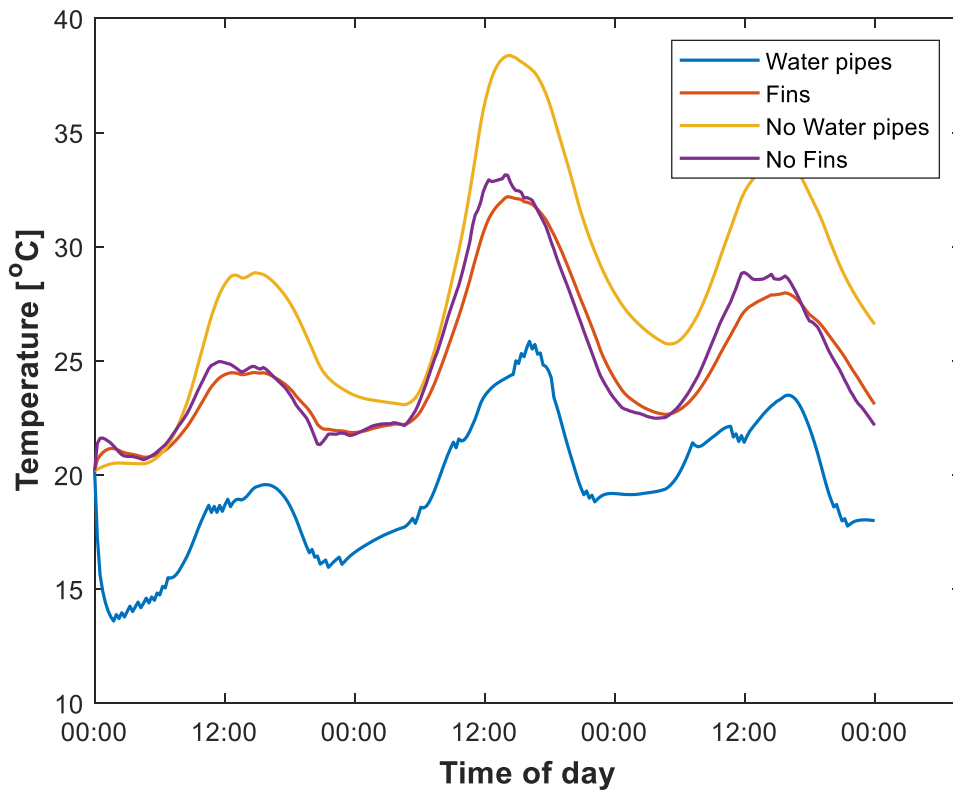


Figure 5-33 Average PV cell temperatures of each configuration for highest ambient temperature day

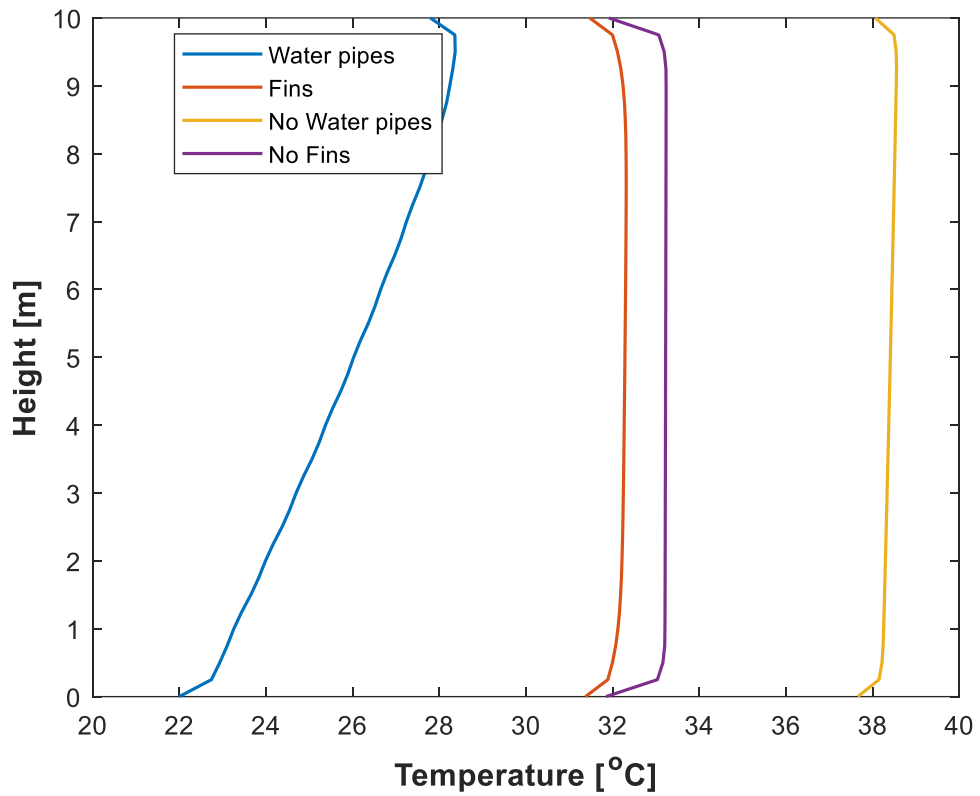


Figure 5-34 Maximum temperature distribution of PV cells in respect of height for each configuration for highest temperature day

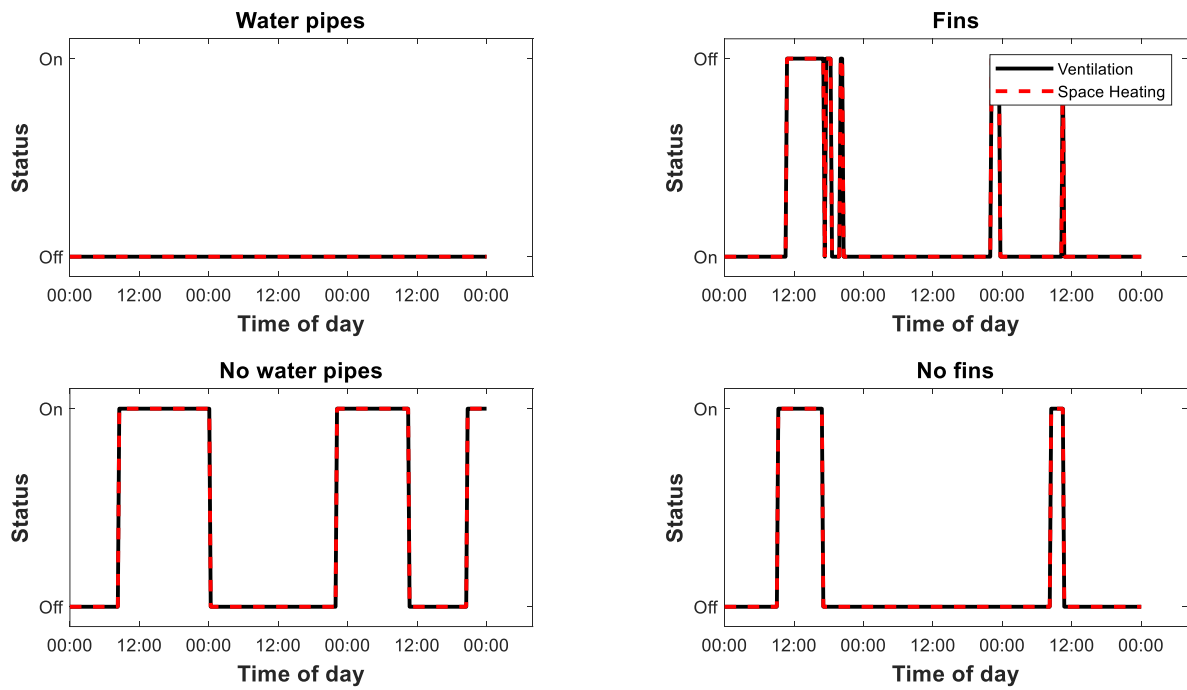


Figure 5-35 Ventilation and heating status (strategy) of each configuration for the highest ambient temperature day

5.3.4 Lowest ambient temperature

This scenario shows the performance of the systems at the day with the lowest average temperature (less than 0°C for the whole day Figure 5-37). However, the irradiance is relatively high that day. Figure 5-36 illustrates the energies of the Water pipe design. Surprisingly, there is a good amount of thermal energy of water generated in such extreme conditions. This is because the PV modules are not directly exposed to the environment.

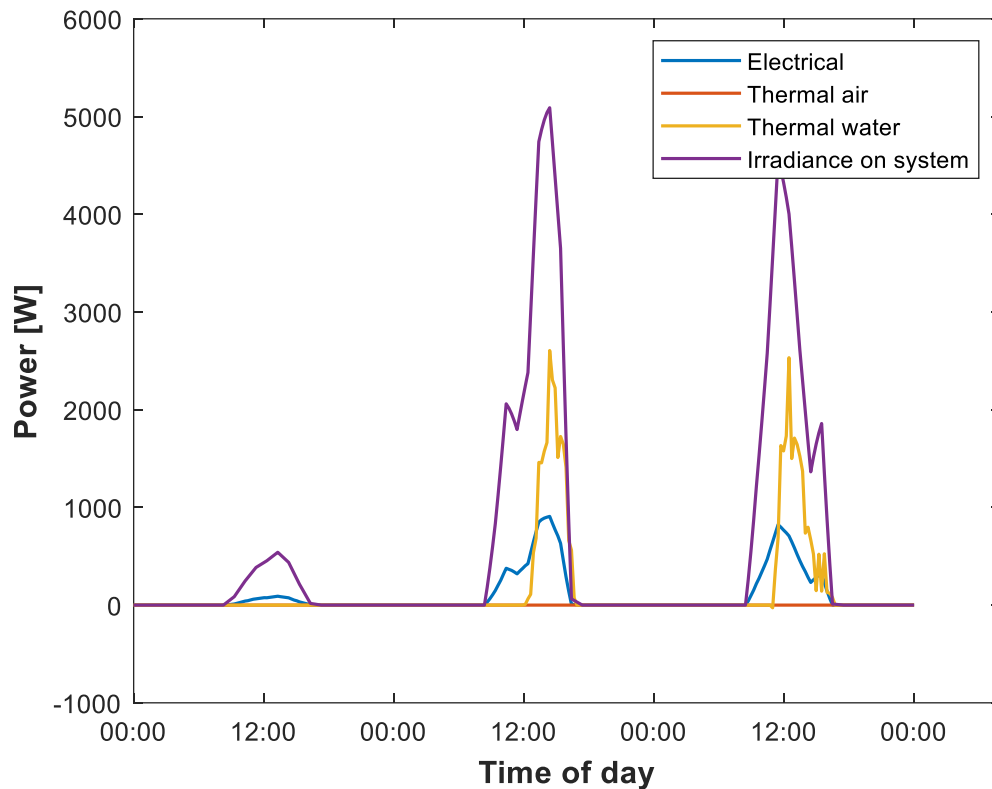


Figure 5-36 Irradiance on system and powers from water pipe design for lowest ambient temperature day (Middle day)

Figure 5-37 illustrates the main temperatures of the Water pipe design. There is a time in the coldest day that the door opening of the room is open so the air of the building can be heated (it can be seen from the yellow line). This is also illustrated in Figure 5-43. This happens because the temperature of the cells is higher than the temperature of the air in the building. However, the outlet temperature of air is not increasing but decreasing. The reason is that the temperature of the front glass is very low and extracts thermal energy from the air in the cavity because of that phenomenon. Therefore, there is zero thermal energy from air even though the strategy is to extract thermal energy from the cavity. Contrarily, the temperature of the water increases significantly during the noon with an increase of about 10°C.

Continuing with Figure 5-38, the mass flow of the water is relatively low because the temperature of the cell is low.

Figure 5-39 illustrates the tank temperatures for such severe conditions. The temperatures of the tank are very high compared to the environmental temperature which is less than zero degrees Celsius.

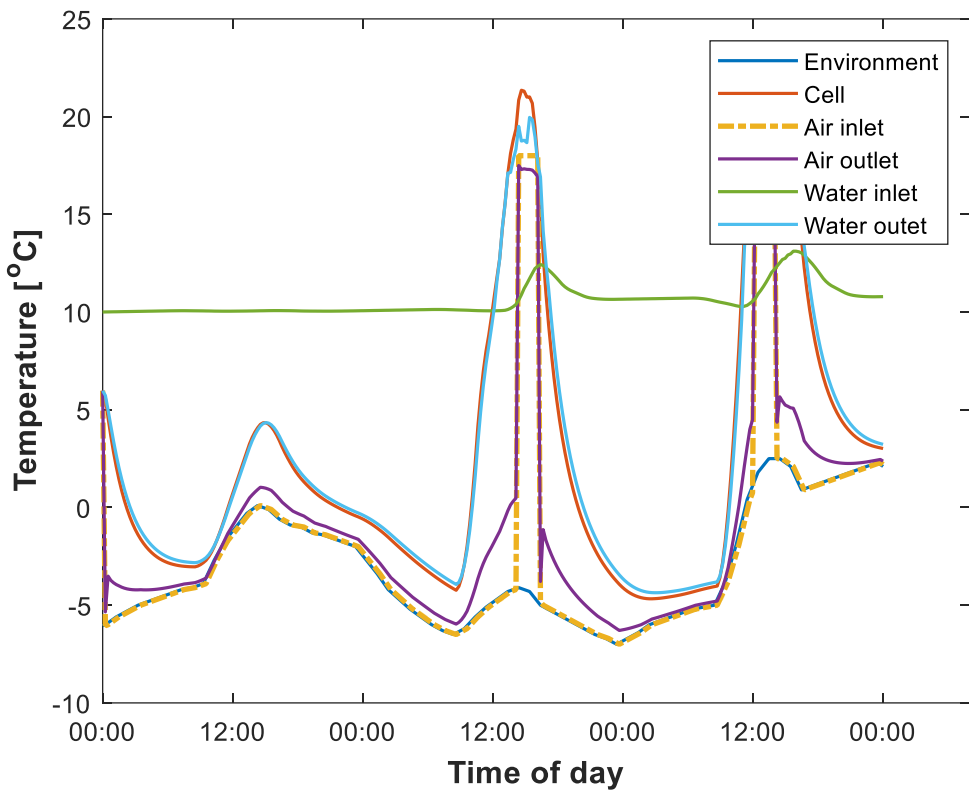


Figure 5-37 Temperatures of water pipe design for lowest ambient temperature day (Middle day)

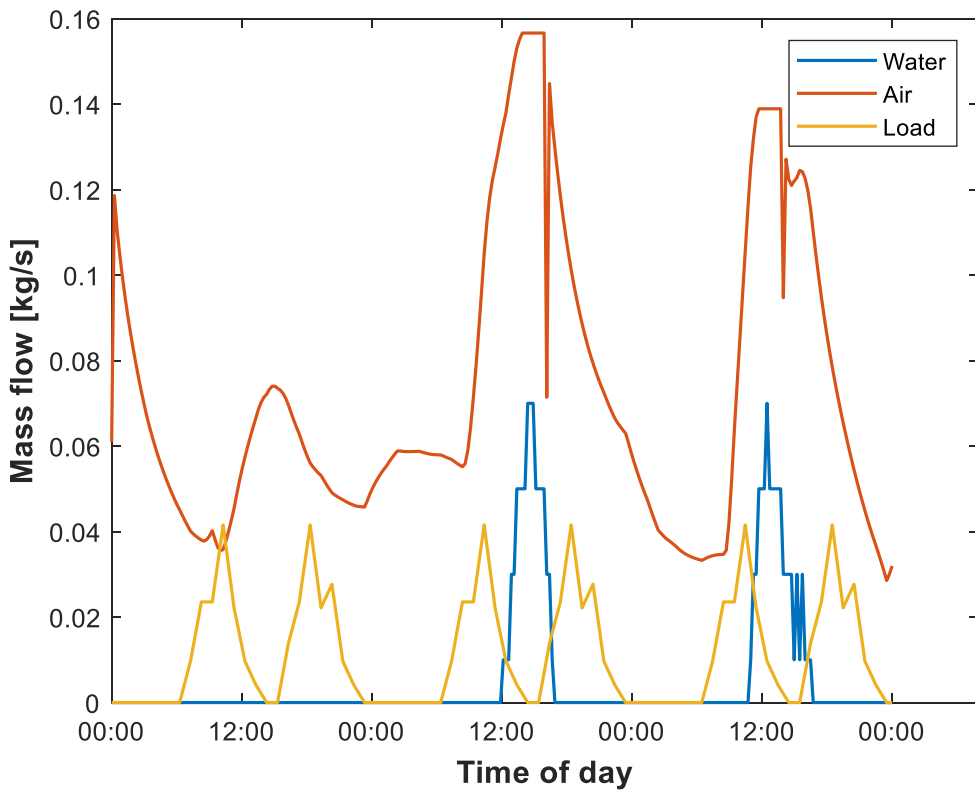


Figure 5-38 Water/air mass flows and water load of water pipe design for lowest ambient temperature (Middle day)

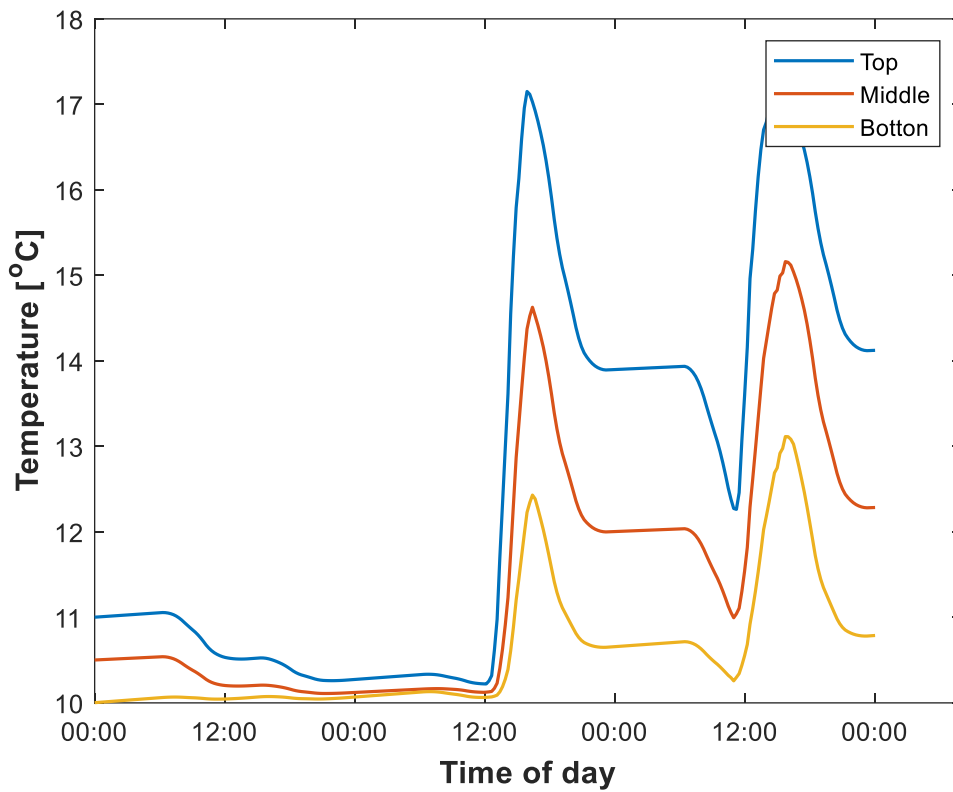


Figure 5-39 Temperatures of water tank levels for lowest ambient temperature day (Middle day)

Figure 5-40 illustrates the electrical power gained from the PV modules for each configuration. Because the temperatures of the cells for all configurations are relatively low and close with each other, the only difference is that the Water pipes and No water pipes designs have smaller power production than the other two configurations due to additional reflection losses.

Figure 5-41 shows that only the No water pipe design extracts thermal energy from the air inside the cavity. The reason is that the temperature of the PV modules is almost 10°C higher than the temperature of the air inside the building.

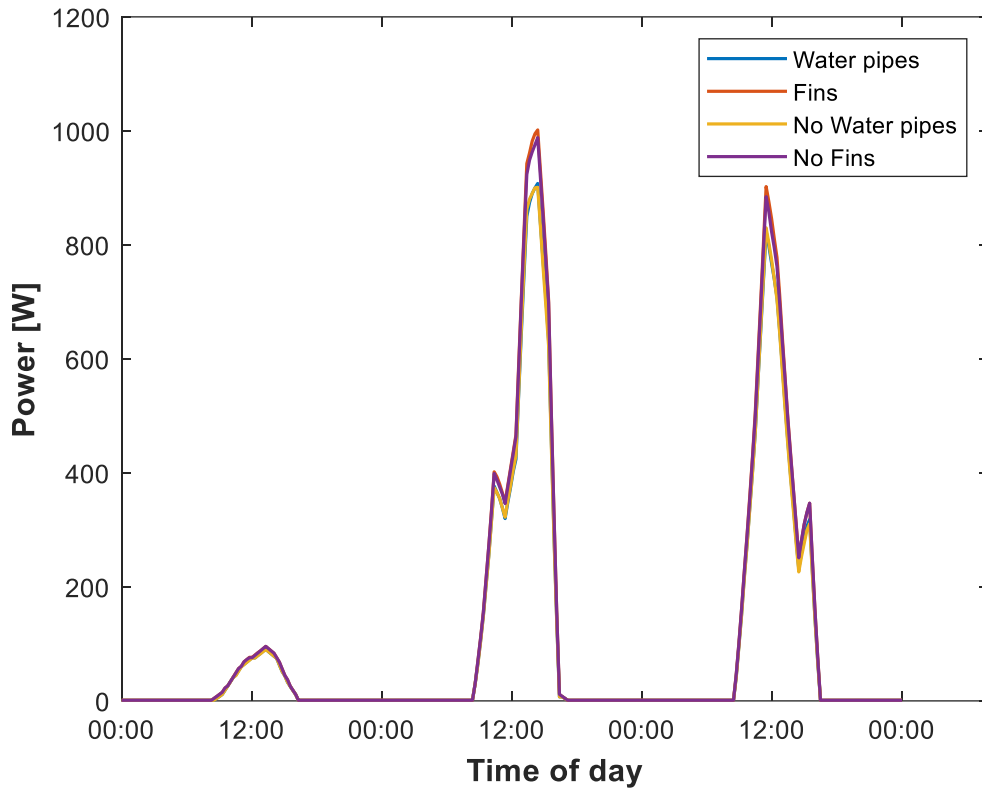


Figure 5-40 Electrical power of each configuration for lowest ambient temperature day (Middle day)

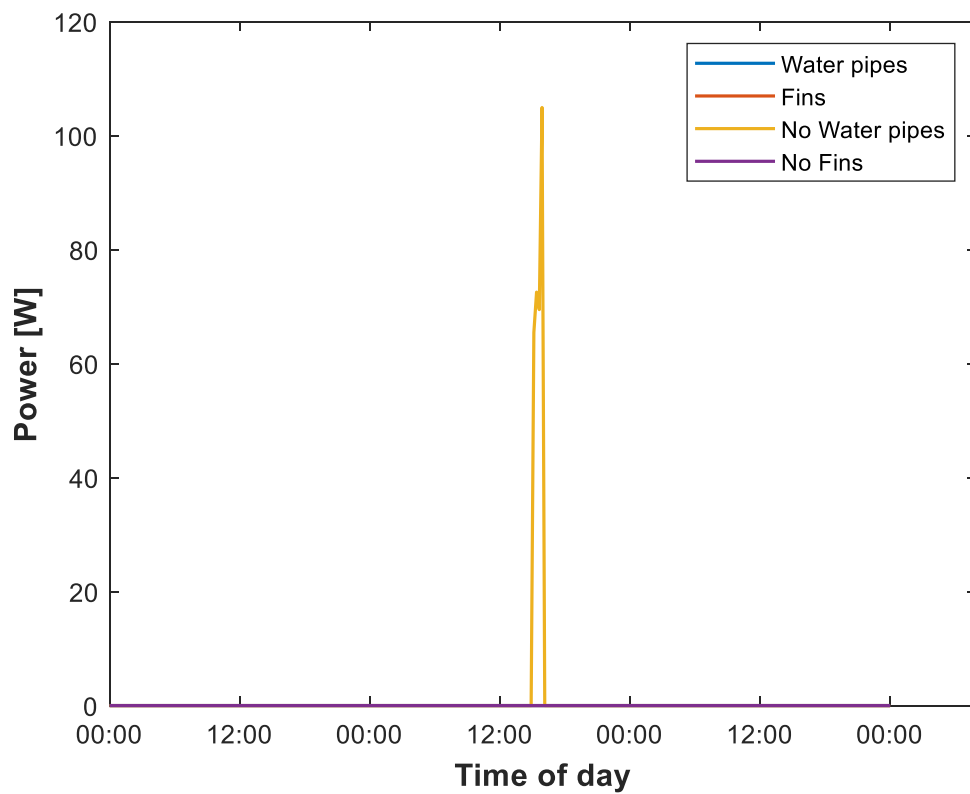


Figure 5-41 Air thermal power of each configuration for lowest ambient temperature day (Middle day)

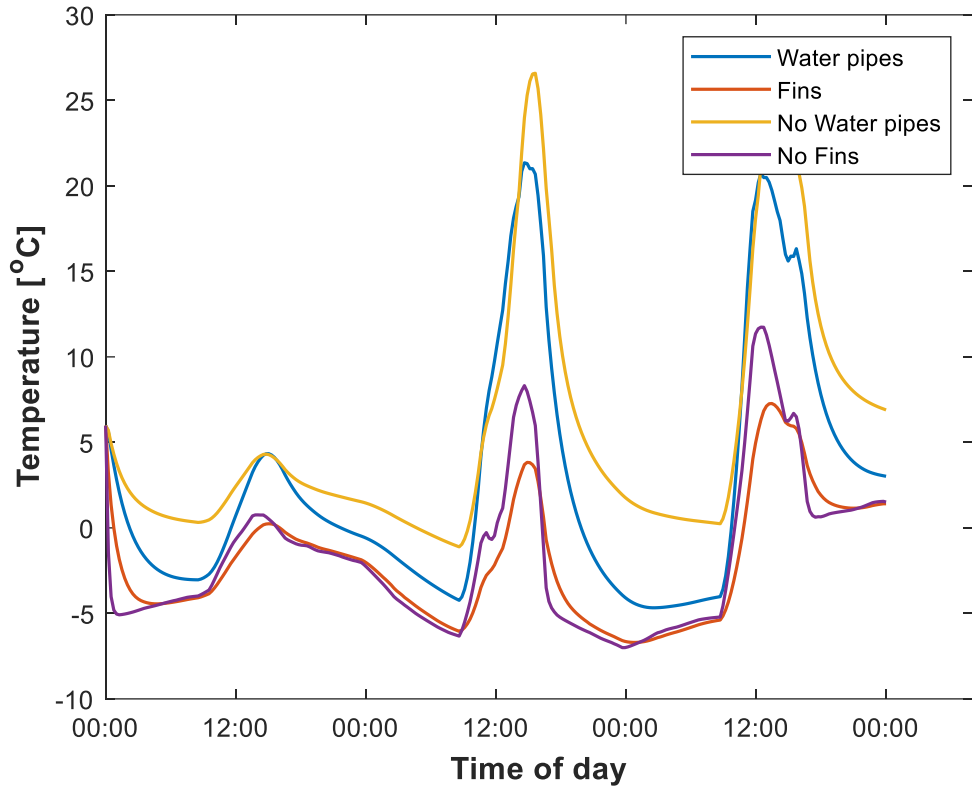


Figure 5-42 Average PV cell temperatures of each configuration for highest irradiance day

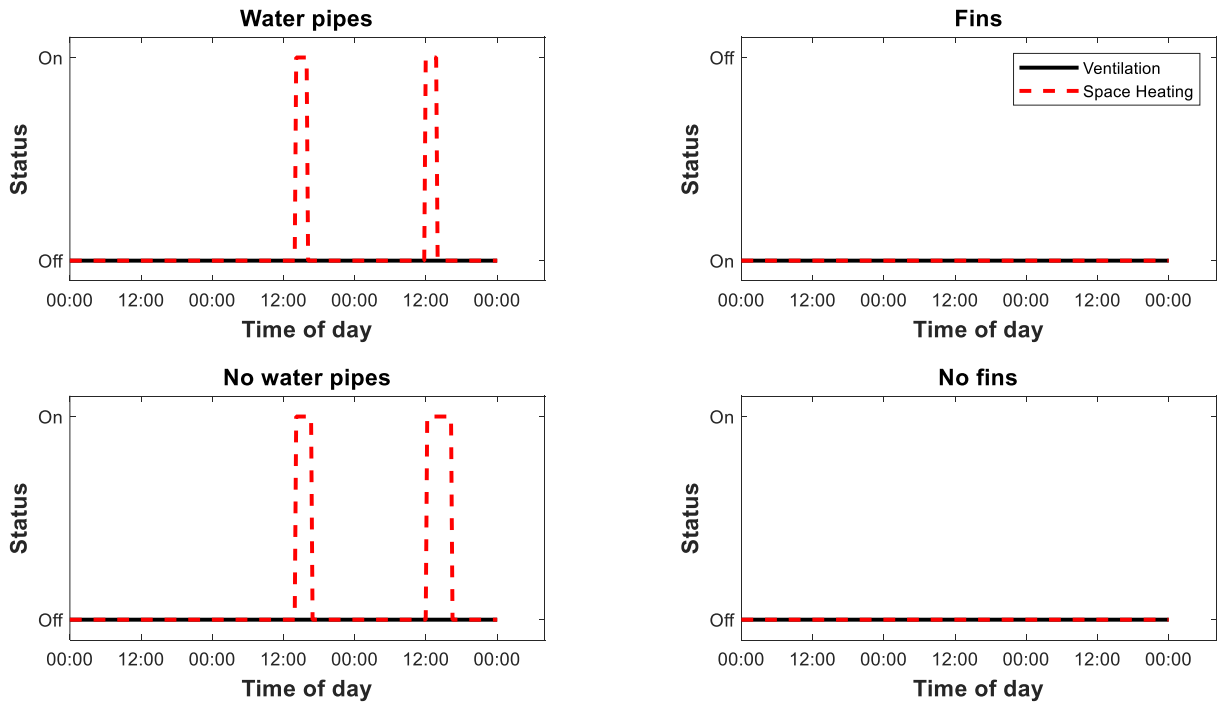


Figure 5-43 Ventilation and heating status (strategy) of each configuration for the lowest ambient temperature day

6 Conclusion

In the Previous study of PV combined with solar chimney (2019) [7], it was concluded that the thermal energy could not be utilised and therefore new designs and strategies needed to be introduced. Consequently, a thermal model was created to find the energetic performance of PV/T combined with solar chimney. Two designs were considered. The PV at the front of the solar chimney with fins (Fins design) and the PV at the back of the solar chimney with water pipe system (Water pipes design). These two designs were also compared with the same systems but without the fins (No fins design) and the water pipes (No water pipes design), to provide results for the location at Delft, Netherlands and a 10m² (10 meters height and 1 meter width) system.

The door openings strategy provided more realistic results and optimized the performance. It was concluded that, ventilation with heating were occurring only during the summer. Heating was available throughout the whole year thanks to the introduction of closed loop heating. In addition, variable water mass flow strategy increased the efficiency of the thermal energy of water and kept the operational temperature of the cells to less than 35°C throughout the year.

The best energetic performance is provided by the Water pipes design because of the high water-thermal energy generation, which amounted for 3336kWh/year (334kWh/m²/year). In addition, the water pipe design has the highest overall yearly efficiency which reaches 64.3%. This is approximately double than the No water pipes design and more than triple than the Fins and No fins designs. The Fins and No fins designs have such lower efficiencies because most of the thermal energy produced is lost in the environment. However, the Fins design performs better in terms of electrical efficiency due to the extra cooling provided from the fins. More precisely it provided 17kWh/year (1.7kWh/m²/year) more than the No fins design. The Water pipes design provides less electricity than the Fins and No fins designs due to the additional reflection losses produced by the solar chimney. But it produced more electricity than the No water pipes design even though a fraction of electrical energy is used to run the water pump. The difference of electrical energy between Water pipe and No water pipe designs is equal to 35kWh/year (3.5kWh/m²/year). The reason is that the cells of the No water pipe design reach very high temperatures (60°C) and the electrical efficiency is much lower. However, due to this high temperature the No water pipes design performs significantly better in the air-thermal energy and ventilation. It provides 4 times more air-thermal energy from the Fins design and about 6 times more air-thermal energy from the No fins and Water pipes designs. Worth mentioning is that the Fins design provides 100kWh/year more thermal energy than the no Fins design due to the higher convection provided from the fins. The Water pipe design has the worst performance in terms of air-thermal energy because most of the thermal energy is driven to the water.

The performance of the four configurations was also simulated for extreme weather conditions. The day with the highest incident irradiance showed that the Water pipe configuration extracts more than 50% of the solar energy thanks to efficient conduction of heat to the water system. In addition, the air-thermal energy of the No water pipes design was delivered continuously throughout the whole night until the next day because of the high PV cell temperatures. The day with the lowest incident irradiance showed that the four designs performed similarly because no thermal energy was generated. The day with the highest temperature showed that water-thermal energy can be extracted due to the high temperatures. However, there is a small error because the temperature of the water coming from the mains is considered constant at 10°C which overestimates the thermal efficiency of the system. Lastly the day with the lowest temperature illustrated that still in such conditions, water-

thermal energy can be generated from the Water pipes designs but also air-thermal energy from the No water pipes designs.

All in all, the best performing configuration is the Water pipes design because not only it can use a huge portion of the incident irradiance but also it can provide three different types of energy (air/water/electricity) which are very important for residential and service buildings. Nonetheless, the Water pipes design is an active system as opposed to the other configurations and has much more components and therefore more initial and maintenance cost will be expected. However, if the priority is electrical energy, the best configuration is the Fins design. Contrarily, if the main priority is air-thermal energy then the best configuration is the No water pipes design. The designs prove that the concept of a solar chimney can have multiple applications with many energetic advantages.

7 Recommendations

The work of this thesis is to determine the energetic performance of PV/T with solar chimney by creating a model in MATLAB. However, there is always room for improvements. The most crucial improvements are introduced below.

- Validation of the model with a full-scale system is essential. In addition, with such experiments, empirical convection coefficient functions can be estimated which will significantly improve the accuracy of the models.
- A model of the optimal pipe diameter for different water mass-flow range is needed to provide more realistic results of electrical energy used from the water pump.
- A function of water temperature that arrives from the mains, with respect to ambient temperature is required to eliminate any possible errors in accuracy on the water-thermal energy calculations.
- Optimization of Fin characteristics (Size and number) is needed for the calculation of the maximum efficiency of the Fins design. In addition, the mass flow model is for flat plates, therefore, a new mass flow model that considers the fins is vital.
- An economic analysis will provide more information of which design is the most cost efficient.
- Lastly, results for other locations (especially hot climates) must be evaluated.

Appendix A: Designs without thermal systems

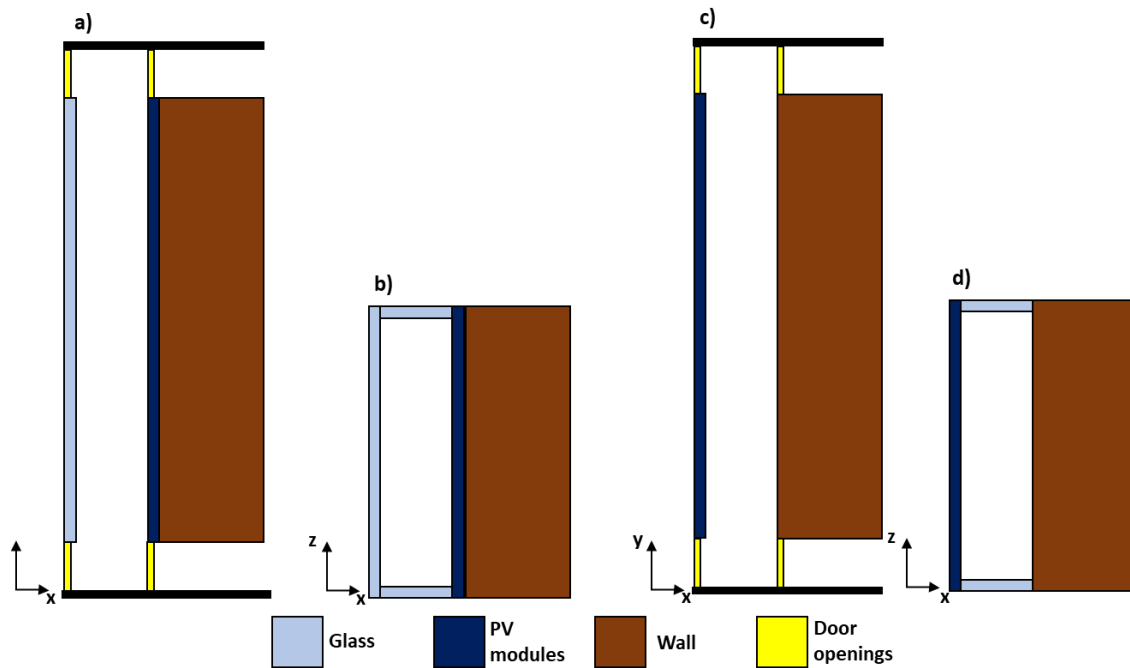


Figure A 1 Designs without thermal systems. a) Without fins, b) Without water pipes

Figure A 1 illustrates the designs without the chosen thermal systems. This means without the water pipes and without the fins as the designs shown in Figure 3-1. These designs are compared with the designs of Figure 3-1 to find out the influence of the water pipe and fins installation. In addition, Figure A 1-a is also excluding the insulation and aluminium bulk. Therefore, the PV modules are directly attached on the wall. The names of this designs are 'No water' pipes and 'No fins'.

Appendix B: Weather data of scenarios

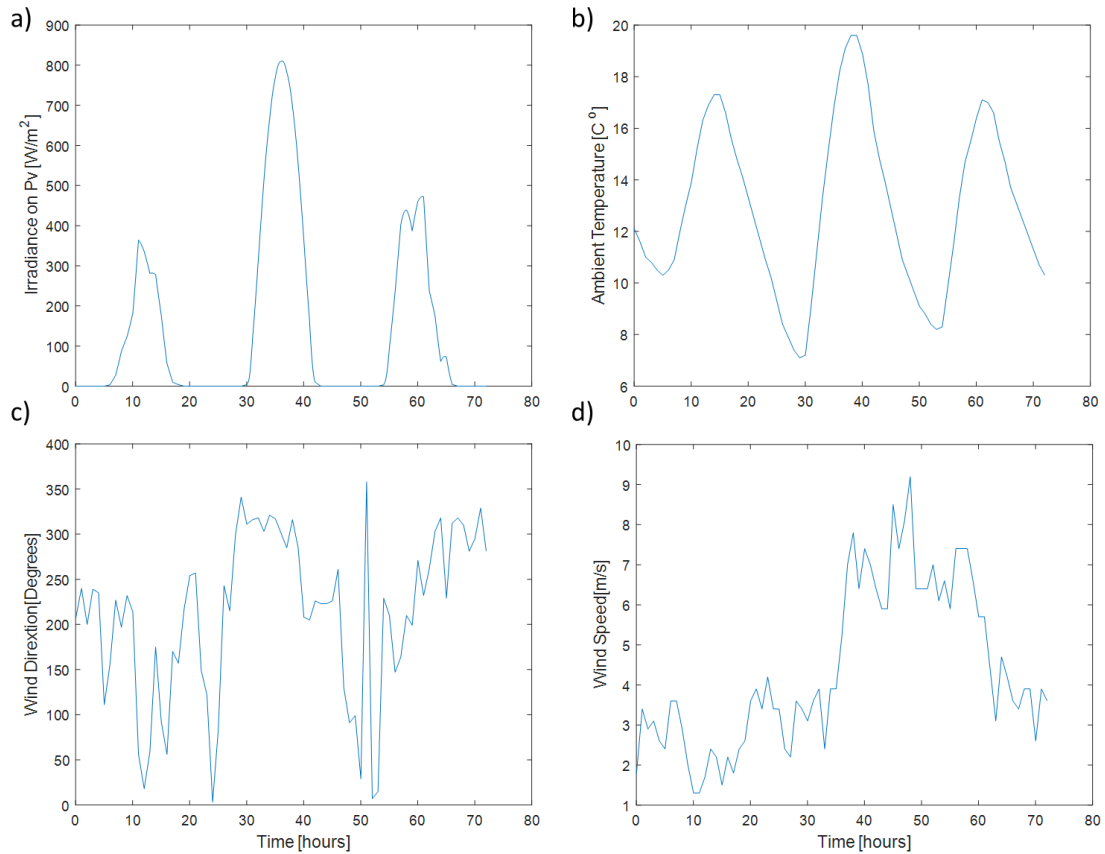


Figure B 1 Weather data for highest irradiance a) Irradiance b) Ambient temperature c) Wind direction d) Wind speed

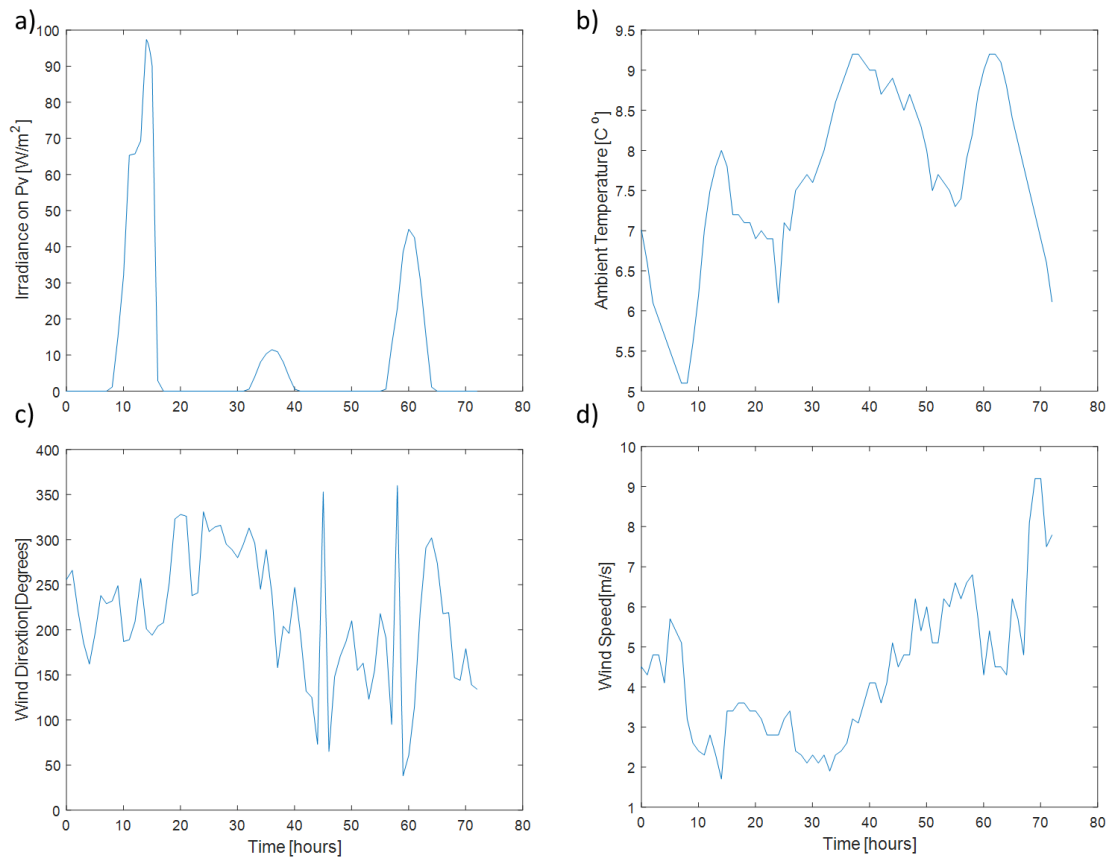


Figure B 2 Weather data for lowest irradiance day. a) Irradiance b) Ambient temperature c) Wind direction d) Wind speed

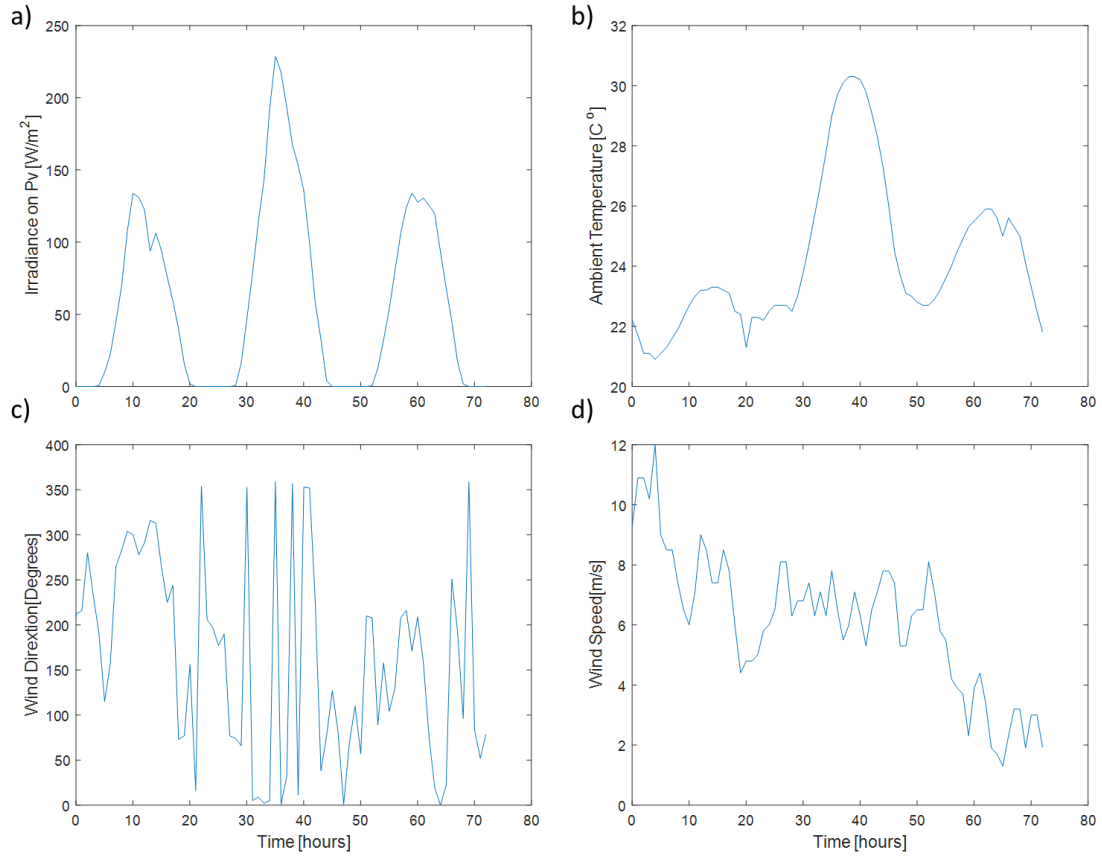


Figure B 3 Weather data for highest temperature day a) Irradiance b) Ambient temperature c) Wind direction d) Wind speed

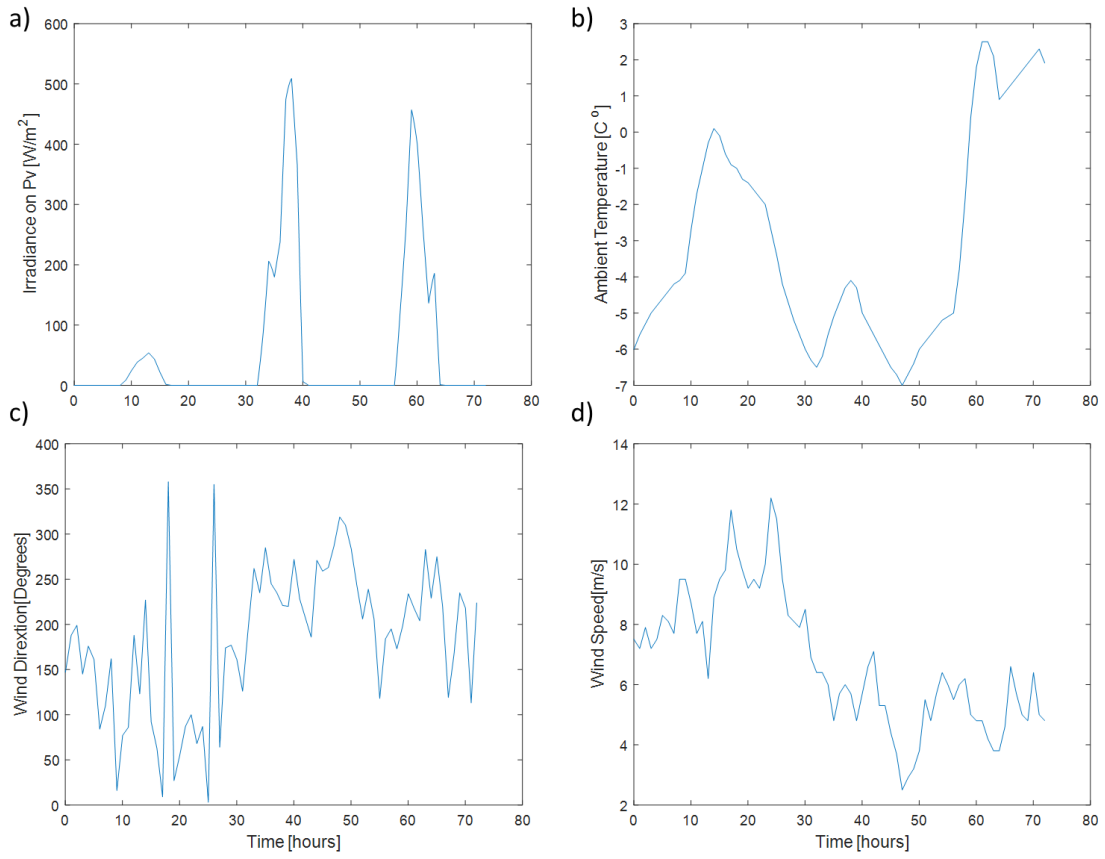


Figure B 4 Weather data for lowest temperature day a) Irradiance b) Ambient temperature c) Wind direction d) Wind speed

Bibliography

- [1] T. F. Stocker *et al.*, “Climate change 2013 the physical science basis: Working Group I contribution to the fifth assessment report of the intergovernmental panel on climate change,” *Clim. Chang. 2013 Phys. Sci. Basis Work. Gr. I Contrib. to Fifth Assess. Rep. Intergov. Panel Clim. Chang.*, vol. 9781107057, pp. 1–1535, 2013, doi: 10.1017/CBO9781107415324.
- [2] “NASA global climate change,” NASA. [Online]. Available: <https://climate.nasa.gov/effects/>.
- [3] “Eurostat statistics explained,” *europa*. [Online]. Available: <https://ec.europa.eu/eurostat>.
- [4] M. C. Brito, S. Freitas, S. Guimarães, C. Catita, and P. Redweik, “The importance of facades for the solar PV potential of a Mediterranean city using LiDAR data,” *Renew. Energy*, vol. 111, pp. 85–94, 2017, doi: 10.1016/j.renene.2017.03.085.
- [5] “Energy education solar chimney,” *University of Calgary*. [Online]. Available: https://energyeducation.ca/encyclopedia/Solar_chimney#:~:text=When solar chimneys are used,two additional vents are present.
- [6] “Energy education trombe wall,” *University of Calgary*. [Online]. Available: https://energyeducation.ca/encyclopedia/Trombe_wall.
- [7] J. C. Ortiz Lizcano *et al.*, “Photovoltaic chimney: Thermal modeling and concept demonstration for integration in buildings,” *Prog. Photovoltaics Res. Appl.*, vol. 28, no. 6, pp. 465–482, 2020, doi: 10.1002/pip.3194.
- [8] S.H.Wapperom, “The energetic performance of a naturally ventilated façade with photovoltaic modules placed as outer façade or at various depths in the air channel,” 2019.
- [9] L. Shi, “Theoretical models for wall solar chimney under cooling and heating modes considering room configuration,” *Energy*, vol. 165, pp. 925–938, 2018, doi: 10.1016/j.energy.2018.10.037.
- [10] K. Sergei, C. Shen, and Y. Jiang, “A review of the current work potential of a trombe wall,” *Renew. Sustain. Energy Rev.*, vol. 130, no. June, p. 109947, 2020, doi: 10.1016/j.rser.2020.109947.
- [11] M. Raghieb Shakeel, J. Al-Sadah, and E. M. A. Mokheimer, “Analytical and Numerical Modeling of Solar Chimney,” *J. Energy Resour. Technol. Trans. ASME*, vol. 139, no. 3, pp. 1–11, 2017, doi: 10.1115/1.4035782.
- [12] A. K. Shukla, K. Sudhakar, and P. Baredar, “Recent advancement in BIPV product technologies: A review,” *Energy Build.*, vol. 140, pp. 188–195, 2017, doi: 10.1016/j.enbuild.2017.02.015.
- [13] A. H. A. Al-Waeli, K. Sopian, H. A. Kazem, and M. T. Chaichan, “Photovoltaic/Thermal (PV/T) systems: Status and future prospects,” *Renew. Sustain. Energy Rev.*, vol. 77, no. April, pp. 109–130, 2017, doi: 10.1016/j.rser.2017.03.126.
- [14] T. M. Sathe and A. S. Dhoble, “A review on recent advancements in photovoltaic thermal techniques,” *Renew. Sustain. Energy Rev.*, vol. 76, no. October 2016, pp. 645–672, 2017, doi: 10.1016/j.rser.2017.03.075.
- [15] S. Dubey and G. N. Tiwari, “Analysis of PV/T flat plate water collectors connected in series,” *Sol. Energy*, vol. 83, no. 9, pp. 1485–1498, 2009, doi: 10.1016/j.solener.2009.04.002.

- [16] H. A. Zondag, D. W. De Vries, W. G. J. Van Helden, R. J. C. Van Zolingen, and A. A. Van Steenhoven, "The thermal and electrical yield of a PV-thermal collector," *Sol. Energy*, vol. 72, no. 2, pp. 113–128, 2002, doi: 10.1016/S0038-092X(01)00094-9.
- [17] T. T. Chow, "Performance analysis of photovoltaic-thermal collector by explicit dynamic model," *Sol. Energy*, vol. 75, no. 2, pp. 143–152, 2003, doi: 10.1016/j.solener.2003.07.001.
- [18] M. I. Sohel, Z. Ma, P. Cooper, J. Adams, and R. Scott, "A dynamic model for air-based photovoltaic thermal systems working under real operating conditions," *Appl. Energy*, vol. 132, pp. 216–225, 2014, doi: 10.1016/j.apenergy.2014.07.010.
- [19] J. K. Tonui and Y. Tripanagnostopoulos, "Air-cooled PV/T solar collectors with low cost performance improvements," *Sol. Energy*, vol. 81, no. 4, pp. 498–511, 2007, doi: 10.1016/j.solener.2006.08.002.
- [20] J. C. Mojumder, W. T. Chong, H. C. Ong, K. Y. Leong, and Abdullah-Al-Mamoon, "An experimental investigation on performance analysis of air type photovoltaic thermal collector system integrated with cooling fins design," *Energy Build.*, vol. 130, pp. 272–285, 2016, doi: 10.1016/j.enbuild.2016.08.040.
- [21] D. Su, Y. Jia, X. Huang, G. Alva, Y. Tang, and G. Fang, "Dynamic performance analysis of photovoltaic-thermal solar collector with dual channels for different fluids," *Energy Convers. Manag.*, vol. 120, pp. 13–24, 2016, doi: 10.1016/j.enconman.2016.04.095.
- [22] T. Yang and A. K. Athienitis, "A review of research and developments of building-integrated photovoltaic/thermal (BIPV/T) systems," *Renew. Sustain. Energy Rev.*, vol. 66, pp. 886–912, 2016, doi: 10.1016/j.rser.2016.07.011.
- [23] J. Jie, Y. Hua, H. Wei, P. Gang, L. Jianping, and J. Bin, "Modeling of a novel Trombe wall with PV cells," *Build. Environ.*, vol. 42, no. 3, pp. 1544–1552, 2007, doi: 10.1016/j.buildenv.2006.01.005.
- [24] A. K. Athienitis, J. Bambara, B. O'Neill, and J. Faille, "A prototype photovoltaic/thermal system integrated with transpired collector," *Sol. Energy*, vol. 85, no. 1, pp. 139–153, 2011, doi: 10.1016/j.solener.2010.10.008.
- [25] T. T. Chow, W. He, and J. Ji, "An experimental study of façade-integrated photovoltaic/water-heating system," *Appl. Therm. Eng.*, vol. 27, no. 1, pp. 37–45, 2007, doi: 10.1016/j.applthermaleng.2006.05.015.
- [26] E. M. Kleinbach, W. A. Beckman, and S. A. Klein, "Performance study of one-dimensional models for stratified thermal storage tanks," *Sol. Energy*, vol. 50, no. 2, pp. 155–166, 1993, doi: 10.1016/0038-092X(93)90087-5.
- [27] M. Haase, F. Marques da Silva, and A. Amato, "Simulation of ventilated facades in hot and humid climates," *Energy Build.*, vol. 41, no. 4, pp. 361–373, 2009, doi: 10.1016/j.enbuild.2008.11.008.
- [28] R. Santbergen, "Optical Absorption Factor of Solar Cells for PVT Systems," 2008.
- [29] "Meteonorm," *Impressum*. [Online]. Available: <https://meteonorm.com/>.
- [30] A. Smets, K. Jager, O. Isabella, R. Van Swaaij, and M. Zeman, *Solar Energy The Physics and Engineering of Photovoltaic Conversion Technologies and Systems*. UIT cambridge, 2015.
- [31] M. E. Hulley, "The urban heat island effect: Causes and potential solutions," *Metrop. Sustain. Underst. Improv. Urban Environ.*, pp. 79–98, 2012, doi: 10.1533/9780857096463.1.79.

- [32] P. Predict, "Optical losses." [Online]. Available: <https://plantpredict.com/algorithm/optical-losses/#reflection-and-refraction>.
- [33] F. P. INCROPERA, D. P. DEWITT, T. L. BERGMAN, and A. S. LAVINE, *Fundamentals of Heat and Mass Transfer*, 6th ed. John Wiley & Sons, Inc, 2007.
- [34] J. A. Palyvos, "A survey of wind convection coefficient correlations for building envelope energy systems' modeling," *Appl. Therm. Eng.*, vol. 28, no. 8–9, pp. 801–808, 2008, doi: 10.1016/j.applthermaleng.2007.12.005.
- [35] W. Elenbaas, "HEAT DISSIPATION OF PARALLEL PLATES BY FREE CONVECTION," *Physica*, no. 1, 1942.
- [36] S. W. Churchill and H. H. S. Chu, "Correlating equations for laminar and turbulent free convection from a vertical plate," *Int. J. Heat Mass Transf.*, vol. 18, no. 11, pp. 1323–1329, 1975, doi: 10.1016/0017-9310(75)90243-4.
- [37] J. M. Mineur, "Laminar flow in narrow ducts and circular tubes: Entrance effects," *Appl. Energy*, vol. 5, no. 1, pp. 1–10, 1979, doi: 10.1016/0306-2619(79)90002-3.
- [38] M. Isidoro, *Radiative view factors*. Isidoro Martinez.
- [39] G. He, J. Zhang, and S. Hong, "A new analytical model for airflow in solar chimneys based on thermal boundary layers," *Sol. Energy*, vol. 136, pp. 614–621, 2016, doi: 10.1016/j.solener.2016.07.041.
- [40] "Seaward," *Seaward Electronic Ltd.*, 2020. [Online]. Available: <https://www.seaward.com/>.
- [41] M. Mathew, "The Mathematics of Pumping Water," 2017.
- [42] S. Ioan and S. Calin, *Solar heating and cooling systems*. Elsevier Science, 2017.
- [43] "The engineering ToolBox," 2001. [Online]. Available: <https://www.engineeringtoolbox.com/>.